Doctoral Thesis

Numerical Methods for Optimal Control of Hydraulic Independent Metering Systems

Dipl.-Ing. Goran Stojanoski

October 2022

MONTANUNIVERSITÄT LEOBEN
www.unileoben.ac.at

AFFIDAVIT

I declare on oath that I wrote this thesis independently, did not use other than the specified sources and aids, and did not otherwise use any unauthorized aids.

I declare that I have read, understood, and complied with the guidelines of the senate of the Montanuniversität Leoben for "Good Scientific Practice".

Furthermore, I declare that the electronic and printed version of the submitted thesis are identical, both, formally and with regard to content.

Date 25.10.2022

Signature Author
Goran Stojanoski

Acknowledgments

There are numerous people I would like to thank who made the writing of this thesis possible. First and foremost, I would like to thank my colleagues, especially Dr. Gerhard Rath and Prof. Paul O'Leary for spending time discussing various technical aspects of this work. Their unconditional support, knowledge sharing, and personal discussions were precious experiences for me. I would also like to thank the mentor of this thesis, Prof. Clemens Brand, for his selfless support throughout my studies and thesis. At this point, I would also like to thank Prof. Mathew Harker for giving me a broader insight into the world of mathematics, especially the methods of the calculus of variations that can be used to control mining machines.

Working in a significant personal environment such as the Institute of Automation in Leoben has helped me a lot in working on my thesis. For this reason, I would to express my gratitude for the physical and moral support during my studies and work there. The diversity at the institute has given me a broader view on technical personal views.

I would also like to take this opportunity to thank Sandvik Mining and Construction GmbH, Zeltweg, as our partner in the EIT Raw Materials Project Rock Vader for their unconditional support and knowledge sharing. My special thanks go to Dipl.-Ing. Uwe Restner, Dipl.-Ing. Martin Gimpel, Dipl.-Ing. Wolfgang Richter and Dipl.-Ing. Hubert Kargl for their support and cooperation during experiments and meetings.

Finally, I would like to thank my family most of all. Without my father Peco and my mother Snezhana I would not have achieved half of what I have achieved today. Finally, I would also like to thank my brother Goce for always being there for me.

Abstract

This thesis encompasses various control methods for numerically stiff independent metering systems used in road-header boring machines. These machines are equipped with state-of-the-art independent metering valves with an already implemented PID control structure. The main topics covered in this thesis are: the bulk modulus as the main indicator of the mechanical stiffness of the system, the development of a new mathematical model for an intelligent independent metering valve, methods of calculus of variations for optimal control with integrated position control, a matrix-based approach for numerically stiff ODEs, and a novel method for computing the optimal PID parameters for a given system.

The Wylie - Yu model for the effective bulk modulus has been improved for the temperature change of the oil and implemented in a simulation environment to observe how the fluctuations of the effective bulk modulus influence the system dynamics. It is concluded that for high pressurized system the temperature of the oil has the highest impact on the value of bulk modulus compared to the other parameters. Additionally, an adaptive controller is implemented to compensate for the energy losses.

Both the optimal control and the path tracking problem have been applied and tested in a simulation environment. For this purpose, a new linear model is derived that includes the complex feedback control structure of the independent metering valves. The linear system is then discretized and solved numerically using the Euler-Lagrange equations. In addition, the mass matrix method and interstitial derivatives are used to improve the numerical stability of the solution.

The optimal control method shows remarkable accuracy and improved energy efficiency compared to conventional solvers. On the other hand, the path tracking method precisely follows the given paths with a maximum deviation of 1%.

Kurzfassung

Die vorliegende Arbeit behandelt Regelungsverfahren für hydraulische Antriebe mit getrennten Steuerkanten, die mathematisch mit steifen Differentialgleichungen zu beschreiben sind, am Beispiel einer Teilschnittmaschine für den Tunnel- und Bergbau. Diese ist mit einem modernen intelligenten Ventil ausgerüstet, das bereits Basisregelreise in Form von PID-Reglern zur Verfügung stellt. Die wissenschaftlichen Beiträge der Arbeit beziehen sich auf den Kompressionsmodul des Fluids als wichtigsten Faktor für die Systemsteifigkeit, die Modellbildung eines intelligenten Ventils mit getrennten Steuerkanten, sowie Methoden der Variationsrechung zur optimalen Regelung einer Reglerkaskade mit Lösungsansatz für gewöhnliche Differentialgleichungen (ODEs) von steifen Systemen auf Basis von Matrizen. Weiters wird eine neue Methode zur Optimierung der Parameter eines PID-Reglers vorgeschlagen. Das Wylie-Yu-Modell für den effektiven Kompressionsmodul wurde erweitert um die Temperaturänderung des Öls und in eine Simulationsumgebung implementiert, um die Systemdynamik zu untersuchen. Es konnte gezeigt werden, dass in Hochdrucksystemen die Temperatur den größten Einfluss auf den Kompressionsmodul hat. Dann wurden die durch die Änderung der Ölnachgiebigkeit verursachten Energieverluste untersucht und ein adaptiver Regler vorgeschlagen, um diese zu reduzieren. Optimale Regelung wurde sowohl auf die Positions- als auch die Pfadfolgeregelung angewendet und in der Simulation verifiziert. Inkludiert wurde dabei auch ein neues Modell für die komplexe Reglerstruktur, die in den Ventilen enthalten ist. Das linearisierte Gleichungssystem wurde diskretisiert und mit Hilfe der Euler-Lagrange-Gleichungen gelöst. Die numerische Stabilität der Lösung konnte verbessert werden durch die Methode der Massenmatrix und mit Hilfe von Interstitial Derivatives unter Verwendung von zusätzlich interpolierten Punkten zur Annäherung der Differentiation. Die Anwendung der optimalen Regelung erzielt eine Verbesserung sowohl der Genauigkeit, als auch des Energiewirkungsgrads im Vergleich zu herkömmlichen Lösungen. Außerdem wird damit die Pfadfolgeregelung verbessert und erreicht Abweichungen, die kleiner als 1% sind.

Contents

Chapter 1

Introduction

1.1 Motivation

The motivation for the work in this dissertation is to improve the performance and efficiency of hydraulic systems used in mining machinery. When operating, both the mechanical and the hydraulic parts of these machines are heavily affected by tremendous external forces which produce vibrations. This means that having a mechanically stiff system is an essential part of the working of these machines. Because the mechanical and the hydraulic system are coupled together, the same applies to the hydraulic system. For this reason, a detailed analysis on the effects of the bulk modulus on the dynamics of such systems was done.
Mining machines used for drilling usually have predefined profiles that need to be excavated. They are usually used for mining various types of minerals that are difficult to extract in different ways. In addition, the state-of-the-art machine that is part of this work should significantly increase the speed of mining and be a substitution for explosives, which are now widely used in this industry. This has motivated the author to apply variational calculus methods such as optimal control and trajectory tracking in such systems. For this reason, a new mathematical model of the system is derived, which has already been implemented on the test-bed. Although this model was simplified, it was strongly influenced by the very high and very low values (very fast and very slow-moving parts) of the system parameters, making it numerically stiff. The physical stiffness in hydraulic systems results with very high and very low values for the system parameters in the ODE which produces numerically stiff system. Therefore the corresponding numerical solution for the continuous problem is stiff. Solving such problems numerically can be a very difficult task.
More precisely, the heart of this thesis lies in the solution of multiple problems which appear at hydraulic machinery used for mining. Firstly, a complete func-

tional model of an intelligent valve was developed and verified. Multiple models for the bulk modulus were tested and compared. A new model was developed and implemented in a simulation environment. The effects of the bulk modulus (the combined effect of: pressure, temperature of the oil and the air content in the oil) on the dynamics of the system was tested and analyzed. A new adaptive controller was implemented which improved the energy efficiency of the system significantly. Additionally, the Euler Lagrange equations for the optimal path and the path tracking problem are solved using a novel method for the solution of stiff numerical equations in hydraulic systems. This is first achieved by implementing the mass matrix, which shifts the very high values from one side of the equations to the other. In addition, interstitial derivatives are used to compute a stable numerical solution for the system.
This work originated during the development of a state of the art mobile mining machine by Sandvik Minning and Construction GmbH as part of the EIT Raw Materials Project 'Rock Vader'.

1.2 Outline

The remainder of the thesis is organized as follows:

Chapter 2 The second chapter of this thesis provides the mathematical background for the algorithms and the methods implemented there. The aim of this chapter is to give a clear overview of the methods and the investigations carried out in this thesis. The method of interpolation is used to derive the collocative and interstitial numerical derivative approximation in matrix form. In addition, a method of matrix discretization is introduced. Once the system of equations is discretized, it can be processed using various numerical techniques of linear algebra. The least squares method is one of the techniques for LTI systems presented in this chapter. Singular value decomposition was then used to solve the least squares problem.

Chapter 3 This chapter introduces the hydraulic and mechanical system used in tunnel boring machines. The valve used to control the cutting motion of this system includes embedded controllers for the flow and pressure. These controllers were included in the linear and nonlinear models of the system derived in this chapter. The bulk modulus is analyzed as one of the leading system parameters for the hydraulic stiffness of the system. If the value of the bulk modulus lowers the mechanical stiffness of the system will decrease which can be the cause of instability and osculations. The Wylie - Yu model was modified for the temperature change and used in a simulation environment to investigate the effects of the temperature and the air content in the oil on the dynamics of hydraulic systems. An adaptive controller is implemented to improve the system's energy efficiency.

Chapter 4 This chapter starts with the basic calculus concepts of variational methods for optimal control. The optimal control problem is derived and implemented for numerically stiff independent metering systems. The method is then compared to an LQR (linear quadratic regulator) and PID (proportional, integral, derivative) controller to show its advantages. Additionally, the path tracking problem for the same system is derived. The solution was then implemented in a simulation environment to verify its results. Both methods show improved energy efficiency and performance.

Chapter 5 The last chapter discusses future methods which can be implemented using techniques already implemented in this thesis. These, nevertheless, should not be overlooked due to their potential and chances of success.

Chapter 2

Matrix Based Approach for Solving Stiff Differential Equations

This chapter introduces the fundamental mathematical background for solving stiff differential equations numerically. These methods are essential for finding stable numerical solutions to the complex system of equations used to describe these systems. The objective is to investigate the methods for solving stiff differential equations, set the basis for matrix formulations of ODEs, discretization, and solving of the ODEs, least-squares approach for solving such systems using the singular value decomposition (SVD). It is concluded that the implicit (backward) Euler methods and the interstitial derivatives perform much better when solving stiff differential equations. Additionally, a mass matrix in the state space representation is introduced, which also improves the numerical stability of the solution.

2.1 Introduction to Stiff Differential Equations

When modeling a dynamic system, one must obey the laws of physics, which bring us to the use of ordinary or partial differential equations (ODEs or PDEs). Although the system of differential equations is well defined and corresponds to the dynamics of the real system, in most cases finding a numerical solution may be impossible by using traditional methods (Runge - Kutta methods). The main reasons for this are their complexity, non-linearity, and the stiffness of the ODEs. The independent metering hydraulic systems presented in chapter 3 have many non-linearities (like friction, bulk modulus) and are usually described with stiff differential equations. The non-linearities are usually included so the system described can represent as close as possible to the real one. The stiffness occurs when two or more variables have a considerable difference in magnitude. From

a mechanical point of view, a stiff system can be considered as such if there are parts of the system which react (move) at a much higher frequency than other parts. Throughout the years, it has been shown that there is no single defined method for the solution of stiff differential equations. However, the Runge - Kutta methods [1] are still an excellent foundation for the commonly used solvers.
The first detection of stiff differential equations was made by two chemists – Curtis and Hirschfelder – [2] in early 1952. They discovered stiffness in their kinetics studies and proposed a multi-step solution using the backward differentiation formula [1], which produced acceptable results. This topic was ignored until 1963, when Dahlquist [3] defined the problem and identified the solvers' numerical instability when solving stiff ODEs. Or, in his words,"Around 1960, things became completely different and everyone became aware that the world was full of stiff problems [4]". Following his paper, the field became more active, and several new approaches were proposed to integrate stiff ODEs. Gear in [5] [6] proposed variable-order backward differentiation methods, which were later modified by Hindmarsh [7] and Byrne [8]. Additionally, Linger and Willoughby [9] and Enright [10] proposed methods based on the second derivative multi-step formulas, which deliver promising results. In the late 20th century, Lindberg studied the trapezoidal rule proposed by Dahlquist [11]. Moreover, Butcher in [12] and Ehle in [13] proposed improved Runge-Kutta methods for solving stiff differential equations. Additional articles on integrating stiff differential equations and the topic of stiffness include [14], [15], [16],[17], [18].
Let us consider the example where the solution of a stiff differential equation has a term e^{-ct} where c is a large positive constant. As the time increases, the solution decays to zero very rapidly compared to other solution terms. This term is called the transient term of the solution. Furthermore, let us consider the case where the component of the solution varies very rapidly on a much shorter time scale. Now, the challenge for the numerical method will be to choose the right step size because the step size is not only dictated by the solution as a whole but also by the rapidly varying local behavior.
Another important numerical approach for solving PDEs is the method of lines [19]. Other applicable techniques include finite difference formulas [20], [21] and spectral methods [22],[19], [21]. The first one to use spectral methods for the numerical solution of ODEs was Lanczos in early 1938 [23]. These methods often include the fast Fourier transformation (FFT) algorithm invented by Cooley and Tukey [24]. More articles on the FFT topic can be found in [25], [26].
Explicit schemes still have difficulty producing stable results when solving stiff differential equations [17]. Using minimal time steps can cause instability in certain steps and excessive error accumulation. On the other hand, implicit methods are advantageous when choosing the time step and offer much better stability properties. However, when using implicit methods for solving non-linear systems

of PDEs, they can be numerically very costly to implement. The reason for this is the discretization of the non-linear PDE, which then leads to a large system of non-linear equations that need to be solved at every time step. The solution of such systems is usually done with the use of implicit - explicit (IMEX) schemes which date back to 1970 [27], [28], [29]. Additional information on the derivation of IMEX and Runge - Kutta IMEX schemes and their stability can be found in [30], [31], [32], [33], [34]. Other applicable schemes include the exponential time differencing (ETD) [35], [36], exponential propagation iterative (EPI) [37], [38], [39],[40] and the IF schemes. More articles about these methods can be found in [14], [20], [41], [42] [43], [44], [45].

2.1.1 Explicit and Implicit Euler Methods and Their Stability

Physical processes in engineering processes are usually described with differential equations (ODEs or PDEs). In many cases, such as the case presented in this thesis, few assumptions are made to reduce the complexity of the system and the solution. Usually, these systems have multiple dependent and independent variables, which are coupled in a system of ordinary differential equations. Hoffman in [46] defines ordinary differential equations as equations that state the relationship between a function of a single independent variable and the total number of derivatives of this function concerning the independent variable. Ordinary differential equations can be classified into a few main groups. The first main group is according to the auxiliary conditions: Initial value differential equations (IVE), where the conditions are specified at a single initial time; and boundary value (BDE), differential equations where the conditions are specified at the initial and the end time. Additionally, the ODEs can be linear and non-linear, of first or higher-order and homogeneous and non-homogeneous. Homogeneous differential equations include terms that involve only the dependent variable or their derivatives. On the other hand, non-homogeneous differential equations involve additional terms (functions, source terms) which do not include the dependent variable [47].
The numerical methods for solving differential equations can be divided into two main groups,

1. Numerical methods for stiff systems (implicit),

2. Numerical methods for non-stiff systems (explicit).

These methods can be additionally divided in single and multi-step methods. Single-step methods use data at a single point n to move forward the solution at

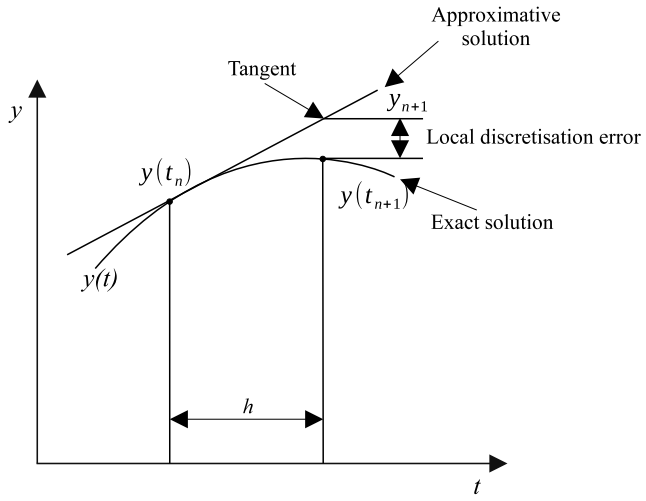

Figure 2.1: Numerical solution using the Euler method, with step size h. The exact solution is approximated using a tangent line in a small neighborhood around the point t_n. This tangent is then used to calculate the value at the next point $t_{n+1} = t_n + h$

$n+1$. On the other hand, multi-step methods use grid points to advance the solution to the next grid points. They use data in multiple known points $(n, n-1, n-2,$ and so on) that help this method to have better accuracy when compared with the single step method. The most popular finite difference methods for solving initial value problems are the Euler explicit and implicit methods. Let's first consider the initial value problem for first order ODE

$$Y' = f(t,Y), \quad Y(t_0) = Y_0, \tag{2.1}$$

where f is a given smooth function. To be able to approximate the solution using the forward (explicit) difference method at point n one gets

$$Y'|_n \approx \frac{Y_{n+1} - Y_n}{h}. \tag{2.2}$$

If one substitutes the forward differentiation method into the ordinary differential equation for y_{n+1} one yields the explicit finite difference Euler equation

$$\begin{aligned} y' \approx \frac{y_{n+1} - y_n}{h} &= f(t_n, y_n) = f_n, \\ y_{n+1} &= y_n + h f_n. \end{aligned} \tag{2.3}$$

If we analyze Eq. 2.3 for a very simple example $y' = -y$ and for the initial condition of $y(0) = 1$ one gets

$$y_{n+1} = y_n - h y_n = y_n(1-h). \tag{2.4}$$

From Eq. 2.4 it is obvious that if the value of the step $h > 2$ then the $|y_{n+1}| > |1-h|y_n$. However, knowing that the exact solution of Eq. 2.4 is e^{-t} the previous statement should not be true. This means that the explicit Euler method shows unstable behavior for certain step sizes. The implicit Euler method can be achieved in a similar manner as the explicit. The backward (implicit) Euler method for Eq. 2.1 can be developed as

$$Y'|_{n+1} \approx \frac{Y_n - Y_{n+1}}{h}. \tag{2.5}$$

If one follows the same steps as for the explicit method one gets

$$y_{n+1} = y_n - hf_{n+1}. \tag{2.6}$$

Following the same steps as for the explicit method for this particular example, the implicit method can be derived as

$$y_{n+1} = \frac{y_n}{1+h}. \tag{2.7}$$

It is obvious from Eq. 2.7 that no matter how high the value of the step is, y_{n+1} is always going to be smaller than y_n. This solves the stability issue that the explicit method has and offers unconditional stability. This is the main advantage of the implicit method and the reason why it works so much better when solving stiff differential equations. Let us consider the following example $y_{n+1} = y_n(1-h)$ where $y(0) = 1$. It is clear from Fig. 2.2 that for a step size of $h = 2$ the explicit

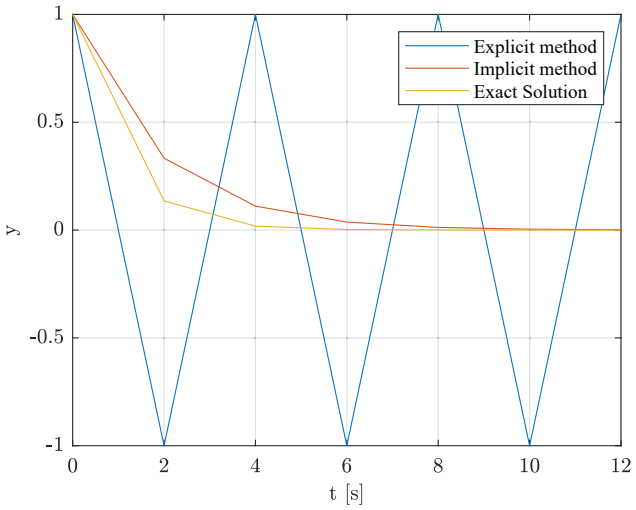

Figure 2.2: Solving Eq. 2.4 by implicit and explicit method with $h = 2$.

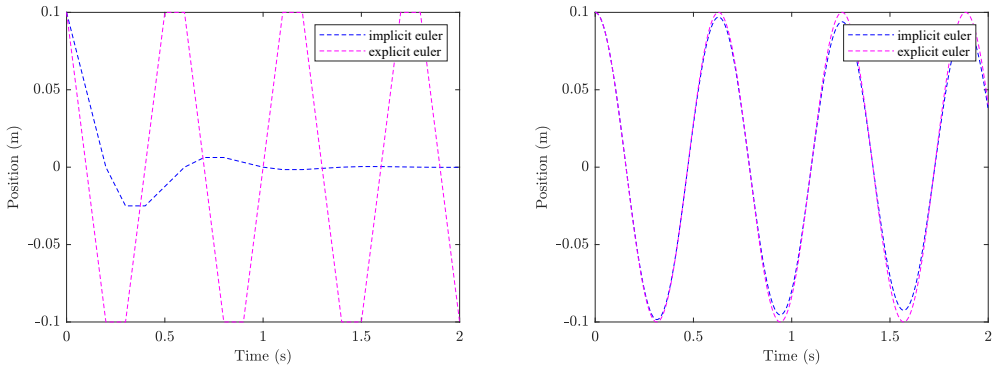

(a) Step size of 0.1 *s*

(b) Step size of 0.001 *ms*

Figure 2.3: Simulation of implicit and explicit Euler methods for different step sizes for the Newton's second law mass spring equation. It is evident that for bigger step-sizes the explicit method shows instability when compared to the implicit method. This damping effect on the implicit method is shown in Eq. 2.7.

method oscillates. The implicit method shows great stability and approximates the exact solution with high accuracy. To illustrate the numerical difficulty solvers face when solving stiff differential equations of real systems, let us consider the second Newton's Law equation which describes a mass spring system,

$$m_a\ddot{y}_1 + b\dot{y}_1 + ky_1 = 0. \tag{2.8}$$

The value of the spring constant is $k = 10\ \frac{kN}{n}$, the mass is $m = 0.1\ kg$ and the damping coefficient b is zero. This system of second order ODE is derived in a manner where two first order ODE's needs to be solved. Two scenarios were simulated, one with step size of 0.1 *s* and one with 1 *ms*. The system presented in Eq. 2.8 was simulated for 1 second with different step size. Yet again, one sees that the implicit method works much better at bigger step size. The reason for this are the stability issues that the explicit method has when solving stiff differential equations.

Both the explicit and implicit methods are first-order methods, and the results are comparable. Additionally, we used these methods as a basis for the implementation of higher-order numerical methods. More information about these methods and their implementation in a simulation environment can be found in [48].

Now, because only the non-linear system presented in section 3.5.1 is solved using these methods, we will not further detail how they work. The focus will be on solving these types of systems using a novel matrix-based approach, the details of which will be explained in the following sections.

2.2 System of Differential Equations (State Space Representation)

Most prototypes of machines and other devices are first tested in a simulation environment before the first prototype is built. For this reason, a very good system representation or an excellent mathematical model of the system is vital. The classical control theory started in the mid-1900s where the systems were mainly developed and analyzed in the frequency domain using the transfer function [49]. One of the disadvantages of this representation was that the system was limited to one input and one output. A few decades later, with the involvement of several known mathematicians and engineers, a pragmatic shift was achieved from the frequency to the time domain. This was possible with the state equation. According to [50] the state can be defined as a set of physical quantities, the specification of which completely determines the evolution of the system. As the systems got more complex, the mathematical representation of the systems included multiple state equations, from which the state space representation was born. More articles on the state space representation can be found in [51], [52], [53]. The state-space for LTI (linear time invariant) system has the general form

$$\begin{aligned} \dot{\boldsymbol{x}} &= \mathsf{A}\boldsymbol{x} + \mathsf{B}\boldsymbol{u}, \\ \boldsymbol{y} &= \mathsf{C}\boldsymbol{x} + \mathsf{D}\boldsymbol{u}, \end{aligned} \tag{2.9}$$

where $\boldsymbol{x}(t)$ is the state vector, $\boldsymbol{u}(t)$ is the input vector and $\boldsymbol{y}(t)$ is the output vector [54]. These are all vectors, not necessarily of the same length, whose scalar components are the state variables. To be able to work with these types of systems outside simulation environments and implement some of the calculus of variations methods, one needs to form the differentiation operators first. Additionally, if the mass matrix is included in the system presented in Eq. 2.9 the system will have the general form

$$\Pi\dot{\boldsymbol{x}} = \mathsf{A}\boldsymbol{x} + \mathsf{B}\boldsymbol{u}. \tag{2.10}$$

The mass matrix Π helps us move the very high or very low values from the right side of the equation to the left side. This reduces the stiffness of the right side of Eq. 2.10, making it easier for the numerical solver and numerical methods to solve this system.

2.3 Interpolation

To discretize a system of differential equations, one must first account for the linear operators. The numerical approximation for these operators can be made using

interpolation. Interpolation is a method (fundamentally considered as an inverse problem) for creating new data points within the range of a discrete set of known data points [55]. The most simple form of interpolation is linear interpolation. To introduce linear interpolation, let us consider a straightforward example. The

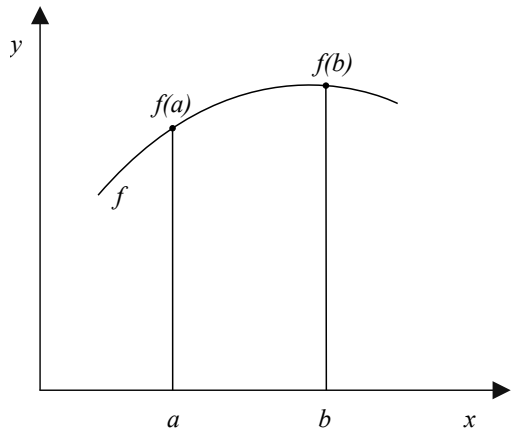

Figure 2.4: Linear interpolation of two points.

points $(a, f(a))$ and $(b, f(b))$ are two points from an unknown function f. The goal is to find a function

$$z(x) = s_0 + s_1 x, \tag{2.11}$$

for which

$$z(a) = f(a), \quad z(b) = f(b). \tag{2.12}$$

This leads to a system of equations, which can be written as follows in matrix form

$$\begin{bmatrix} 1 & a \\ 1 & b \end{bmatrix} \begin{bmatrix} s_0 \\ s_1 \end{bmatrix} = \begin{bmatrix} f(a) \\ f(b) \end{bmatrix}. \tag{2.13}$$

If the coefficients were to be calculated, one would have to first compute the inverse

$$\begin{bmatrix} s_0 \\ s_1 \end{bmatrix} = \begin{bmatrix} 1 & a \\ 1 & b \end{bmatrix}^{-1} \begin{bmatrix} f(a) \\ f(b) \end{bmatrix}, \quad \begin{bmatrix} s_0 \\ s_1 \end{bmatrix} = \frac{1}{b-a} \begin{bmatrix} b & -a \\ -1 & 1 \end{bmatrix} \begin{bmatrix} f(a) \\ f(b) \end{bmatrix} \tag{2.14}$$

from which one gets

$$\begin{aligned} s_0 &= \frac{b}{b-a} f(a) - \frac{a}{b-a} f(b) \\ s_1 &= -\frac{1}{b-a} f(a) + \frac{1}{b-a} f(b) \end{aligned} \tag{2.15}$$

which leads to

$$z(x) = \frac{b-x}{b-a} f(a) + \frac{x-a}{b-a} f(b), \tag{2.16}$$

or if $a = x_1$ and $b = x_2$, one gets the general form for the linear interpolation

$$z(x) = \frac{x-x_2}{x_1-x_2} f(x_1) + \frac{x-x_1}{x_2-x_1} f(x_2). \tag{2.17}$$

It can be seen from Eq. 2.16 that the functions evaluated at given points are multiplied by functions of x. These functions are known as the linear Lagrange interpolation polynomials,

$$l_1(x) = \frac{x-x_2}{x_1-x_2}, \quad l_2(x) = \frac{x-x_1}{x_2-x_1}. \tag{2.18}$$

which have the following properties

$$\begin{aligned} l_1(x_1) &= 1 \qquad l_2(x_1) = 0 \\ l_1(x_2) &= 0 \qquad l_2(x_2) = 1. \end{aligned} \tag{2.19}$$

2.3.1 Quadratic Interpolation

If the idea presented in 2.3 is now extended to 3 points, we can use quadratic polynomials to approximate the solution. Similar to before, the interpolation polynomials will have the form

$$z(x) = l_1(x) f(x_1) + l_2(x) f(x_2) + l_3(x) f(x_3), \tag{2.20}$$

where,

$$\begin{aligned} l_1(x_1) &= 1, \qquad l_2(x_1) = 0, \qquad l_3(x_1) = 0 \\ l_1(x_2) &= 0, \qquad l_2(x_2) = 1, \qquad l_3(x_2) = 0 \\ l_1(x_3) &= 0, \qquad l_2(x_3) = 0, \qquad l_3(x_3) = 1. \end{aligned} \tag{2.21}$$

Using the same analogy as before, the Lagrangian interpolation polynomials [56] are

$$\begin{aligned} l_1(x) &= \frac{(x-x_2)(x-x_3)}{(x_1-x_2)(x_1-x_3)}, \\ l_2(x) &= \frac{(x-x_1)(x-x_3)}{(x_2-x_1)(x_2-x_3)}, \\ l_3(x) &= \frac{(x-x_1)(x-x_2)}{(x_3-x_1)(x_3-x_2)}. \end{aligned} \tag{2.22}$$

Using the structure as before, one can very easily generalize the interpolation polynomials for the case of n points

$$l_k(x) = \frac{(x-x_1)(x-x_2)\dots(x-x_{k-1})(x-x_{k+1})\dots(x-x_n)}{(x_k-x_1)(x_k-x_2)\dots(x_k-x_{k-1})(x_k-x_{k+1})\dots(x_k-x_n)} \tag{2.23}$$

The advantages of interpolating polynomials are their uniqueness and calculation of the interpolating error that can be done without difficulty. Other techniques for calculating the interpolation polynomials include the method of divided differences or the linear combination of monomials to establish the Vandermonde matrix [57].

2.4 Numerical Differentiation

Numerical differentiation is one of the most crucial tasks when it comes to numerically solving differential equations. It is particularly useful because it can be performed simply by matrix multiplication. This allows a system of ODE's to be discretized and then solved numerically by solving a system of ordinary linear equations.

2.4.1 Collocation Derivatives

In Fig.,2.5 we have n points $x_1, x_2, ...x_n$ for which a function f is evaluated. The points are such that $x_1 < x_2 < ... < x_n$. The collocation derivatives are the ones that are evaluated at the same points where the function is being evaluated. In

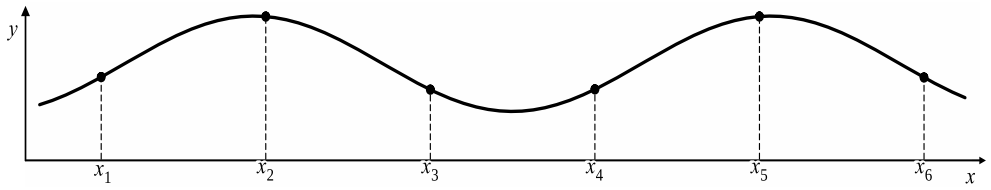

Figure 2.5: Collocation points for numerical differentiation.

the same analogy as before, a Lagrange interpolating function polynomial can be constructed

$$z(x) \approx l_1(x)f(x_1) + l_2(x)f(x_2) + \ldots + l_n(x)f(x_n). \tag{2.24}$$

This can be differentiated k times

$$z^{(k)}(x) \approx l_1^{(k)}(x)f(x_1) + l_2^{(k)}(x)f(x_2) + \ldots + l_n^{(k)}(x)f(x_n). \tag{2.25}$$

Evaluated at the interpolation points (the 'collocation part)

$$z^{(k)}(x_i) \approx l_1^{(k)}(x_i) f(x_1) + l_2^{(k)}(x_i) f(x_2) + \ldots + l_n^{(k)}(x_i) f(x_n), \tag{2.26}$$

or written in matrix form,

$$\begin{bmatrix} z^{(k)}(x_1) \\ z^{(k)}(x_2) \\ \vdots \\ z^{(k)}(x_n) \end{bmatrix} \approx \begin{bmatrix} l_1^{(k)}(x_1) & l_2^{(k)}(x_1) & \ldots & l_n^{(k)}(x_1) \\ l_1^{(k)}(x_2) & l_2^{(k)}(x_2) & \ldots & l_n^{(k)}(x_2) \\ \vdots & \vdots & \ddots & \vdots \\ l_1^{(k)}(x_n) & l_2^{(k)}(x_n) & \ldots & l_n^{(k)}(x_n) \end{bmatrix} \begin{bmatrix} f(x_1) \\ f(x_2) \\ \vdots \\ f(x_n) \end{bmatrix}. \tag{2.27}$$

To construct the matrix form, let us consider a simple example for $n = 3$ points. To simplify, the points should be evenly spaced, $x_1 = a$, $x_2 = a+h$, $x_3 = a+2h$. The Lagrangian interpolation polynomials for these points can be written as

$$\begin{aligned} l_1(x) &= \frac{(x-x_2)(x-x_3)}{(x_1-x_2)(x_1-x_3)} = \frac{(x-(a+h))(x-(a+2h))}{2h^2}, \\ l_2(x) &= \frac{(x-x_1)(x-x_3)}{(x_2-x_1)(x_2-x_3)} = -\frac{(x-a)(x-(a+2h))}{h^2}, \\ l_3(x) &= \frac{(x-x_1)(x-x_2)}{(x_3-x_1)(x_3-x_2)} = \frac{(x-a)(x-(a+h))}{2h^2}. \end{aligned} \tag{2.28}$$

The derivatives for the Lagrangian interpolating polynomials given in Eq. 2.28 evaluated at the given nodes are as follows

$$\begin{aligned} l_1'(a) &= -\frac{3}{2h}, & l_2'(a) &= \frac{2}{h}, & l_3'(a) &= -\frac{1}{2h}, \\ l_1'(a+h) &= -\frac{1}{2h}, & l_2'(a+h) &= 0, & l_3'(a+h) &= \frac{1}{2h}, \\ l_1'(a+2h) &= \frac{1}{2h}, & l_2'(a+2h) &= -\frac{2}{h}, & l_3'(a+2h) &= \frac{3}{2h}. \end{aligned} \tag{2.29}$$

After calculating the derivative, one can very easily construct the matrix form equation

$$\begin{bmatrix} z'(a) \\ z'(a+h) \\ z'(a+2h) \end{bmatrix} \approx \begin{bmatrix} -\frac{3}{2h} & \frac{2}{h} & -\frac{1}{h} \\ -\frac{1}{2h} & 0 & \frac{1}{2h} \\ \frac{1}{2h} & -\frac{2}{h} & \frac{3}{2h} \end{bmatrix} \begin{bmatrix} f(a) \\ f(a+h) \\ f(a+2h) \end{bmatrix} \tag{2.30}$$

or simplified

$$\begin{bmatrix} z'(a) \\ z'(a+h) \\ z'(a+2h) \end{bmatrix} \approx \underbrace{\frac{1}{2h} \begin{bmatrix} -3 & 4 & -1 \\ -1 & 0 & 1 \\ 1 & -4 & 3 \end{bmatrix}}_{\mathsf{D}_1} \begin{bmatrix} f(a) \\ f(a+h) \\ f(a+2h) \end{bmatrix}. \tag{2.31}$$

From Eq. 2.31, it can be seen that the numerical differentiation can be performed by simple multiplication with a matrix that is already calculated [58]. If the idea is for the matrix to be extended for a large set of data, interpolating with a polynomial of the degree $n-1$ numerically it is not very accurate. What can be done is to use polynomials of a small degree locally and perform interpolation at every step. This means that one can use the two end formulas $z'(a)$ and $z'(a+2h)$ at each of the endpoints and the central formula $z(a+h)$ at all internal points. Taking this into account, the differentiation operator for n points can be

$$\begin{bmatrix} z'(x_1) \\ z'(x_2) \\ z'(x_3) \\ \vdots \\ z'(x_{n-1}) \\ z'(x_n) \end{bmatrix} \approx \frac{1}{2h} \begin{bmatrix} -3 & 4 & -1 & 0 & \dots & 0 \\ -1 & 0 & 1 & 0 & \dots & 0 \\ 0 & -1 & 0 & 1 & \dots & 0 \\ \vdots & \vdots & \vdots & \vdots & \ddots & \vdots \\ 0 & \dots & 0 & -1 & 0 & 1 \\ 0 & \dots & 0 & 1 & -4 & 3 \end{bmatrix} \begin{bmatrix} f(x_1) \\ f(x_2) \\ f(x_3) \\ \vdots \\ f(x_{n-1}) \\ f(x_n) \end{bmatrix} \tag{2.32}$$

2.4.2 Interstitial Derivatives

The interstitial derivatives are the ones that are being evaluated at the points between each given node. In a similar manner, the interpolating function defined in Eq. 2.48 can be used here. It is able to consequently differentiate this function and then be evaluated at each interstitial $N-1$ node shown in Fig. 2.6. This means

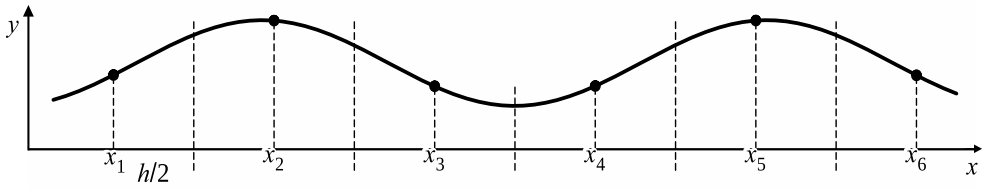

Figure 2.6: Interstitial points for numerical differentiation.

that the differentiation matrix is no longer square as the number of interstitial points will always be smaller by one than the nodes used for interpolations. The discretized differential operator (matrix) will have the dimension $(N-1)\times(N)$. Following the analogy presented in Eq. 2.28 the Lagrangian interpolating func-

tions for Fig. 2.6 using a 5th order polynomial can be written as

$$
\begin{aligned}
l_1(x) &= \frac{(x-x_2)(x-x_3)(x-x_4)(x-x_5)(x-x_6)}{(x_1-x_2)(x_1-x_3)(x_1-x_4)(x_1-x_5)(x_1-x_6)},\\
l_2(x) &= \frac{(x-x_1)(x-x_3)(x-x_4)(x-x_5)(x-x_6)}{(x_2-x_1)(x_2-x_3)(x_2-x_4)(x_2-x_5)(x_2-x_6)},\\
l_3(x) &= \frac{(x-x_1)(x-x_2)(x-x_4)(x-x_5)(x-x_6)}{(x_3-x_1)(x_3-x_2)(x_3-x_4)(x_3-x_5)(x_3-x_6)},\\
l_4(x) &= \frac{(x-x_1)(x-x_2)(x-x_3)(x-x_5)(x-x_6)}{(x_4-x_1)(x_4-x_2)(x_4-x_3)(x_4-x_5)(x_4-x_6)},\\
l_5(x) &= \frac{(x-x_1)(x-x_2)(x-x_3)(x-x_4)(x-x_6)}{(x_5-x_1)(x_5-x_2)(x_5-x_3)(x_5-x_4)(x_5-x_6)},\\
l_6(x) &= \frac{(x-x_1)(x-x_2)(x-x_3)(x-x_4)(x-x_5)}{(x_6-x_1)(x_6-x_2)(x_6-x_3)(x_6-x_4)(x_6-x_5)}.
\end{aligned}
\tag{2.33}
$$

It is obvious from Fig. 2.6 that the interpolating function has 5 interstitial points. The distance between the interpolating points is the same as in section 2.4.1 h. However, the distance between the interpolation and interstitial points is defined as $\frac{h}{2}$. Following this, the Lagrangian interpolating functions presented in Eq. 2.33 are firstly evaluated at $x_1 = a$, $x_2 = a+h$, $x_3 = a+2h$, $x_4 + a + 3h$, $x_5 = a+5h$ and $x_6 = a+6h$. Additionally, the Lagrangian functions are then evaluated at each interstitial point defined as $x = a + \frac{h}{2}$, $x = a + \frac{3h}{2}$, $x = a + \frac{5h}{2}$, $x = a + \frac{7h}{2}$ and, $x = a + \frac{9h}{2}$. Doing this, one can very easily compute the zero order derivative or the identity operator (interpolation matrix) for the interstitial points. In matrix form

$$
D_0 = \frac{1}{16}\begin{bmatrix}
5 & 15 & -5 & 1 & 0 & 0\\
-1 & 9 & 9 & -1 & 0 & 0\\
0 & -1 & 9 & 9 & -1 & 0\\
0 & 0 & -1 & 9 & 9 & -1\\
0 & 0 & 1 & -5 & 15 & 5
\end{bmatrix}
\tag{2.34}
$$

If one is to calculate the first derivative matrix for the interstitial points, the functions given in Eq. 2.33 must be first differentiated. Following the same steps as for the identity operator, the derivative at each of the interval midpoints can be written in matrix form as

$$
D_1 = \frac{1}{24h}\begin{bmatrix}
-23 & 21 & 3 & -1 & 0 & 0\\
1 & -27 & 27 & -1 & 0 & 0\\
0 & 1 & -27 & 27 & -1 & 0\\
0 & 0 & 1 & -27 & 27 & -1\\
0 & 0 & 1 & -3 & -21 & -23
\end{bmatrix}
\tag{2.35}
$$

This can be then extended for n number of points by using local polynomial interpolation

$$D_1 = \frac{1}{24h}\begin{bmatrix} -23 & 21 & 3 & -1 & 0 & 0 & \dots & 0 \\ 1 & -27 & 27 & -1 & 0 & 0 & \dots & 0 \\ 0 & 1 & -27 & 27 & -1 & 0 & \dots & 0 \\ \vdots & \ddots & \ddots & \ddots & \ddots & \vdots & \vdots & \vdots \\ 0 & \dots & 0 & 0 & 1 & -27 & 27 & -1 \\ 0 & \dots & 0 & 0 & 1 & -3 & -21 & -23 \end{bmatrix} \tag{2.36}$$

Interstitial derivatives are derived in this section because of their improved performance when solving a system of stiff differential equations. Given the observation in section 2.4.2, interstitial derivatives show superior performance when solving stiff differential equations compared to collocation derivatives.

2.5 Discretization of Linear Operators

To be able to use techniques of numerical linear algebra on a system of differential equations, it is crucial first to discretize that system. In the early 1960s, Ortega [59] was one of the first people to discretize a system of differential equations to apply the Newton method. With the introduction of interpolation in chapter 2.3 a general approach to the discretization of linear operators like differentiation or integration can be obtained. Let us consider a linear ODE for a given interval

$$a_1(x)y^{(\alpha_1)}(x) + a_2(x)y^{(\alpha_2)}(x) + ... + a_p(x)y^{(\alpha_p)}(x) = f(x), \tag{2.37}$$

for the interval

$$a = x_1 < x_2 < ... < x_{n-1} < x_n = b. \tag{2.38}$$

If Eq. 2.37 is evaluated at every point, one gets

$$\begin{aligned} &a_1(x_1)y^{(\alpha_1)}(x_1) + a_2(x_1)y^{(\alpha_2)}(x_1) + ... + a_p(x_1)y^{(\alpha_p)}(x_1) = f(x_1), \\ &a_1(x_2)y^{(\alpha_1)}(x_2) + a_2(x_2)y^{(\alpha_2)}(x_2) + ... + a_p(x_2)y^{(\alpha_p)}(x_2) = f(x_2), \\ &\qquad\qquad\qquad\qquad\qquad\qquad\qquad\qquad\qquad\qquad\qquad\qquad \vdots \\ &a_1(x_n)y^{(\alpha_1)}(x_n) + a_2(x_n)y^{(\alpha_2)}(x_n) + ... + a_p(x_n)y^{(\alpha_p)}(x_n) = f(x_n), \end{aligned} \tag{2.39}$$

or written in matrix form

$$\begin{bmatrix} a_1(x_1)y^{(\alpha_1)}(x_1) \\ a_1(x_2)y^{(\alpha_1)}(x_2) \\ \vdots \\ a_1(x_n)y^{(\alpha_1)}(x_n) \end{bmatrix} + \begin{bmatrix} a_2(x_1)y^{(\alpha_2)}(x_1) \\ a_2(x_2)y^{(\alpha_2)}(x_2) \\ \vdots \\ a_2(x_n)y^{(\alpha_2)}(x_n) \end{bmatrix} + \dots + \begin{bmatrix} a_P(x_1)y^{(\alpha_p)}(x_1) \\ a_p(x_2)y^{(\alpha_p)}(x_2) \\ \vdots \\ a_p(x_n)y^{(\alpha_p)}(x_n) \end{bmatrix} = \begin{bmatrix} f(x_1) \\ f(x_2) \\ \vdots \\ f(x_n) \end{bmatrix}, \tag{2.40}$$

or the discretization for one term

$$\begin{bmatrix} a_k(x_1)y^{(\alpha_k)}(x_1) \\ a_k(x_2)y^{(\alpha_k)}(x_2) \\ \vdots \\ a_k(x_n)y^{(\alpha_k)}(x_n) \end{bmatrix} = \begin{bmatrix} a_k(x_1) & 0 & \dots & 0 \\ 0 & a_k(x_2) & \dots & 0 \\ \vdots & \vdots & \ddots & \vdots \\ 0 & 0 & \dots & a_k(x_n) \end{bmatrix} \begin{bmatrix} y^{(\alpha_k)}(x_1) \\ y^{(\alpha_k)}(x_2) \\ \vdots \\ y^{(\alpha_k)}(x_n) \end{bmatrix}, \tag{2.41}$$

or each term discretized as,

$$a_k(x)y^{(a_k)}(x) \rightarrow \mathsf{A_k}\boldsymbol{y}^{(a_k)} \tag{2.42}$$

With the introduction of a consistent approximation term for differentiation, one can rearrange Eq. 2.41 in

$$\mathsf{A}_1\mathsf{D}^{(\alpha_1)}\boldsymbol{y} + \mathsf{A}_2\mathsf{D}^{(\alpha_2)}\boldsymbol{y} + \ldots + \mathsf{A_p}\mathsf{D}^{(\alpha_p)}\boldsymbol{y} = \boldsymbol{f}, \tag{2.43}$$

where D is an approximation to the derivative matrix. With this approach, the system of ODE can be discretized in one step with a simple linear operator

$$\mathsf{K}\boldsymbol{y} = \boldsymbol{f}, \tag{2.44}$$

where,

$$\mathsf{K} = \mathsf{A}_1\mathsf{D}^{(\alpha_1)} + \mathsf{A}_2\mathsf{D}^{(\alpha_2)} + \ldots + \mathsf{A_p}\mathsf{D}^{(\alpha_p)}. \tag{2.45}$$

In the case of differential equations, the matrix K is theoretically not invertible since the matrices $\mathsf{D}^{(\alpha_p)}$ are not invertible. This concurs with the fact that a linear differential equation has an infinite number of solutions, based on the number of independent homogeneous solutions which is the equal to the order of the differential equation. However, for a lower number of points, it can be numerically invertible due to discretization error.

2.5.1 Discretization of Initial and Boundary Values

The solution of ODE is not unique if one has not defined its initial or boundary conditions. Following the analogy from the previous section 2.5, the boundary conditions need to be discretized in a similar manner. Differential constraints such as initial or boundary conditions at a given point σ can be written in a general form as

$$\psi_1 y(\sigma) + \psi_2 y'(\sigma) + \ldots + \psi_k y^{(k)}(\sigma) = d, \tag{2.46}$$

The application of the constraints for a given point σ is done in such a manner that the nearest solution nodes N need not be unique, but, if possible, should be the

exact nodes used for the derivative or integral approximation. The nearest nodes interval can be defined as

$$x_{i_1} < x_{i_2} < ... < x_{i_{N-1}} < x_{i_N}. \tag{2.47}$$

The interpolating function for $y(x)$ for the points defined in Eq 2.47 is defined as $z(x)$ which gives

$$z(x) \approx \gamma_{i_1}(x)y(x_{i_1}) + \gamma_{i_2}(x)y(x_{i_2}) + ... + \gamma_{i_N}(x)y(x_{i_N}). \tag{2.48}$$

where γ_{i_1} are the basis functions for the interpolation (for example the Lagrange interpolation polynomials). So one can approximate equation Eq. 2.46 as

$$\psi_1 z(\sigma) + \psi_2 z'(\sigma) + ... + \psi_k z^{(k)}(\sigma) = d, \tag{2.49}$$

Substituting Eq. 2.48 in Eq. 2.49 one gets

$$\begin{aligned} &\psi_1(\gamma_{i_1}(\sigma)y(x_{i_1}) + \gamma_{i_2}(\sigma)y(x_{i_2}) + ... + \gamma_{i_N}(\sigma)y(x_{i_N})) + \\ &\psi_2(\gamma'_{i_1}(\sigma)y(x_{i_1}) + \gamma'_{i_2}(\sigma)y(x_{i_2}) + ... + \gamma'_{i_N}(\sigma)y(x_{i_N})) + \\ &... + \psi_k(\gamma^{(k)}_{i_1}(\sigma)y(x_{i_1}) + \gamma^{(k)}_{i_2}(\sigma)y(x_{i_2}) + ... + \gamma^{(k)}_{i_N}(\sigma)y(x_{i_N})) = d, \end{aligned} \tag{2.50}$$

which can also be written as

$$\begin{aligned} &(\psi_1\gamma_{i_1}(\sigma) + \psi_2\gamma'_{i_1}(\sigma) + ... + \psi_k\gamma^{(k)}_{i_1}(\sigma))y(x_{i_1}) + \\ &(\psi_1\gamma_{i_2}(\sigma) + \psi_2\gamma'_{i_2}(\sigma) + ... + \psi_K\gamma^{(k)}_{i_2}(\sigma))y(x_{i_2}) + \\ &... + (\psi_1\gamma_{i_n}(\sigma) + \psi_2\gamma'_{i_n}(\sigma) + ... + \psi_k\gamma^{(k)}_{i_N}(\sigma))y(x_{i_N}) = d, \end{aligned} \tag{2.51}$$

or written in a matrix form

$$W_1 y(x_{i_1}) + W_2 y(x_{i_2}) + \ldots + W_n y(x_{i_N}) = d, \tag{2.52}$$

or simplified

$$\begin{bmatrix} 0 & \ldots & 0 & W_1 & \ldots & W_N & 0 & \ldots & 0 \end{bmatrix} \begin{bmatrix} y(x_1) \\ y(x_2) \\ \vdots \\ y(x_n) \end{bmatrix} = d. \tag{2.53}$$

Given multiple constrains of the form like in Eq. 2.53 one could combine them in a single matrix equations

$$\mathsf{G}^{\mathsf{T}}\boldsymbol{y} = \boldsymbol{d}, \tag{2.54}$$

where each row in G^{T} corresponds to one constraint.

2.6 Least Squares Estimation

The least-squares technique in regression analysis is used to approximate the solution of a system where the number of equations and unknowns is not the same (over-determined system). Harker defined it in [57] as a method for estimating the model parameters from a discretized system given a set of measured data. The first use of such methods was in the fields of astronomy and geodesy, which helped the exploration missions in the early 18th century with the navigation through the seas. Lagrange published the least-squares method for the first time in [60]. He used this method to determine the orbit of the comets, the ellipticity of the Earth, and the meter's length. Although Gauss used the method first he published it later to compute the orbits of the celestial bodies [61]. Additionally, he improved the methods by connecting the least squares to the probability and the normal distribution [62], [63]. The most common distribution which prompts the least-squares method is the normal distribution (Gaussian distribution). If x is the parameter that is being measured, the Gaussian distribution can be defined as

$$P(x) = \frac{1}{\sqrt{2\pi}\sigma} \exp\left(-\frac{(x-\mu)^2}{2\sigma^2}\right), \tag{2.55}$$

where σ is the standard deviation, σ^2 is the variance, and μ is the mean value [64], [65], [66]. The variance determines the width (spread) of the bell curve. The

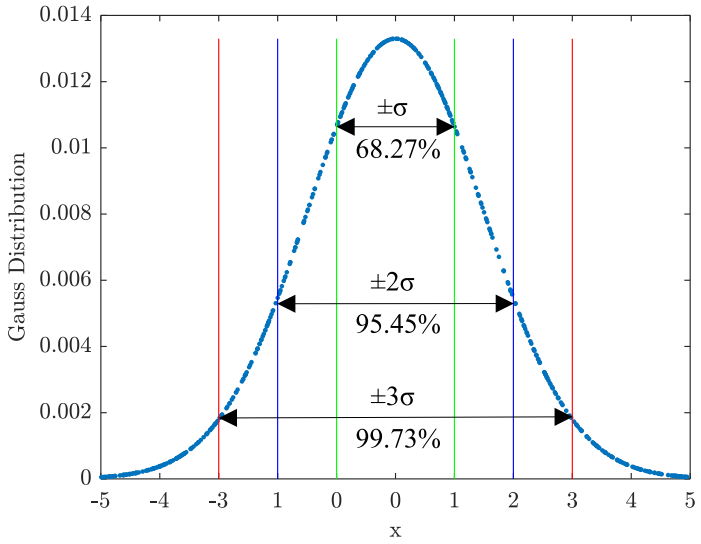

Figure 2.7: Gaussian distribution for a given set of data. For normal distribution 68.27 % of the values fall within one standard deviation (95.45 % within two and 99.73 % within three standard deviations).

larger the variance is, the larger the spread of the data points will be. When the mean value μ is zero, the graph shown in Fig. 2.7 is centered around the 0 point. The Gaussian distribution given in Eq. 2.55 has the property that 68.27% of the measured data lie within $\mu \pm \sigma$. The Maximum Likelihood principle can lead to the method of least squares only if the measured data behaves according to the Gaussian distribution. The least-square method can be substituted in two main groups: linear and non-linear least squares [67], [68]. The solution of the linear least squares is shown in section 2.6.2. On the other hand, the non-linear least squares are usually solved with iterative algorithms where, at each iteration, the system is approximated by a linear one which brings us back to solving a linear least square system.

2.6.1 Maximum Likelihood Principle of Least Squares

The maximum likelihood method (estimation) MLE is one of the most widely used methods for obtaining the values for the parameters that define a model [69]. This is done, so that the values maximize the likelihood that the method portrayed by the model delivered the observed data. Fisher [70] was one of the first authors in the early 20th century who widely popularized the use of this method.
Let us consider a random sample of n measurements of a sample x. The first step will be finding the model which best describes the given data. In our case, let us consider the residuals in the measurements behaving according to the Gaussian distribution. To be able to find the true value of x for a given measurement x_k one has to substitute the measured values into the probability distribution 2.55 which results in the likelihood function

$$L_k(\mu,\sigma) = \frac{1}{\sqrt{2\pi\sigma}} \exp\left(-\frac{(x_k-\mu)^2}{2\sigma^2}\right), \tag{2.56}$$

It can be seen from Eq. 2.56 that the likelihood function is dependent on two parameters: μ the mean and σ the standard deviation. Different values of these parameters yield different Gaussian curves. This method (MLE) idea is to find the optimal values for these two parameters that result in a curve that best fits the measurements. If Eq. 2.56 is extended for all the measurements (estimators) for the same true value x, the collective likelihood can be written as a product of the likelihood functions

$$L(\mu,\sigma) = \prod_{k=1}^{n} L_k. \tag{2.57}$$

If Eq. 2.56 for the Gaussian distribution is now substituted in Eq. 2.57 one gets

$$L(\mu,\sigma) = \frac{1}{\sqrt{(2\pi)^n}\sigma^n} \exp\left(-\frac{1}{2\sigma^2}\sum_{k=1}^{n}(x_k-\mu)^2\right), \tag{2.58}$$

Since the exponential function is an increasing function, the location of the maximum of the likelihood function corresponds to the minimum of the exponent (we are looking for exponent that is small in magnitude). Hence, the maximum can be found by minimizing the term

$$\varepsilon(\mu) = \sum_{k=1}^{n} (x_k - \mu)^2. \tag{2.59}$$

Differentiating Eq. 2.59 with respect to μ and equating to zero, one gets

$$\mu = \frac{1}{n} \sum_{k=1}^{n} x_k. \tag{2.60}$$

which is the well known formula for the mean value. In a comparable way, Eq. 2.59 is differentiated w.r.t. σ, which yields the expression for the variance

$$\sigma^2 = \frac{1}{n} \sum_{k=1}^{n} (x_k - \mu)^2. \tag{2.61}$$

Equation 2.60 and Eq. 2.61 express the maximum likelihood estimators for the mean and the variance.

2.6.2 Linear Least Squares

Linear least squares (also known as 'linear regression') is the most widely used method for fitting a model through data [71]. The simplest model is fitting a straight line through data,

$$y_m = ax + b. \tag{2.62}$$

Assuming that all errors are in y_m and the values in x are known exactly, the residuals in the vertical distance can be calculated as

$$d = y_m - (ax + b). \tag{2.63}$$

Taking into account that the error follows a Gaussian distribution with zero mean, the likelihood function for all point estimates can be calculated as a product of all likelihood functions

$$L(a,b) = \frac{1}{\sqrt{(2\pi)^n}\sigma^n} \exp\left(-\frac{1}{2\sigma^2} \sum_{k=1}^{n} (y_{m_k} - (ax_k + b))^2 \right). \tag{2.64}$$

Similar as in section 2.6.1 the likelihood function has an extrema

$$\varepsilon(\mu) = \sum_{k=1}^{n} (y_{m_k} - (ax_k + b))^2. \tag{2.65}$$

when the sum of the squared residuals has a minimum. This can be done by differentiating the likelihood function w.r.t. both parameters a and b.
Now, to generalize this, one must first find an efficient way to approximate a set of data. Principally, a set of data can be approximated in a linear manner using linear basis functions. The basis of this functions $b_k(x)$ must be linear in the parameters

$$y_m(x) = \sum_{k=1}^{d} \alpha_k b_k(x). \tag{2.66}$$

This can then be rewritten in a matrix form for n points x_k for $k = 1,...,n$ and n equations and $d+1$ unknowns

$$\begin{bmatrix} y_m(x_1) \\ y_m(x_2) \\ \vdots \\ y_m(x_n) \end{bmatrix} \approx \begin{bmatrix} b_0(x_1) & b_1(x_1) & \dots & b_d(x_1) \\ b_0(x_2) & b_1(x_2) & \dots & b_d(x_2) \\ \vdots & \vdots & \vdots & \vdots \\ b_0(x_n) & b_1(x_n) & \dots & b_d(x_n) \end{bmatrix} \begin{bmatrix} \alpha_0 \\ \alpha_1 \\ \vdots \\ \alpha_d \end{bmatrix} \tag{2.67}$$

or in matrix - vector notation,

$$\boldsymbol{y_m} \approx \mathsf{B}\boldsymbol{\alpha}. \tag{2.68}$$

This is a similar problem to the one defined in equation Eq. 2.45. This is basically a linear system of equations that can be written in general form

$$\mathsf{H}\boldsymbol{\gamma} = \boldsymbol{b}. \tag{2.69}$$

The difference between the model parameters (linear model) a_k and the vector $\boldsymbol{b}$ is corrupted by Gaussian noise and assumed to have the true values can be defined with a residual vector

$$\boldsymbol{r} = \mathsf{H}\boldsymbol{\gamma} - \boldsymbol{b}. \tag{2.70}$$

The goal is to find the vector of $\boldsymbol{\gamma}$, which minimizes the norm of the residual. Taking this into account, the cost function for the linear least squares is

$$\varepsilon(\boldsymbol{\gamma}) = ||\mathsf{H}\boldsymbol{\gamma} - \boldsymbol{b}||_2^2. \tag{2.71}$$

Equation 2.71 is minimized w.r.t. $\boldsymbol{\gamma}$ by taking the first derivative and setting the equation to 0

$$\frac{\partial \varepsilon(\boldsymbol{\gamma})}{\partial \boldsymbol{\gamma}} = \mathbf{0}. \tag{2.72}$$

Before taking the cost function derivative, one must first expand Eq. 2.71. The cost function can be expressed as

$$\varepsilon(\boldsymbol{\gamma}) = (\boldsymbol{b}^T - \boldsymbol{\gamma}^T \mathsf{H}^T)(\boldsymbol{b} - \mathsf{H}\boldsymbol{\gamma}), \tag{2.73}$$

which when expanded yields

$$\varepsilon(\boldsymbol{\gamma}) = \boldsymbol{b}^T\boldsymbol{b} - \boldsymbol{b}^{\mathrm{T}}\mathsf{H}\boldsymbol{\gamma} - \boldsymbol{\gamma}^T\mathsf{H}^T\boldsymbol{b} + \boldsymbol{\gamma}^T\mathsf{H}^T\mathsf{H}\boldsymbol{\gamma}. \tag{2.74}$$

Because the product $\boldsymbol{b}^{\mathrm{T}}\mathsf{H}\boldsymbol{\gamma}$ is a scalar it can be transposed without changing anything. Thus, rearranging Eq. 2.74, one gets

$$\varepsilon(\boldsymbol{\gamma}) = \boldsymbol{b}^T\boldsymbol{b} - 2\boldsymbol{\gamma}^T\mathsf{H}^T\boldsymbol{b} + \boldsymbol{\gamma}^T\mathsf{H}^T\mathsf{H}\boldsymbol{\gamma}. \tag{2.75}$$

The derivative with regards to $\boldsymbol{\gamma}$ is expressed as

$$\frac{\partial\varepsilon(\boldsymbol{\gamma})}{\partial(\boldsymbol{\gamma})} = (\mathsf{H}^T\mathsf{H} + (\mathsf{H}^T\mathsf{H})^T)\boldsymbol{\gamma} - 2\mathsf{H}^T\boldsymbol{b} = \mathbf{0}, \tag{2.76}$$

which yields

$$\boldsymbol{\gamma} = (\mathsf{H}^T\mathsf{H})^{-1}\mathsf{H}^T\boldsymbol{b}. \tag{2.77}$$

The matrix $\mathsf{H}^T\mathsf{H}$ is invertable if H has linearly independent columns. In that case the matrix $(\mathsf{H}^T\mathsf{H})^{-1}\mathsf{H}^T$ is called the Moore - Penrose pseudo inverse [72]. The case when the matrix $\mathsf{H}^T\mathsf{H}$ will be dealt with in the next section.

2.7 Singular Value Decomposition and the Least Squares

If H is a symmetric $n \times n$ real matrix, there are orthogonal matrices U and V and a diagonal matrix S such that [73]

$$\mathsf{H} = \mathsf{U}\mathsf{S}\mathsf{V}^T. \tag{2.78}$$

This means that the product of $\mathsf{U}\mathsf{U}^T$ or $\mathsf{V}\mathsf{V}^T$ will be equal to the identity matrix. On the other side, the matrix S is a diagonal matrix

$$\mathsf{S} = diag(\sigma_1, \sigma_2, \ldots \sigma_n), \tag{2.79}$$

where the diagonal elements are the singular values ordered such that

$$\sigma_1 \geq \sigma_2 \geq \ldots \geq \sigma_n \geq 0. \tag{2.80}$$

If the least squares solution given in Eq. 2.71 is to be extended with the SVD, one gets

$$\varepsilon(\boldsymbol{\gamma}) = ||\mathsf{U}\mathsf{S}\mathsf{V}^T\boldsymbol{\gamma} - \boldsymbol{b}||_2^2. \tag{2.81}$$

Equation 2.81 can be extended to

$$\varepsilon(\boldsymbol{\gamma}) = ||\mathsf{U}^T(\mathsf{U}\mathsf{S}\mathsf{V}^T\boldsymbol{\gamma} - \boldsymbol{b}||_2^2 = ||\mathsf{S}\mathsf{V}^T\boldsymbol{\gamma} - \mathsf{U}^T\boldsymbol{b}||_2^2, \tag{2.82}$$

because multiplying a vector with the unitary matrix from the left does not change its norm. Using the orthogonal substitution $\boldsymbol{\gamma} = \mathsf{V}\boldsymbol{z}$ one gets

$$\varepsilon(\boldsymbol{z}) = ||\mathsf{S}\mathsf{V}^T\mathsf{V}\boldsymbol{z} - \mathsf{U}^T\boldsymbol{b}||_2^2 = ||\mathsf{S}\boldsymbol{z} - \mathsf{U}^T\boldsymbol{b}||_2^2, \tag{2.83}$$

The vector $\boldsymbol{z}$ can be partitioned such that

$$\boldsymbol{\gamma} = \mathsf{V}\boldsymbol{z} = \begin{bmatrix}\mathsf{V}_\mathsf{r} & \tilde{\mathsf{V}}\end{bmatrix}\begin{bmatrix}\boldsymbol{\alpha}\\ \boldsymbol{\beta}\end{bmatrix} = \mathsf{V}_\mathsf{r}\boldsymbol{\alpha} + \tilde{\mathsf{V}}\boldsymbol{\beta}, \tag{2.84}$$

where U_r and V_r are the matrices which are contained in the first r column (where r is the rank of the matrix) of U and V. The matrices $\tilde{\mathsf{U}}$ and $\tilde{\mathsf{V}}$ are respectively the remaining columns, and the matrix S_r is a diagonal matrix with the singular values at the diagonal. Following this, the cost function can be written as

$$\varepsilon(\boldsymbol{\alpha},\boldsymbol{\beta}) = \left\| \begin{bmatrix}\mathsf{S}_\mathsf{r} & 0\\ 0 & \Delta\end{bmatrix}\begin{bmatrix}\boldsymbol{\alpha}\\ \boldsymbol{\beta}\end{bmatrix} - \begin{bmatrix}\mathsf{U}_\mathsf{r}{}^T\\ \tilde{\mathsf{U}}\end{bmatrix}\boldsymbol{b}\right\|_2^2 \tag{2.85}$$

where Δ is a diagonal matrix. More information about this matrix and its properties can be found in [57]. If Eq. 2.85 is multiplied, it can be rewritten as a sum of two norms

$$\varepsilon(\boldsymbol{\alpha},\boldsymbol{\beta}) = ||\mathsf{S}_\mathsf{r}\boldsymbol{\alpha} - \mathsf{U}_\mathsf{r}{}^T\boldsymbol{b}||_2^2 + ||\Delta\boldsymbol{\beta} - \tilde{\mathsf{U}}_\mathsf{r}^T\boldsymbol{b}||_2^2. \tag{2.86}$$

The matrix Δ is a diagonal matrix containing the singular values which are zero or very small when calculated numerically. This give us the partitioning of the $\mathsf{U} = [\mathsf{U}_\mathsf{r}\tilde{\mathsf{U}}]$, $\mathsf{V} = [\mathsf{V}_\mathsf{r}\tilde{\mathsf{V}}]$. The subscript r is the rank of the matrix. The rank of the matirx H can be defined as the number of non zero singular values of the matrix. Consequently the cost function is no longer dependent on the vector coefficient $\boldsymbol{\beta}$. This leaves us with

$$\varepsilon(\alpha) = ||\mathsf{S}_\mathsf{r}\boldsymbol{\alpha} - \mathsf{U}_\mathsf{r}{}^T\boldsymbol{b}||_2^2 + ||\tilde{\mathsf{U}_\mathsf{r}}{}^T\boldsymbol{b}||_2^2. \tag{2.87}$$

The second term of Eq. 2.87 is a norm of $\mathsf{U}_\mathsf{r}{}^T\boldsymbol{b}$, which is basically a scalar product of the columns of the matrix of U with the vector $\boldsymbol{b}$. To get a normal solution, for which one needs to minimize the cost function, Eq. 2.87 must be differentiated w.r.t. the coefficient vector $\boldsymbol{\alpha}$. This yields the equation

$$\mathsf{S}_\mathsf{r}{}^T\mathsf{S}_\mathsf{r}\boldsymbol{\alpha} = \mathsf{S}_\mathsf{r}{}^T\mathsf{U}_\mathsf{r}{}^T\boldsymbol{b}, \tag{2.88}$$

which leads to the minimizing solution for $\boldsymbol{\alpha}$

$$\boldsymbol{\alpha} = \mathsf{S}_\mathsf{r}{}^{-1}\mathsf{U}_\mathsf{r}{}^T\boldsymbol{b}. \tag{2.89}$$

Substituting Eq. 2.97 into the Eq. 2.84 one gets the general solution for the least squares problem

$$\boldsymbol{\gamma} = \mathsf{V}_\mathsf{r}\mathsf{S}_\mathsf{r}{}^{-1}\mathsf{U}_\mathsf{r}{}^T\boldsymbol{b} + \tilde{\mathsf{V}}\boldsymbol{\beta}, \tag{2.90}$$

where the first part of the equation is the one that influences the cost function and the second part doesn't influence the cost function because it doesn't contain $\boldsymbol{b}$. Furthermore, one can define the Moore-Penrose pseudo inverse matrix as

$$\mathsf{H}^{+} = \mathsf{V}_{\mathsf{r}}\mathsf{S}_{\mathsf{r}}{}^{-1}\mathsf{U}_{\mathsf{r}}{}^{T}. \tag{2.91}$$

This is a unique matrix Y, which must satisfy four conditions

$$\begin{aligned} \mathsf{HYH} &= \mathsf{H}, \\ \mathsf{YLY} &= \mathsf{Y}, \\ (\mathsf{HY})^{T} &= \mathsf{HY}, \\ (\mathsf{YH})^{T} &= \mathsf{YH}. \end{aligned} \tag{2.92}$$

The solution of Eq. 2.92 is dependent on the properties of the matrix L. If the matrix $\mathsf{H}^{T}\mathsf{H}$ is invertible, the solution will be expressed through the formula $\mathsf{H}^{+} = (\mathsf{H}^{T}\mathsf{H})^{-1}\mathsf{H}^{T}$. In the case of L not being full rank, the solution will entirely depend on the null space and the vector $\boldsymbol{\beta}$ (there is infinite family of solutions, with $\boldsymbol{\beta}$ arbitrary parameters). To be able to determine a unique solution, one must then define supplementary conditions such as boundary conditions.

2.8 Least Squares for Solving ODE with Equality Constraints (LSE) via SVD

In the previous sections, a few steps for solving differential equations were introduced. These steps included: introducing numerical differentiation matrices (collocative and interstitial), discretization of linear operators and boundary conditions and introduction to the least square problem. Following this, one can very easily formulate the least square problem with equality constraints (LSE)

$$\min ||\mathsf{H}\boldsymbol{\gamma} - \boldsymbol{b}||_2^2 \quad \text{subject to} \quad \mathsf{G}^{T}\boldsymbol{\gamma} = \boldsymbol{d}. \tag{2.93}$$

where $\mathsf{G} \in \mathbb{R}^{n\times p}$ and $\boldsymbol{d} \in \mathbb{R}^{p}$, where p is the number of constraints. As mentioned in section 2.7 the solution of Eq. 2.90 depends on the properties of the matrix H. This leads to the generalized form of the solution given in Eq. 2.90 where the solution is written in terms of a particular solution and a set of homogeneous solutions to the differential equations. This can be rewritten in terms of the differential operators as

$$H = \begin{bmatrix} \mathsf{U}_{n-p} & \tilde{\mathsf{U}} \end{bmatrix} \begin{bmatrix} \mathsf{S}_{n-p} & 0 \\ 0 & \Delta \end{bmatrix} \begin{bmatrix} \mathsf{V}^{\mathsf{T}}{}_{n-p} \\ \tilde{\mathsf{V}}^{\mathsf{T}} \end{bmatrix} \tag{2.94}$$

Equation 2.94 shows that the matrices S and V are partitioned according to the number of nodes and the number of constraints. This means that if the problem

is well structured then the matrix S_{n-p} will be square, invertible and in the limit $n \to \infty$ Δ will be zero. Now, this will lead to the solution similar as in Eq. 2.84

$$\boldsymbol{\gamma} = \mathsf{V}_{n-p}\boldsymbol{\alpha} + \tilde{\mathsf{V}}\boldsymbol{\beta}, \tag{2.95}$$

from which the cost function can be expressed as

$$\varepsilon(\boldsymbol{\alpha}, \boldsymbol{\beta}) = ||\mathsf{S}_{n-p}\boldsymbol{\alpha} - \mathsf{U}_{n-p}^{T}\boldsymbol{b}||_2^2 + ||\Delta\boldsymbol{\beta} - \tilde{\mathsf{U}}^{T}\boldsymbol{b}||_2^2. \tag{2.96}$$

If Eq. 2.96 is solved in a similar manner and minimized, the solution for cost function for $\boldsymbol{\alpha}$ can be expressed as

$$\boldsymbol{\alpha} = \mathsf{S}_{\mathsf{n-p}}{}^{-1}\mathsf{U}_{\mathsf{n-p}}{}^{T}\boldsymbol{b}. \tag{2.97}$$

Following this, the solution of Eq. 2.95 can be put down as

$$\boldsymbol{\gamma} = \mathsf{V}_{n-p}\mathsf{S}_{n-p}^{-1}\mathsf{U}_{n-p}^{T}\boldsymbol{b} + \tilde{\mathsf{V}}\boldsymbol{\beta}, \tag{2.98}$$

which leads to

$$\boldsymbol{\gamma} = \mathsf{L}^{-}\boldsymbol{b} + \tilde{\mathsf{V}}\boldsymbol{\beta}, \tag{2.99}$$

where the matrix L^{-} is expressed as

$$\mathsf{L}^{-} = \mathsf{V}_{n-p}\mathsf{S}_{n-p}^{-1}\mathsf{U}_{n-p}^{T}. \tag{2.100}$$

which is the generalized inverse of the matrix L. The generalized inverse in this case approximates the linear differential operator by truncating the SVD. This matrix is different from the Moore-Pseudo inverse Eq. 2.91 in that it does not satisfy all four conditions given in Eq. 2.92 [57]. Moreover, it is obvious that the solution of the first term of Eq. 2.99 is dependent on the vector of function values $\boldsymbol{b}$. For this reason, the first term is usually illustrated as the particular solution to the system of differential equations, and the second term as the homogeneous solution of the equation. If the solution Eq. 2.99 is substituted in the general constraints equations, one gets

$$\mathsf{G}^{T}\boldsymbol{\gamma} = \mathsf{G}^{T}\mathsf{L}^{-}\boldsymbol{b} + \mathsf{G}^{T}\tilde{\mathsf{V}}\boldsymbol{\beta} = \boldsymbol{d}. \tag{2.101}$$

This leads to

$$G^{\mathrm{T}}\tilde{\mathsf{V}}\boldsymbol{\beta} = \boldsymbol{d} - \mathsf{G}^{T}\mathsf{L}^{-}\boldsymbol{b}. \tag{2.102}$$

Now, since the number of p constraints corresponds to the number of p parameters (ODE specific method), the coefficient matrix $\mathsf{G}^{T}\tilde{\mathsf{V}}$ is square and invertible. Following this, the solution for the parameters of the homogeneous solution can be expressed as

$$\boldsymbol{\beta} = (\mathsf{G}^{T}\tilde{\mathsf{V}})^{-1}(\boldsymbol{d} - \mathsf{G}^{T}\mathsf{L}^{-}\boldsymbol{b}). \tag{2.103}$$

Substituting the solution for the homogeneous parameters back into the general solution Eq. 2.99 one gets

$$\boldsymbol{\gamma} = \mathsf{L}^{-}\boldsymbol{b} + \tilde{\mathsf{V}}(\mathsf{G}^{T}\tilde{\mathsf{V}})^{-1}(\boldsymbol{d} - \mathsf{G}^{T}\mathsf{L}^{-}\boldsymbol{b}). \tag{2.104}$$

By rearranging Eq. 2.104

$$\begin{aligned}\boldsymbol{\gamma} &= \mathsf{L}^{-}\boldsymbol{b} + \tilde{\mathsf{V}}(\mathsf{G}^{T}\tilde{\mathsf{V}})^{-1}\boldsymbol{d} - \tilde{\mathsf{V}}(\mathsf{G}^{T}\tilde{\mathsf{V}})^{-1}\mathsf{G}^{T}\mathsf{L}^{-}\boldsymbol{b} \\ &= (\mathsf{I} - \tilde{\mathsf{V}}(\mathsf{G}^{T}\tilde{\mathsf{V}})^{-1}\mathsf{G}^{T})\mathsf{L}^{-}\boldsymbol{b} + \tilde{\mathsf{V}}(\mathsf{G}^{T}\tilde{\mathsf{V}})^{-1}\boldsymbol{d},\end{aligned} \tag{2.105}$$

where I is the identity matrix. Equation 2.105 shows that the solution may be explicitly determined in terms of the forcing function and the values of the specified constraints after the linear differential operator and differential constraints have been established. The first term in this entire solution is, once again, a particular solution of the ODE. However, this time, a particular solution fulfills homogeneous constraints provided by the matrix G. The second term denotes the solution that satisfies each of the differential constraints separately.

Chapter 3

Fluid Power Systems for Mobile Machinery

The main research done in this chapter is the development of a new control system for high inertia loads. Additionally, different models (linear and non-linear) have been developed and studied. These models have been used to study the concepts of energy efficiency, damping, adaptive, flow, and pressure control.

3.1 Introduction to Fluid Power Systems for Mobile Machinery

A fluid power system is an apparatus that is used to convert and transfer energy. One of its main advantages is the high weight-to-power ratio, enabling these types of systems to handle large amounts of power. Hydraulic oil is the main medium used in these systems. The characteristics of the oil allow it to transfer and absorb huge amounts of energy. When absorbing energy, the oil gets hot, which leads to a lower bulk modulus value and decreases the energy efficiency of the whole system. This is the main reason for using of remote coolers in mobile machinery. Traditionally, fluid power systems were designed to focus mainly on performance and functionality and less on efficiency. A fluid power system consists of multiple parts: hydraulic pump, actuator, valves, etc. All these parts are combined to form a system design that will give us the desired performance. Pumps are usually hydrostatic or displacement types that convert mechanical energy into a fluid one. In mobile machinery, usually, one pump is used to supply multiple load actuators. The most common configuration used today is the load sensing system (LS) [74]. The LS is a system configured from one variable displacement pump for every actuator. This type of system improves the overall system's efficiency and performance [74]. Lately, in the mining industry, there has been a trend of us-

ing valveless systems because this improves the energy efficiency of the systems significantly [75], [76], [77]. However, because of the high inertia loads, using a valveless system configuration for the type of machine described in section 3.1.2, would not be desirable. To be able to achieve the fast changes in directions and handle the active and passive inertia loads, state-of-the-art valves were used [78]. These independent metering valves are equipped with different operating modes that can handle different kinds of load very accurately. The valve-operated systems are separated into two main groups: constant pressure systems and constant flow systems.

3.1.1 Hydraulic Independent Metering Systems

Hydraulic load systems often consist of two parts, i.e., motors and cylinders. Traditionally, these types of systems have been controlled with one valve with a meter in (inlet) and a meter out (outlet) orifice that are mechanically connected. This makes the system much more robust and easy to control, but, on the other hand, it lacks flexibility. Its lack of flexibility can cause numerous types of losses. For example, losses due to the synchronous work of the orifice with different pressure demand, unnecessary losses on the meter outside with dimensions adjusted for overrunning loads, and so on. This is not desirable when handling restrictive (positive) loads. In order to overcome these shortcomings, a second valve can be implemented [79] [80] [81] [82] [75]. The system, which consists of at least two valves (meter in - meter out) that are independently controlled, goes under the umbrella name ”Independent metering valves” (see Fig. 3.1). In the literature, numerous terms are used for independent metering valves: programmable valves [83], multi-functional valve [84], separate meter in – meter out [85], [86]. Dynamic performance improvement and energy-saving aspects are the main research objective, as well as the use of this type of valve configuration. Additionally, by separating the meter in and meter out orifice, features like regeneration and recuperation can be utilized to further improve the efficiency of these systems [81]. Independent metering systems usually come with a load sensing (LS) feature. This means that the system uses a variable displacement pump. The control of the LS margin can be done on the pump or electronically. The main advantage of the LS system is the improved energy efficiency and the improved performance. The downsides are: increased oscillation and excessive pressure margin. The properties of the LS system have been the subject of research in [74].
Electronic devices have improved the accuracy of hydraulic control systems using closed-loop techniques in many applications. With the introduction of a second valve, the possibility to control an additional variable has been introduced; for example, it can be pressure. This way, pressure on the meter out side can be controlled independently of the flow requirements on the meter in. This means that

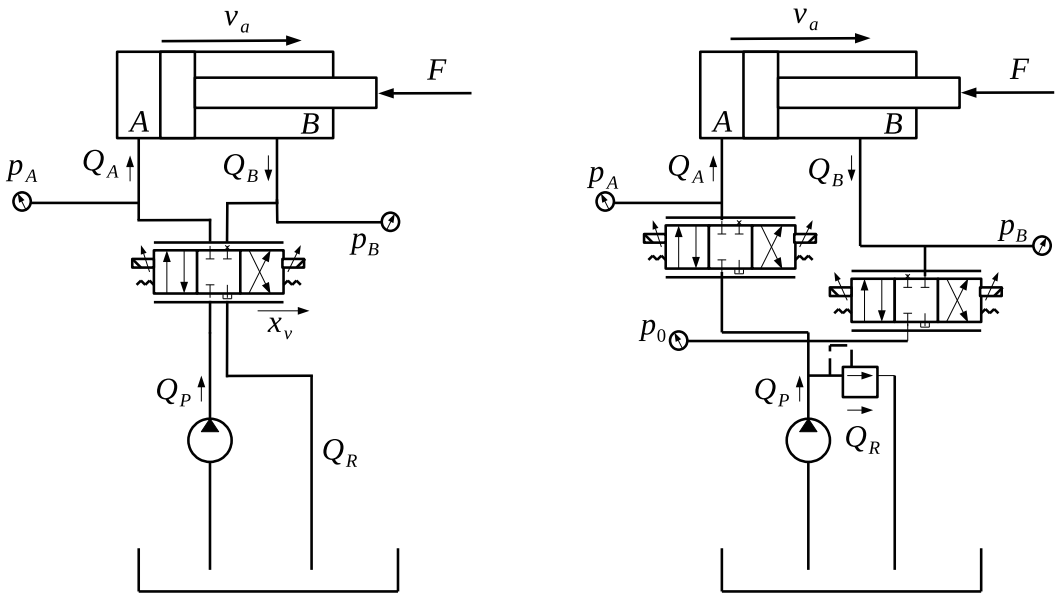

Figure 3.1: Conventional system with one independent metering vale on the left which allows the control system to control only one system variable (example: flow or pressure). Independent metering system on the right with two metering valves with which we can control two system variables (example: flow and pressure).

the resistance on the meter out side will be adjusted to meet the requirements for the set value. This can improve the system's stability and improve its ability to handle cavitation.
The downside of the independent metering systems is their complexity and the strong dependence on knowledge of the systems.

3.1.2 Introduction to Rapid Mine Development System

This section discusses the issues arising during the control of hydraulic systems. The first problem arising is the active and passive loads which cause vibration and pressure fluctuations. Additionally, the active loads (puling forces) can lead to cavitation and disruption or collapse of the pipelines if they are not adequately managed. There are multiple ways of how one can damp the oscillations that appear as a result of external forces during the working process. Passive damping is usually done with hydro-pneumatic accumulators [87]. Another way of damping is to use active vibration damping [88], [89], [90], [91]. In mining machinery, some kind of oscillation source feedback is very often needed to find out more about the source. Such feedback can be acceleration, pressure, or force feedback.

Figure 3.2: Rapid mining development system Sandvik MX650 ((C) 2020 By courtesy of Sandvik Mining and Construction.)

Optimal control theory is a research area that shows very promising results in active vibration damping [92], [93], [94]. This is one of the reasons why optimal control theory will be considered in this thesis.
The Sandvik MX650 (Fig.3.2) has two cutting arms which rotate and carry out the cutting process. Sometimes, if the pulling forces are in the same direction as the movement of the arm, the machine needs to be stopped and reset. The Eaton CMA valve offers multiple control methods that handle these types of loads very efficiently. In [95], all of these methods are simulated and tested. The pressure and flow control methods described in section 3.5 show improved performance compared to some of the methods described in [48]. The second problem investigated was the issue of the bulk modulus. At high temperatures and high air content, the value of the bulk modulus tends to get very low. This lowers the hydraulic system's stiffness, which will lower the mechanical system's natural frequency accordingly. As a result, the system exhibits oscillatory behavior, which lowers its performance. For this reason, multiple models for estimation of the effective bulk modulus were tested and compared. This model was then implemented in a simulation environment where multiple aspects were considered. It is concluded that the pressure and the flow controller do not have equal contribution to the mechanical stiffness of the system. Additionally, an adaptive back pressure controller was implemented to improve the energy efficiency of the whole system [96], [97].

3.2 Modelling and Simulation of Hydraulic Independent Metering Systems

Simulations are one of the most powerful tools, especially when developing new products. They offer the possibility to test the system and its performance before it is developed. Furthermore, they are very affordable and can prevent damage to the equipment or personnel. When designing a tunnel boring machine like the one described in chapter 3.1.2, it is very important to test the controllers for real-time capabilities and performance. This is especially important because of the high inertia loads that the hydraulic systems need to handle. Testing mining machines in the harsh conditions in which they work can cost a lot of money and time. Taking all this into account, simulation of these systems is essential. Additionally, a test rig was constructed for this system at Sandvik Mining and Construction in Zeltweg. The rig was used to test some of the capabilities of these systems.
The hydraulic system implemented in the mining machines is very complex and operates at very high pressures. Furthermore, these machines use state-of-the-art valves with an embedded controller, making this system highly nonlinear [78]. The independent metering valves in these systems react much faster than the natural frequency of the load system. This creates a very stiff problem, numerically. This section will define the nonlinear and linear mathematical models for the system. Furthermore, the developed models with the implemented controllers will be tested in a simulation environment.

3.2.1 Non-Linear Model of the Independent Metering System

The rapid mine development system has multiple cylinders driven by hydraulic servo valves. These valves are equipped with embedded controllers, which include different control strategies. The goal is to test the system's controllers and compare them with the actual model. In this section, the cylinder and the servo valves are presented with nonlinear state-space differential equations derived from the fundamental laws of physics.
When modeling these systems, one needs to be mindful to include all the effects that affect the system's dynamics. A complex nonlinear model should give a significant insight into the simulation model's behavior that can then be related to the real machine or test rig. In the present section 3.2, these systems are described as numerically stiff. The difference in reaction time results in a big magnitude difference in values between the servo valve and the load system. Additionally, this system has multiple feedback loops for the PID controllers implemented in the valves and the controllers for the load systems, making the system highly nonlinear. This is a nightmare for numerical solvers used for solving systems of

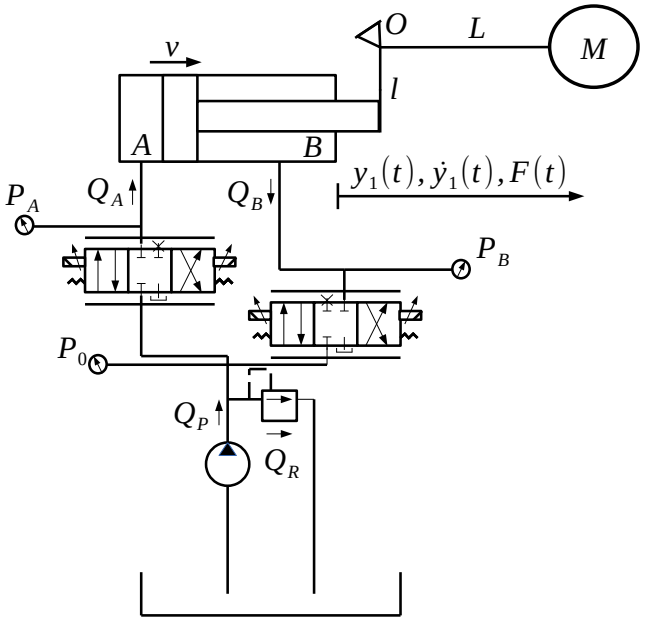

Figure 3.3: Simplified hydraulic and mechanical model of the system implemented in the machine. The mass makes rotation movements while cutting the profile. When the mass moves in positive direction the system flow is controlled on the active side of the cylinder and the pressure on the passive side of the cylinder.

differential equations. The model was developed in Matlab/Simulink. Multiple published works in this area have been used for creating the model. In [98] and [99], it is shown that the mathematical models for these systems can be a good basis for modeling independent metering systems.
As shown in Fig. 3.2, the rapid mine development system has multiple actuators, which are controlled with multiple independent metering valves. The main force responsible for motion is a product of the pressure difference between the piston (A) and rod (B) sides in the cylinder. When the system moves in positive direction the piston side is flow controlled and the rod side is pressure controlled. This force is resisted by the friction (nonlinear) and the load forces. The fiction force in the hydraulic cylinder is nonlinear and difficult to model. A complete mathematical model of the friction includes the Stribeck and stiction effect and viscous and Coulomb friction [100]. The LuGre friction model was used in the simulation. Additionally, the oil's elasticity (bulk modulus) can be affected by multiple parameters, such as air content, temperature, piston position. Low bulk modulus values can cause oscillations and decrease the system's stability. Different models of the bulk modulus are investigated and implemented in the simulation environment. Additionally, the influence on the flow and pressure controllers is

illustrated.

3.2.2 Mathematical Modeling of the Non Linear System

The system shown in Fig. 3.3 consists of a hydraulic pump, two independent metering valves, and a hydraulic cylinder that actuates the mechanical load. Newton's Second Law equations of motion are:

$$\frac{dy_1}{dt} = v_a. \tag{3.1}$$

$$m_a\ddot{y}_1 = p_A A_A - p_B A_B - F_f - F_{ext}. \tag{3.2}$$

where A_A is the area on the piston side and A_B is the area on the rod side. The restrictive forces coming from the load are designated as F_f for the friction force and F_{ext} for the external (load) force. The friction force is directly related to the velocity. When the machine is carrying out its cutting process, it is assumed that the friction force is mostly viscous, and it is described as $F_f = bv_a$, where b represents the coefficient of viscous friction. The additional friction forces will be explained in a designated subsection 3.3.
The flow through the valve orifice is nonlinear and introduced as Q_A and Q_B [98] [99]:

$$Q_A = C_d w x_v(t)\sqrt{\frac{2(p_s - p_a)}{\rho}} = C_v x_v(t)\sqrt{p_s - p_A}, \tag{3.3}$$

$$Q_B = C_d w x_v(t)\sqrt{\frac{2(p_B - p_T)}{\rho}} = C_v x_v(t)\sqrt{p_B - p_T}. \tag{3.4}$$

$$C_v = C_d w\sqrt{\frac{2}{\rho}} \tag{3.5}$$

In [98], the value of the discharge coefficient C_d = 0.61 and w is the area gradient whose value can be found in the valve catalog. The value of C_v Eq. 3.5 can also be calculated using the valve's catalog values for nominal flow Q_N, the maximum orifice opening $x_{v_{max}}$, and the nominal pressure differential Δ_{P_N}. The supply pressure is denoted as p_s and the tank pressure as p_T.

$$C_v = \frac{Q_N}{\sqrt{\frac{\Delta_{P_N}}{2}}}\frac{1}{x_{v_{max}}}. \tag{3.6}$$

The compressibility of the fluid plays an integral part in these systems. Its value is expressed through the bulk modulus β, which varies with pressure (p) and

strongly depends on the fluid's temperature (T) and air content (x_{air}). The amount of volume change that occurs while the fluid is being pressurized is defined as bulk modulus. Additionally, very low bulk modulus values can cause system instability. Consequently, the modeling of this parameter needs to be considered carefully.

$$\beta(p,t,x_{air},T) = -\frac{\Delta_p}{\Delta_v}V, \tag{3.7}$$

If Eq. 3.7 is to be used in a simulation environment, it needs to be rearranged in the following form:

$$\frac{dp}{\mathrm{d}t} = \frac{\beta}{V}\frac{\Delta_V}{\mathrm{d}t}. \tag{3.8}$$

According to [48], the compression rate of the fluid in volume V is given as follows:

$$\frac{dV}{\mathrm{d}t} = \left(\sum_{i=1}^{i=m} Q_{in} - \sum_{i=1}^{i=m} Q_{out}\right), \tag{3.9}$$

where Q_{in} is the flow that goes into and Q_{out} the flow that goes out of the system. Using the equations above, the volume change can now be expressed as a rate of change in pressure:

$$\frac{dp}{\mathrm{d}t} = \frac{\beta(t)}{V(t)}\left(\sum_{i=1}^{i=m} Q_{in} - \sum_{i=1}^{i=m} Q_{out}\right), \tag{3.10}$$

$$\frac{dp_A}{\mathrm{d}t} = \left(\frac{\beta(t)}{V_A + A_A y_1}\right)(Q_A - A_A v_a), \tag{3.11}$$

$$\frac{dp_B}{\mathrm{d}t} = \left(\frac{\beta(t)}{V_B + A_B(l_a - y_1)}\right)(A_B v_a - Q_B). \tag{3.12}$$

Four differential equations now describe the system: Eq. 3.1, Eq. 3.2, Eq. 3.11, and Eq. 3.12. This means that the system has four state variables. According to [101], a state variable is a first-order differential equation that describes the system's motion. In our case, the state variables are y_1, $v_a(y_2)$, p_A and p_B. Moreover, when simplifying the model, one can additionally replace the terms $\frac{\beta}{V+Ay_1}$ with the hydraulic capacitance $C = \frac{V}{\beta}$.

3.2.3 Mathematical Modeling of the Linear System

For the purpose of analysis and further usage in the numerical methods, a linear model of the system was developed. This model was used in real-time Simulink and Matlab environments. To develop the linear model, we must start with the

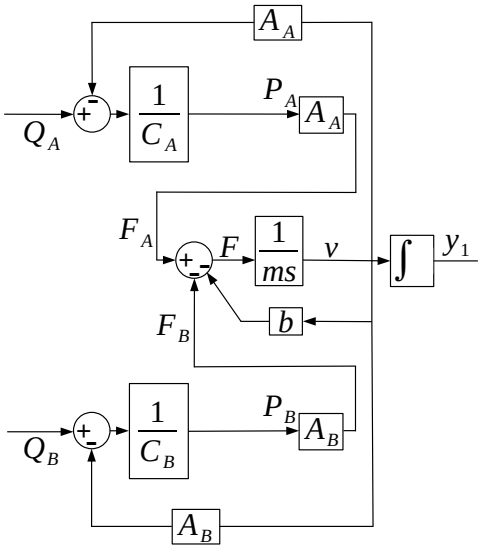

Figure 3.4: Nonlinear model of the hydraulic and mechanical system.

equations for the nonlinear model described in section 3.2.2. Flow through the valve can be expressed as

$$Q = Cvx_v(t)\sqrt{\Delta_P}. \tag{3.13}$$

To develop the linear equations for flow through both orifices, it is necessary to apply the method of small perturbations [102]. The flow on each side depends on the pressure change and the orifice position Eq. 3.3, Eq. 3.4. By linearizing both equations, one gets

$$\begin{aligned}
\Delta_{Q_A} &= \frac{\partial Q_A}{\partial x_v} x_{v_s} + \frac{\partial Q_A}{\partial p_A} p_{A_s}, \\
\frac{\partial Q_A}{\partial x_v} &= C_v\sqrt{p_s - p_1} = C_{q_1}, \\
\frac{\partial Q_A}{\partial p_A} &= -\frac{1}{2}\frac{C_v x_v}{\sqrt{p_s - p_1}} = C_p, \\
q_A &= C_{q_1} x_v - C_p p_1,
\end{aligned} \tag{3.14}$$

$$\begin{aligned}
\Delta_{Q_B} &= \frac{\partial Q_B}{\partial x_v} x_{v_s} + \frac{\partial Q_B}{\partial p_B} p_{B_s}, \\
\frac{\partial Q_B}{\partial x_v} &= C_v \sqrt{p_2} = C_{q_2}, \\
\frac{\partial Q_B}{\partial p_B} &= \frac{C_v x_v}{2\sqrt{p_2}} = C_p, \\
q_B &= C_{q_2} x_v + C_p p_2.
\end{aligned} \tag{3.15}$$

Because of the symmetry of the valve characteristics arising from the use of the same actuators area one gets

$$\begin{aligned}
\frac{\partial Q_A}{\partial x_v} &= \frac{\partial Q_B}{\partial x_v} = C_{q_1} = C_{q_2}, \\
\frac{\partial Q_A}{\partial p_1} &= -\frac{\partial Q_B}{\partial p_2} = -C_p.
\end{aligned} \tag{3.16}$$

Now, if one combines Eq. 3.14, Eq. 3.15, and Eq. 3.11, Eq. 3.12, pressures for both sides can be easily calculated.

$$\begin{aligned}
p_A &= \frac{C_{q_1} x_v - A_A v}{\frac{V_A}{\beta} s + C_p}, \\
p_B &= \frac{A_B v - C_{q_2} x_v}{\frac{V_B}{\beta} s + C_p}.
\end{aligned} \tag{3.17}$$

The system shown in Fig. 3.5 shows and incorporates the pressure equations into the equation of motion. In this system, no feedback loops or controllers are implemented. It shows that, as input on both sides, one gets the position of the orifice, better known as the spool opening.

3.3 Friction in Hydraulic Systems

Friction in hydraulic systems is nonlinear. A poorly modeled friction curve can deteriorate the performance hydraulic machines and cause a steady-state error for high precision motion machines. In [95], it is shown that when using a simplified friction model, the simulation results do not fully match the behavior of the real system. Multiple parts in a hydraulic system can be a source of friction: the oil flow through the valve orifice, the steel construction, and the load's movement. Additionally, the hydraulic cylinder has a highly nonlinear friction behavior.
Friction models are, by nature, divided into two main groups: static and dynamic. Static friction models are solely dependent on the direction of the velocity. The

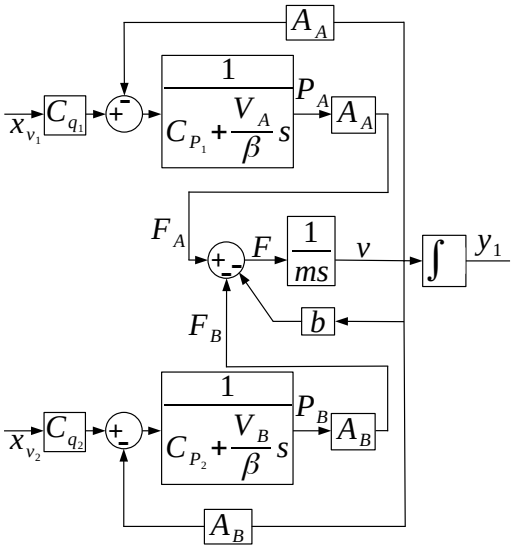

Figure 3.5: A linear model of the hydraulic linear and mechanical system obtained by combining Eq. 3.17 and Eq. 3.2.

static models are not accurate enough for applications that operate at velocities around zero. Because of this, dynamic models which introduce additional state are used to tackle this problem.

3.3.1 Steady State Friction Models

Steady state friction models are used for application depending of the direction of the velocity. The most basic models contain the Columb and the linear viscous friction [103]. The Columb friction force shown in Fig. 3.6 a is given by

$$F_c = \mu F_n \text{sign}(v). \tag{3.18}$$

where F_n is the normal force, μ is the friction coefficient and v is the relative velocity of the object in motion. The viscous friction force is linear with the velocity and can be expressed as

$$F_v(v) = bv. \tag{3.19}$$

where b is the viscous friction coefficient. Viscous friction is often added to the Columb friction (see Fig. 3.6 b). However, the friction force at rest is higher than the Columb friction level. At the beginning of the 20th century, Richard Stribeck shows that the friction force does not decrease discontinuously (see Fig. 3.6 c). Moreover, he showed that the dependence on velocity is continuous (see Fig. 3.6

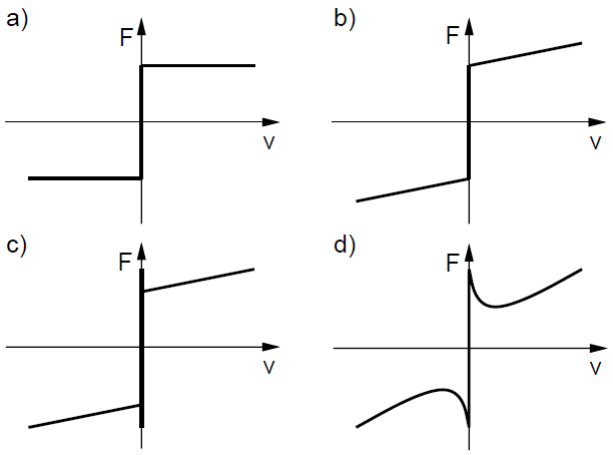

Figure 3.6: Steady state friction models: a) Columb Friction (no static friction). b) Columb and viscous friction (no static friction). c) Stiction, Columb, and viscous friction. d) Columb and viscous friction with the Stribeck effect

d) [104] [105] [106]. The Stribeck friction model, which incorporates all three effects can be expressed as

$$F_f(v) = F_C + (F_s - F_c)e^{(-|\frac{v}{v_s}|)^{\delta_s}} + F_v, \tag{3.20}$$

where F_c is the Columb friction force, F_s is the stiction force and v_s is the characteristic velocity of the Stribeck friction. In Fig.3.7, the Stribeck friction force is simulated for a positive movement. As input, we take a ramp function with a maximum velocity of $v = 0.5\,\mathrm{m\,s^{-1}}$. Additionally, for the simulation, $F_s = 1000\,\mathrm{N}$, $F_c = 800\,\mathrm{N}$, $v_s = 0.1\,\mathrm{m\,s^{-1}}$ and $b = 100\,\mathrm{N\,s\,m^{-1}}$. All above mentioned basic (steady state) friction models describe the friction forces very well at steady-state velocities. These models are not accurate enough for velocities around $v = 0$ and give numerical difficulties. Karnopp addresses this problem in [107] by setting the friction force equal to the force acting on the object for velocities around zero. However, this model showed numerical difficulties. Leine develops a switch friction model in [108], which consists of three differential equations for stick, slip, and the transition phase. Although this model improves the numerical solution, it still lacks the ability to describe friction completely, especially for the elastic part.

3.3.2 Dynamic Friction Models

The seven parameter models were developed to incorporate the presliding displacement, the Columb and the viscous friction, and the Stribeck effect with the

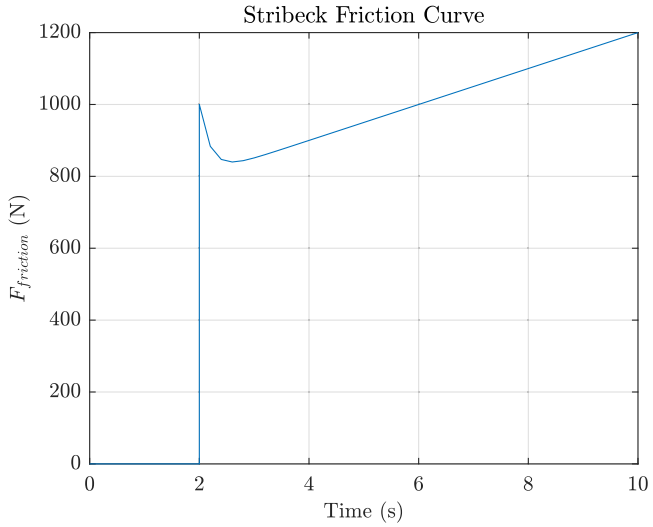

Figure 3.7: Stribeck friction force simulated according to Eq. 3.20.

frictional lag in one model [109] [110]. These models usually consist of two separate parts, one for the stiction phase and the other for the sliding phase. The stiction phase can be simply expressed as a spring

$$F_f(y_1) = \sigma_0 y_1, \tag{3.21}$$

where σ_0 is the micro stiffness and y_1 is the displacement of the object subjected to the force. The sliding phase of the friction can be expressed as

$$F_f(v,t) = \left(F_c + F_v|v| + F_s(\gamma,t_1)\frac{1}{1+\frac{v(t-\tau_l)}{v_s}^2} \right), \tag{3.22}$$

where γ is the temporal parameter of the rising static friction, τ_l is the time constant of frictional memory and t_2 is the dwell time. In Eq. 3.22, an attempt was made to describe the presliding and sliding regime with the introduction of time delay. However, as there is no apparent transition between the two equations, this model fails to describe the two regimes successfully.
Dahl observed in [111] that when an object is under small displacement, it returns to its primary position. However, if the displacement is larger, the bonding interface will undergo permanent displacement. Additionally, he states in [112] that the friction force is not only a function of the Coulomb friction force but also of the displacement. This model managed to describe the predisplacement much better than previous models but failed to capture many other phenomena like the Stribeck effect and the stick-slip motion. Although this model gives only an approximation of the presliding phenomenon, it was later used as a basis for more

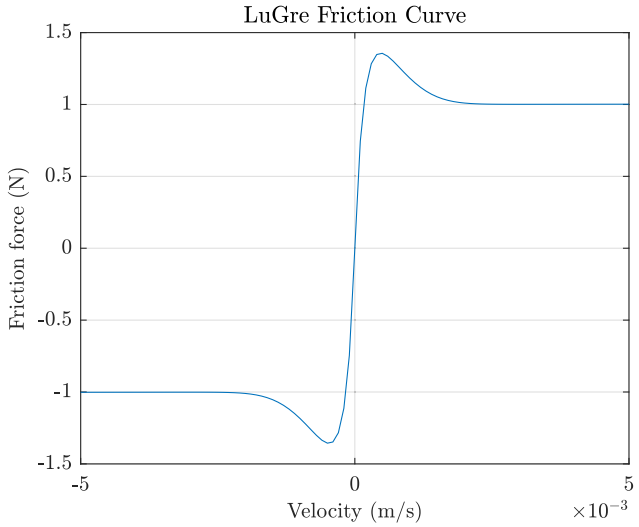

Figure 3.8: LuGre friction force simulated according to Eq. 3.24 and Eq. 3.25.

advanced models.
A significant breakthrough in friction modeling was made with the introduction of the LuGre model [113]. Using the Dahl model as a basis, the LuGre model introduced a new state variable $z = \frac{F_f}{\sigma_0}$. According to this, the Dahl model [112] can be modified as

$$\frac{dz}{dt} = \frac{1}{\sigma_0}\frac{dF_f}{dy_1}\frac{dy_1}{dt} = \frac{1}{\sigma_0}\frac{dF_f}{dy_1}v = v - \sigma_0\frac{|v|}{F_c}z. \tag{3.23}$$

This model replaces the constant term for the Columb friction force F_c with a velocity-dependent function $g(v)$. Additionally, it adds damping σ_0 associated with the micro displacement and a memory-less term dependent on the velocity $f(v)$. If Eq. 3.23 is modified accordingly, the LuGre friction model can be expressed as

$$\dot{z} = v - \sigma_0\frac{|v|}{g(v)}z = v - h(v)z, \tag{3.24}$$

$$F_f = \sigma_0 z + \sigma_1\dot{z} + f(v), \tag{3.25}$$

where z is the internal friction state. In Fig.3.8, the LuGre friction model is simulated for F_s = 1.5 N, F_c = 1 N, v_s = 0.001 m s^{-1}, σ_0 = 10^5 N m rad^{-1}, σ_1 = 316 N m s rad^{-1}. Additionally, the velocity is varying from v = -0.005 m s^{-1} to v = -0.005 m s^{-1}.

3.4 Effective Bulk Modulus

The compressibility of the hydraulic oil can be expressed through the value of the bulk modulus 3.2.2. It reflects both the stiffness of the oil and the speed of transmission of pressure waves [114]. Its value can be affected by the oil pressure and temperature, air content in oil, pipe rigidity, and molecular structure of the oil. The equivalent of the bulk modulus, which includes all of these parameters, can be expressed through the value of the effective bulk modulus [98]. Furthermore, it is shown in [115] that the compressibility of the oil has the highest effect on the mechanical stiffness of the hydraulic actuator.
If the process is adiabatic or isothermal and if tangent or secant definition of the bulk modulus is used, four types of bulk modulus can be defined. The secant bulk modulus can be expressed as

$$\beta_s = -V_0 \left(\frac{\Delta_P}{\Delta_V} \right)_{(S,T)}, \tag{3.26}$$

where V_0 is the initial volume of the fluid, Δ_P is the change in pressure, Δ_V is the change in volume and S and T represent the adiabatic and isothermal process respectively. The tangent bulk modulus can be defined as

$$\beta_t = -V \left(\frac{\partial P}{\partial V} \right)_{(S,T)}. \tag{3.27}$$

The secant bulk modulus Eq. 3.26 is more suitable for big pressure changes in comparison with the tangent bulk modulus Eq. 3.27, which is more adequate for smaller pressure changes. In this thesis, the tangent bulk modulus Eq. 3.27 will be mostly used and referred to as β.
Several theoretical models for the effective bulk modulus have been introduced to incorporate all of these effects. In the mid-1960s, Merrit introduced a theoretical model for calculating the effective bulk modulus but did not include the effects of the air content [98]. In [116], Nykanen added air content into the equation. Cho improved the Nykanen model by using the correct definition for the tangent bulk modulus [117]. Additionally, Gholizadeh [114] also modified the Nykanen model for the true value of the tangent bulk modulus. However, in [118], Yu developed a model which gives the pressure a dependent variation of free and dissolved air. Wylie used the Yu model as a basis for his model [119]. Kajaste [120] modified the Wylie model for the non-isothermal process and labeled it the "Wylie-Yu model". He further modified the model for pressure increase according to [121], [122], where it is shown that the relationship between the pressure and bulk modulus is often referred to as linear. Shunghun introduced a theoretical model where he incorporated the temperature influence of the oil [123]. In his dissertation,

Gholizadeh introduces a new model which consists of two equations [114], one for the value of the pressure below the critical value (air is not dissolved) and one for pressure above the critical value (air is dissolved).

3.4.1 Merrit model

In [98], Merrit defined the effective bulk modulus as an air-oil mixture in a flexible container. In addition, multiple assumptions were made: air bubbles were uniformly distributed, secant bulk modulus was used, the air was treated as a perfect gas, the oil and air had the same temperature. Following these assumptions, the Merrit model can be expressed as

$$\beta_{\text{Merrit}} = \frac{\beta_0}{1 + x_{air}\left(\frac{\beta_0}{nP} - 1\right)}, \tag{3.28}$$

where β_0 is the start value for the bulk modulus, x_{air} is the air content in oil and n is the polytropic constant. The value for the effective bulk modulus using Eq. 3.28 will always be lower when compared with the other models, because Merrit did not consider the effect of rising pressure on the air content in the oil.

3.4.2 Nykanen model

The model Nykanen introduces in [116] is a two-phase model for the oil-air mixture. Here, he used the secant bulk modulus from Eq. 3.26 to find the values for β_0. Furthermore, as in the previous section, 3.4.1, the assumption made for the temperature is that it is constant.

$$\beta_{\text{Nykanen}} = \frac{x_{air}\left(\frac{P_0}{P}\right)^{\left(\frac{1}{n}\right)} + (1 - x_{air})e^{-\left(\frac{P}{\beta_0}\right)}}{\frac{x_{air}}{nP}\left(\frac{P_0}{P}\right)^{\left(\frac{1}{n}\right)} + \frac{(1-x_{air})e^{-\left(\frac{P}{\beta_0}\right)}}{\beta_0}}. \tag{3.29}$$

The Merrit model 3.4.1 incorporates the standard definition of the secant bulk modulus, but Nykanen used the unconventional definition of the tangent bulk modulus. Due to this, the Nykanen model will not converge to the specified oil bulk modulus value.

3.4.3 Nykanen modified and Cho model

Cho [117] develops a novel model under the same assumptions as the Merrit model described in 3.4.1. As opposed to the Nykanen model, his definition of

the tangent of the bulk modulus corresponds well with the standard definition of the tangent bulk modulus. He defines the total instantaneous volume as the sum of the air and oil volumes.

$$V = V_g + V_l, \tag{3.30}$$

where V_l is the volume of the liquid and V_g is the volume of the air when compressed in accordance with the ideal gas law. The ideal gas law states that

$$V_g = \left(\frac{P_0}{P}\right)^{\frac{1}{n}} V_{g0}, \tag{3.31}$$

where V_{g_0} is an initial value for the gas volume. Additionally, Cho assumes a constant bulk modulus for the oil, which can be defined as

$$V_l = V_{l_0} e^{\left(\frac{P_0}{P}\right)^{\frac{1}{n}}}, \tag{3.32}$$

where V_{l_0} is the initial volume of the liquid. If Eq. 3.30, Eq. 3.31 and Eq. 3.32 are combined, one gets

$$V = \left(\frac{P_0}{P}\right)^{\frac{1}{n}} V_{g0} + V_{l_0} e^{\left(\frac{P_0}{P}\right)^{\frac{1}{n}}}, \tag{3.33}$$

If Eq. 3.33 is differentiated and inserted into the tangent bulk modulus formula, one gets

$$\beta_{Cho} = \beta_l \left(\frac{x_{Cho} + \left(\frac{P}{P_0}\right)^{\left(\frac{1}{n}\right)} e^{\left(\frac{P-P_0}{\beta_l}\right)}}{\frac{x_{Cho}}{n}\frac{\beta_l}{P} + \left(\frac{P}{P_0}\right)^{\left(\frac{1}{n}\right)} e^{-\left(\frac{P-P_0}{\beta_l}\right)}} \right). \tag{3.34}$$

If it is assumed that the oil bulk modulus is much larger than the pressure difference $P - P_0$, the term $e^{-\left(\frac{P-P_0}{\beta_l}\right)}$ can be replaced by unity. Accordingly, Eq. 3.34 can be approximated as,

$$\beta_{Cho} = \frac{x_{Cho} + \left(\frac{P}{P_0}\right)^{\left(\frac{1}{n}\right)}}{\frac{x_{Cho}}{n}\frac{\beta_l}{P} + \left(\frac{P}{P_0}\right)^{\left(\frac{1}{n}\right)}}. \tag{3.35}$$

Cho defined the air volumetric fraction x_{Cho} as

$$x_{Cho} = \frac{V_{g0}}{V_{l_0}}, \tag{3.36}$$

which can also be expressed as

$$x_{Cho} = \frac{x_{air}}{1 - x_{air}}. \tag{3.37}$$

If Eq. 3.37 is replaced in Eq. 3.35, the Cho model can be expressed as

$$\beta_{Cho} = \frac{1 - x_{air} + \left(\frac{P_0}{P}\right)^{\left(\frac{1}{n}\right)} x_{air}}{\frac{x_{air}}{nP}\left(\frac{P}{P_0}\right)^{\left(\frac{1}{n}\right)} + \frac{1-x_{air}}{\beta_l}}. \tag{3.38}$$

In his dissertation [114], Gholizadeh modifies the Nykanen model (Eq. 3.29) for the correct definition of the tangent bulk modulus of the volumetric fraction Eq. 3.36 and receives Eq. 3.38 as for the model given by Cho.

3.4.4 Yu Model

The previous models describe the compression of the air in the oil very precisely. However, they fail to describe both compression and dissolving of the volumetric fraction when subject to different pressures and temperatures. In [118], Yu introduces a new theoretical model based on the Merrit model 3.4.1. In order to include the dissolving effect of air, Yu defines a new variable named c_1, which was defined as the air bubble volume variation. This variable describes the ratio variation of the entrained and dissolved air content in oil. According to this, Yu introduced the following polytropic equation:

$$(V_{g_0} - c_1 V_{g_0}(P - P_0))^n P_0 = P V'_{gcd}, \tag{3.39}$$

where V_{gcd} is the instantaneous volume of entrained air which is a result of the compression and loss of mass of entrained air due to dissolving. Using the tangent bulk modulus, the Yu model can be expressed as

$$\beta_{Yu} = \frac{\beta_l}{1 + x_{Yu}\left(\frac{P_0}{P}\right)^{\left(\frac{1}{n}\right)} + (1 - c_1(P - P_0))\left(\frac{\beta_l}{nP} - 1\right)}, \tag{3.40}$$

where x_{Yu} is the air volumetric fraction by Yu which can be expressed as

$$x_{Yu} = \frac{V_{g_0}}{V_{gcd} + V_l} = \frac{x_{air}}{V_{g_0}\left(\frac{P_0}{P}\right)^{\left(\frac{1}{n}\right)} + (1 - x_{air})}. \tag{3.41}$$

Moreover, Yu provided a simplified model ($c_1 = 0$) by neglecting the dissolving effect.

$$\beta_{Yu_{simplified}} = \frac{\beta_l}{1 + x_{Yu}\left(\frac{P_0}{P}\right)^{\left(\frac{1}{n}\right)}\left(\frac{\beta_l}{nP} - 1\right)}. \tag{3.42}$$

If we implement the second part of Eq. 3.41 in the simplified model Eq.3.42, we get

$$\beta_{Yu_{simplified}} = \frac{1 - x_{air} + \left(\frac{P_0}{P}\right)^{\left(\frac{1}{n}\right)} x_{air}}{\frac{x_{air}}{nP}\left(\frac{P}{P_0}\right)^{\left(\frac{1}{n}\right)} + \frac{1-x_{air}}{\beta_l}}. \tag{3.43}$$

If we compare the Cho, the modified Nykanen, and the Yu simplified models, we can conclude that when the effect of air dissolving is neglected, they are all the same.

3.4.5 Wylie - Yu Model modified by Kajeste

Wylie [119] describes the effective bulk modulus as the ratio between the pressure difference and the volume change of the fluid. Additionally, the air content of the fluid has also a big effect on its value. The Wylie model for isothermal conditions can be expressed as

$$\beta_W = \frac{\beta_l}{1 + \left(m_g \frac{RT}{P}\right)^{\left(\frac{1}{n}\right)} \left(\frac{\beta_l}{nP} - 1\right)}, \tag{3.44}$$

where R is the gas constant and m_g is the mass of free gas. Kajeste further modified Eq. 3.44 for non-isothermal conditions and labeled it the "Wylie-Yu" model.

$$\beta_{Wk} = \frac{\beta_l}{1 + x_{air}\left(\frac{P_0}{P}\right)^n \left(\frac{\beta_l}{nP} - 1\right)}, \tag{3.45}$$

To be able to express the pressure change on the effective bulk modulus, Kajeste modifies the value β_l as presented in [122]. Additionally, the value of β_l is being modified for the temperature change as given in [124] [123].

$$K_l = K_0 + m_p P + n_T T. \tag{3.46}$$

In Eq. 3.46, m_p represents the pressure-related term and n_T the temperature-related term, which describe the pressure and temperature change in a linear manner. Additionally, K_l stands for the liquid bulk modulus and K_0 for the starting value of the bulk modulus.

3.4.6 IFAS model

In [123], Kim introduces a new model for the effective bulk modulus labeled as the "IFAS" model. He addresses the tangent bulk modulus of oil with the pressure-

related term already implemented in the theoretical equation.

$$\beta_{IFAS} = \frac{(1-x_{air})\left(1+\frac{m_p(P-P_0)}{\beta_0}\right)^{-\frac{1}{m_p}} + x_{air}\left(\frac{P_0}{P}\right)^{\frac{1}{n}}}{\frac{1}{\beta_0}(1-x_{air})\left(\frac{P_0}{P}\right)^{\frac{1}{n}}\left(1+\frac{m_p(P-P_0)}{\beta_0}\right)^{-\frac{m_p+1}{m_p}} + \left(\frac{x_{air}}{nP_0}\right)\left(\frac{P_0}{P}\right)^{\frac{n+1}{n}}}. \quad (3.47)$$

3.4.7 Gholizadeh Model

In his dissertation [114], Gholizadeh separates the models into two main groups. In the first one, the models include the volumetric compression of air ('compression only'), and in the second, the models include the compression and dissolving of air ('compression and dissolve'). In order to improve the application of the compression-only models for higher air content and to solve the discontinuity at critical pressures for the compression dissolve models, Gholizaden introduces a new model [125]. In his model, when the critical pressure is reached, all the air in the oil is dissolved, and the remaining air will tend to follow a 'compression only' bulk modulus curve. Additionally, he defines two polytropic indices: n_1 before and n_2 after reaching the saturation point. The volume of the air for pressure values which are less than the critical one is given by

$$V_{gcd}(P,T) = \left(\frac{P_0}{P}\right)^{\frac{1}{n_1}} \frac{T}{T_0} x_{air}\theta, \quad (3.48)$$

where the volumetric fraction of air θ at $P < P_C$ is found by

$$\theta = \left(\frac{P_c - P}{P_c - P_0}\right)\left(1 - \frac{(x_{air})_c}{x_{air}}\right) + \frac{(x_{air})_c}{x_{air}}, \quad (3.49)$$

and for $P > P_c$, the remaining air will not be dissolved and will follow the compression rule

$$V_{gcd}(P,T) = \left(\frac{P_0}{P}\right)^{\frac{1}{n_2}} \frac{T}{T_0}(x_{air})_c. \quad (3.50)$$

According to this, two equations are introduced, one for when $P < P_c$,

$$\beta_{Gholizadeh} = \frac{V_l + V_{gcd}}{\frac{V_l}{\beta_l} + \frac{1}{K_{g1}}V_{gcd}}. \quad (3.51)$$

and one for when $P > P_c$

$$\beta_{Gholizadeh} = \frac{V_l + \left(\frac{P_0}{P}\right)^{\frac{1}{n_2}} \frac{T}{T_0}(x_{air})_c}{\frac{V_l}{\beta_l} + \frac{1}{K_{g2}}\left(\frac{P_0}{P}\right)^{\frac{1}{n_2}} \frac{T}{T_0}(x_{air})_c}. \quad (3.52)$$

where

$$\begin{aligned} K_{g_1} &= n_1 P, \qquad K_{g_2} = n_2 P, \\ \beta_l &= V_{l_0} + m(P - P_0), \\ V_l &= V_{l_0}(1 + \frac{m}{\beta_{l_0}}(P - P_0))^{-\frac{1}{m}}. \end{aligned} \tag{3.53}$$

where m is the pressure related term.

3.5 Control of Hydraulic Independent Metering System for Tunnel Boring Machines

The hydraulic independent metering system for tunnel boring machines is a very complex nonlinear system that presents many challenges when it needs to be controlled. For the first time in this type of machine, a novel independent metering valve was implemented and used. The Eaton CMA valve is an advanced CAN-enabled electro-hydraulic section mobile valve, which consists of two separate valves: the CV (conditioning valve) and the PV (pivot valve) [78], [126]. The CV has two main margins: the CV margin added on top of the highest load sensing margin for each PV, and the other is the LS margin for each PV. The LS margin is usually set to 20 *bar* and the CV margin to 5 *bar*. The valve shown in Fig. 3.9

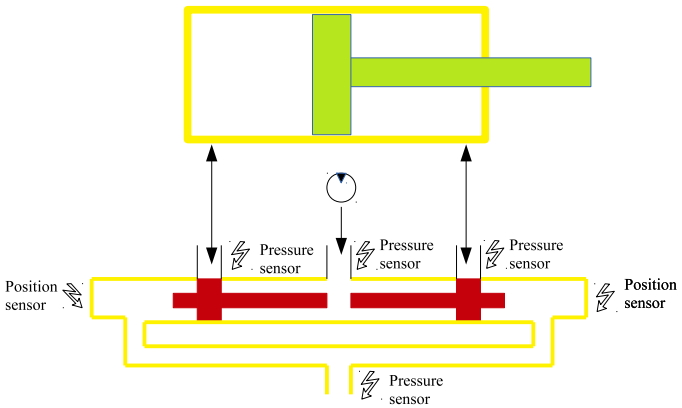

Figure 3.9: Electro - hydraulic section mobile valve Eaton CMA90 equipped with embedded controllers and sensors. These allows to control the valve pressure, flow and the spool position very accurately.

has a pressure and position sensor on every spool. It is also equipped with flow sensors for the piston and rod sides. The main problem during the cutting process are the high inertia loads which lead to active and passive loads. Passive loads act in the opposite direction of the movement of the working cylinder. On the other

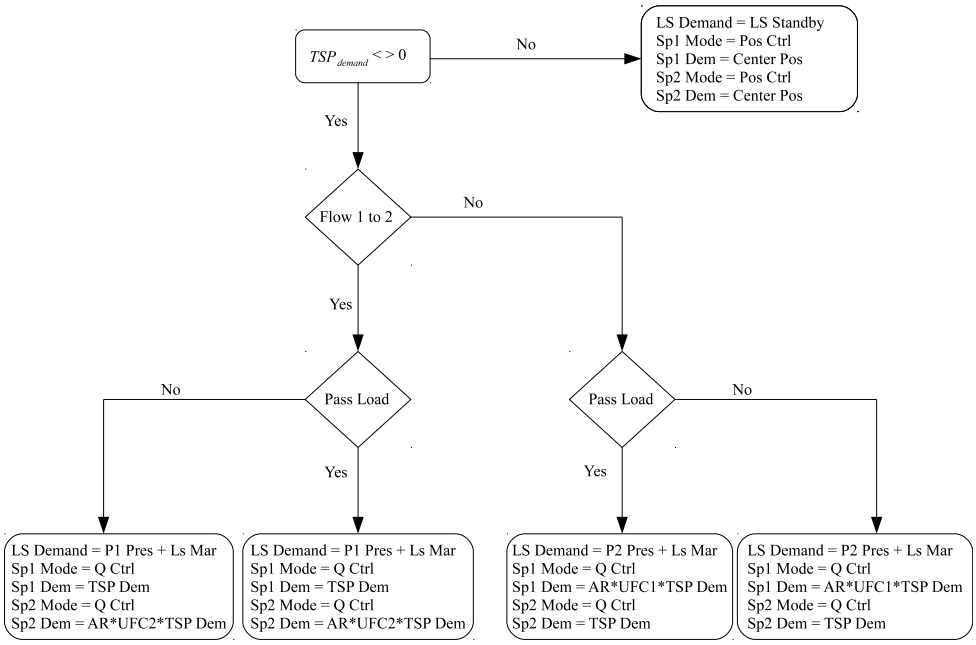

Figure 3.10: UFC - Universal flow control logic.

hand, active loads act in the direction of the movement of the working cylinder. In [127], Will illustrates that active loads act independently of the motion direction and by standstill, always in one direction. That being, there is no change in the force direction on the piston side. When this scenario occurs, the valve needs to break on the rod side in order to maintain constant flow and pressure.
The Eaton CMA90 valve has an incorporated control logic that efficiently handles this type of load. It consists of pressure and flow controllers whose inner-work depends on the load type. The UFC (universal flow control) implements flow controllers on both sides of the cylinder. This opens the possibility to limit the speed of the valve opening, which directly increases or decreases the system's speed of motion. It can be seen from Fig. 3.10 that, depending whether the load is active or passive, the system implements flow controllers on both sides, but with a small difference on the active side. For the active side, the area difference AR and the flow limiting factor $UFC1$ or $UFC2$ are considered. On the other side, the IFC incorporates flow and pressure controllers for both sides. What makes the IFC more efficient is the PI pressure controller, which controls the pressure to the set value on the active side. This allows the system to maintain constant velocity and avoid oscillations. This is possible because the valve has a very flexible control system that allows the control of multiple variables simultaneously.

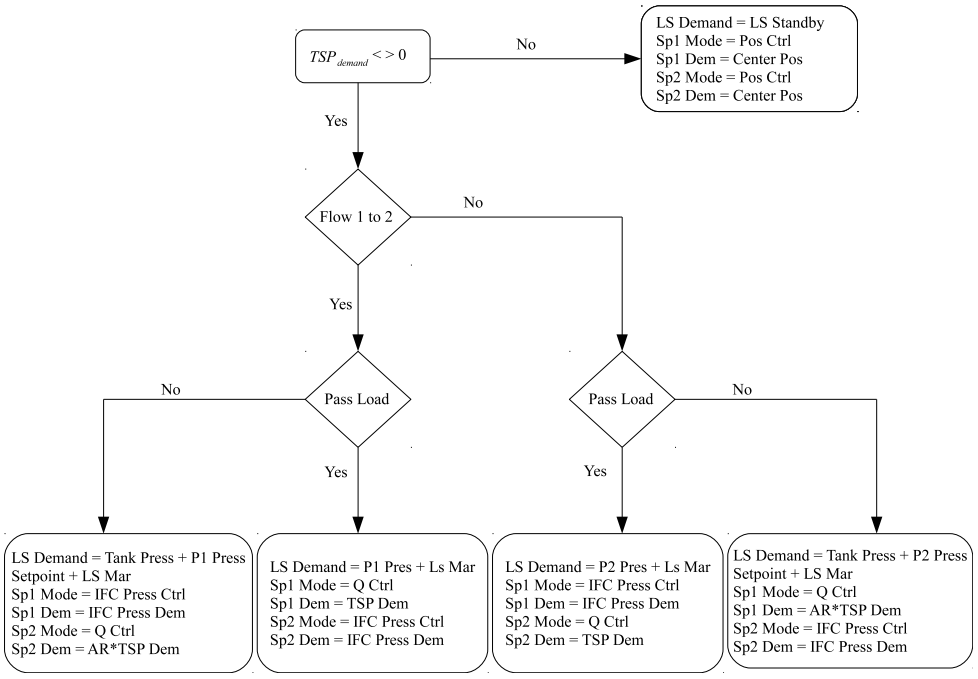

Figure 3.11: IFC - Intelligent flow control logic.

3.5.1 Control of Nonlinear Hydraulic Independent Metering System

The equations for the nonlinear system are already shown in the last section 3.2.2. Figure 3.4 shows that the inputs on both sides are the flows for this type of system. As explained in section 3.5, the system has flow and pressure controllers implemented on both sides. In addition, there is an external position controller that regulates the actuator's position. The position controller also determines the flow demand that the system requires to achieve a specific position. The controllers implemented in the system are PI controllers. In Fig. 3.12, $Q_{A_{valve}}$ is the flow that leaves the independent metering valve. The control illustrated in Fig. 3.12 is only for the passive loads and when the system moves in a positive direction. When the machine moves in a negative direction or the loads are active, the system follows the control logic illustrated in Fig. 3.11. This system was used and tested for multiple load and position scenarios. Furthermore, this model was used to test the influence of the bulk modulus on this type of system.

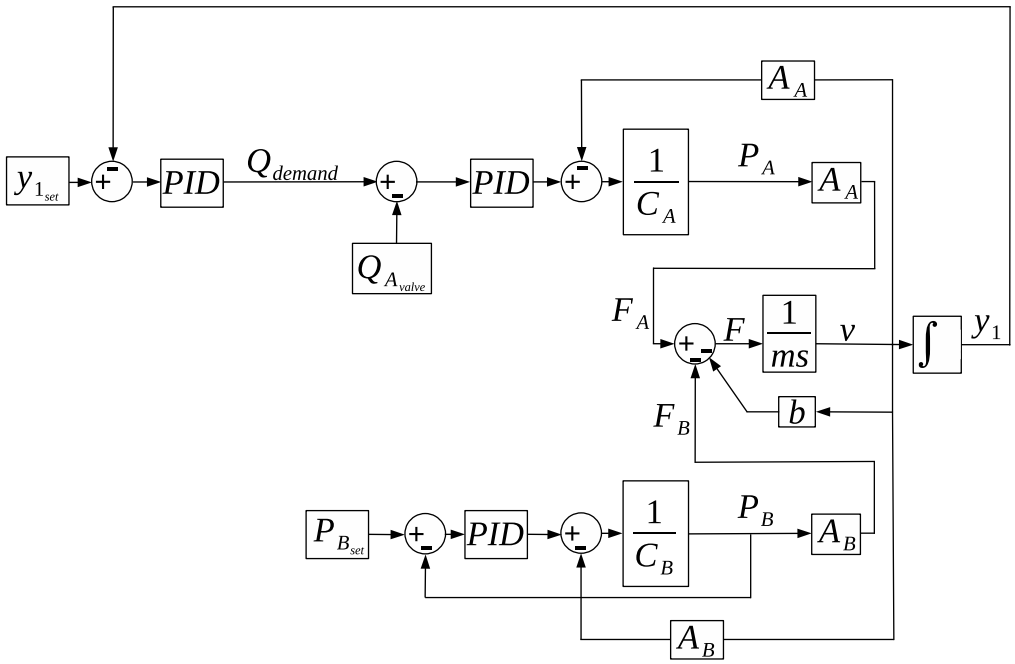

Figure 3.12: A hydraulic nonlinear system with control. The non linear model of the valve is not included in this figure but in the working model. Implemented pressure controller on the rod side and flow controller on the piston side. Additionally, an external flow controller is implemented.

3.5.2 Control of Linear Hydraulic Independent Metering System

The linear system equations were illustrated and derived in section 3.2.3. In equation 3.17, the pressures for the linear system are shown. Additionally, from Fig. 3.5 it can be seen that inputs in the system for both sides are the orifice openings x_{v_1} and x_{v_2}. If the same control is to be implemented for the linear as for the nonlinear system, some modifications need to be made. Since the servo valve reacts much faster than the natural frequency of the mechanical system [128], the flow controller on the piston side was not implemented. The rod side is always pressure-controlled for passive loads and actuation in the positive direction. The state-space representation of the system shown in Fig. 3.13 which includes the feedback loops for the pressure, the flow and the position of the system can be written as

$$\dot{\boldsymbol{x}} = \mathsf{A}\boldsymbol{x} + \mathsf{B}\boldsymbol{u} \tag{3.54}$$

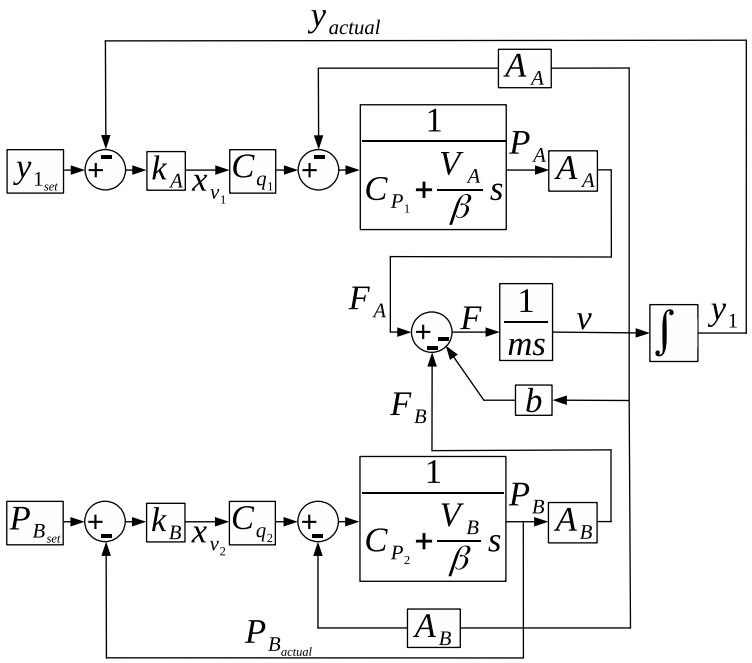

Figure 3.13: Hydraulic linear system with control. Implemented P position controller on the piston side and P pressure controller on the rod side.

where

$$\mathsf{A} = \begin{bmatrix} -C_{p1}\frac{\beta}{V_A} & 0 & -k_A C_{q1}\frac{\beta}{V_A} & -A_A\frac{\beta}{V_A} \\ 0 & -\left(k_B C_{q2} + C_{p2}\right)\frac{\beta}{V_B} & 0 & -A_B\frac{\beta}{V_B} \\ 0 & 0 & 0 & 1 \\ \frac{A_A}{m} & -\frac{A_B}{m} & 0 & -\frac{b}{m} \end{bmatrix}, \boldsymbol{x} = \begin{bmatrix} P_A \\ P_B \\ y_1 \\ v \end{bmatrix},$$

$$\mathsf{B} = \begin{bmatrix} k_A C_{q1}\frac{\beta}{V_A} & 0 \\ 0 & -k_B C_{q2}\frac{\beta}{V_B} \\ 0 & 0 \\ 0 & 0 \end{bmatrix}, \qquad \boldsymbol{u} = \begin{bmatrix} y_{set} \\ P_{Bset} \end{bmatrix}. \tag{3.55}$$

Chapter 4

The Effect of the Bulk Modulus on the Dynamics of Controlled Independent Metering System

In this chapter the models for effective bulk modulus presented in the previous chapter were firstly compared for isotermal conditions. The IFAS and the Wiley-Yu (Kajeste) models were further compared for non constant temperature. This was done firstly to investigate and improve the already existing models for modeling the effective bulk modulus and then test the influence of low bulk modulus values on the system performance and dynamics. This lead to the development of a new energy-efficient adaptive controller for this type of system. Multiple conclusions arise from these investigations. Firstly, for lower bulk modulus values, the pressure controller has an advantage over the flow controller. Secondly, for highly pressurized systems, the temperature has a more considerable influence on the bulk modulus value than the air content or the pressure.

4.1 Comparison of the Compression and Dissolve Models

In the previous chapter, multiple models for modeling the bulk modulus of oil were presented. In these models, multiple definitions for the tangent bulk modulus were observed. It is shown that the use of the secant bulk modulus leads to lower values for the effective bulk modulus. Because of this, the tangent bulk modulus definition was preferred. Additionally, the influence of the pressure and the temperature increase on the bulk modulus was discussed. To be able to compare the models, they were simulated under the same conditions x_{air} = 1 %, n = 1 (isothermal conditions), P_0 = 1 bar, m_p = 11.4, β_0 = 15 000 bar and P = [0 - 50]

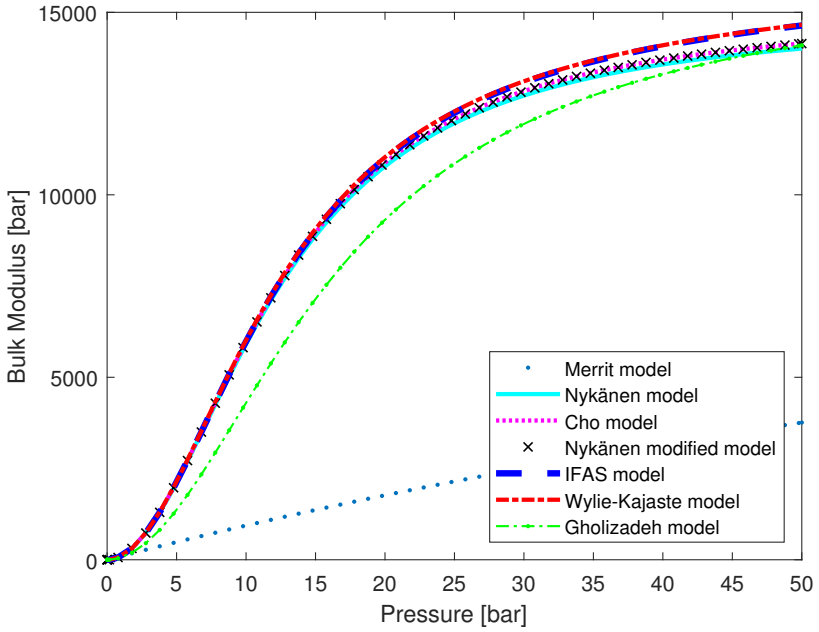

Figure 4.1: Comparison of the different models under the same conditions, x_{air} = 1 %, n = 1 (isothermal conditions), P_0 = 1 bar, m_p = 11.4, β_0 = 15 000 bar and P = [0 - 50] bar.

bar. The models were principally investigated and compared. Fig. 4.1 illustrates the results for the different bulk modulus values. Compared to the results presented in [123], the Wylie-Yu (Kajeste) 3.4.5 and the IFAS model 3.4.6 show the most consistent results. For this reason, these two models were further compared for non-isothermal conditions and non-constant temperature.

4.1.1 Comparison of the Wylie-Yu (Kajeste) and IFAS Models for non-constant temperature

In this section, the two models were compared for non-isothermal conditions. Pressure ranges between p = [0 - 80] bar and temperature between T = [0 - 60]°C. The additional values were as follows: the air content x_{air} = 0.0013 %, the bulk modulus β_0 = 18670 bar (ISO VG 46 oil), the temperature-related term n_T = -80 $\frac{bar}{°C}$, the pressure-related term m_p = 11.4 and the polytropic constant n = 1.4.
Additionally, Figure 4.2 shows that both models correspond well with the measurements done in [123]. In order to illustrate the difference between the two models, an error plot is needed. Fig. 4.3 shows that the difference between the two models is very small. Due to this and the results stated in [129], the Wylie-Yu model was incorporated in the simulation model.

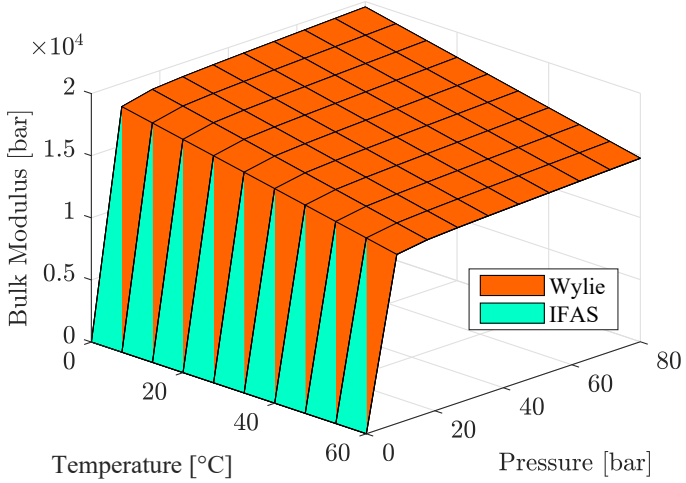

Figure 4.2: Comparison of the different models under the same conditions, x_{air} = 0.0013 %, n = 1.4 (isothermal conditions), P_0 = 1 bar, m_p = 11.4, β_0 = 18 670 bar, n_T = -80 $\frac{bar}{°C}$, T = [0 - 60]$°C$ and P = [0 - 80] bar.

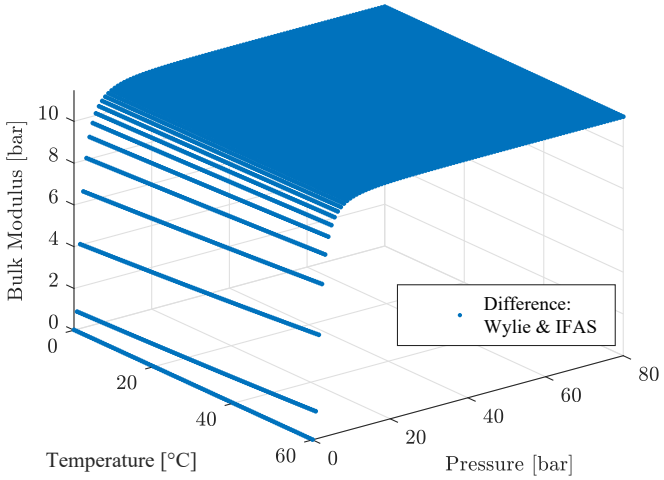

Figure 4.3: Error plot for the Wylie - Yu and IFAS model for non isothermal conditions.

4.2 Case Study

The hydraulic system consists of a pump, two servo valves, a hydraulic actuator, and a mass that needs to be moved. The servo valves offer the possibility to control the back pressure. When the bulk modulus values decrease due to increased oil temperature or increased air content, the system's natural frequency goes down. To compensate for that, one can increase the backpressure, which will increase the pressure on the active side of the cylinder. This will increase the natural frequency of the system. Although this option is not energy-efficient, it is very often used in hydraulics to avoid any oscillations.
In [130], Cetin introduces a combined PID - Fuzzy logic controller, which results better than a regular PID controller at lower bulk modulus values. However, the question of energy efficiency was not considered. In [131], Wang presents a method where he successfully lowers the air content in the system by 0.01 %. In [132], Anwer shows that more power is needed when the oil temperature increases. Additionally, Anwer and Hassan both verify in their experiments [133] that the increasing temperature decreases the supply pressure on the system. However, none of the previous works show how the bulk modulus values affect the pressure or flow controllers of the system and, further to this, what is the energy loss due to increased oil temperature or increased air content into the oil.
To investigate the effects of the bulk modulus on the system controllers first, and then on the energy consumption, the nonlinear system 3.5.1 presented in Fig. 3.3 was tested and simulated in Matlab Simulink ®. The system's mass is $M = 400,000\,\text{kg}$, the viscous friction parameter b = $10^7 \frac{Ns}{m}$, identified from measurements during cutting operations. The hydraulic cylinder areas are given as A_A = $0.0616\,m^2$, $A_B = 0.0302\,m^2$ and the length of the cylinder $h = 0.65$ m. The system input is a position controller with a set value of 0.01 m. The back pressure varies from 30 to 80 bars. As shown in Fig. 3.12, the flow controller directly depends on the flow demand of the system and the flow that goes through the valve. Depending on the load conditions, the system modifies its control to achieve its position and maintain a constant velocity [95]. The system's performance was analyzed for different temperature values and air content. From Fig. 4.4 it can be seen that as the bulk modulus value decreases due to the increased temperature and air content into the oil, the system position delays, and the system peak velocity decreases. Additionally, the peak pressure on the active side is significantly higher when compared with the pressure on the rod side, which is pressure-controlled. On the other side, in Fig. 4.5 the system's controllers and power consumption are analyzed. When the bulk modulus value decreases, the system flow demand increases, which leads to increased power consumption. This actuates the flow controller accordingly. The pressure controller only delays its signal to the valve. This leads to the delayed performance and lower pressure values shown in Fig. 4.4. It is

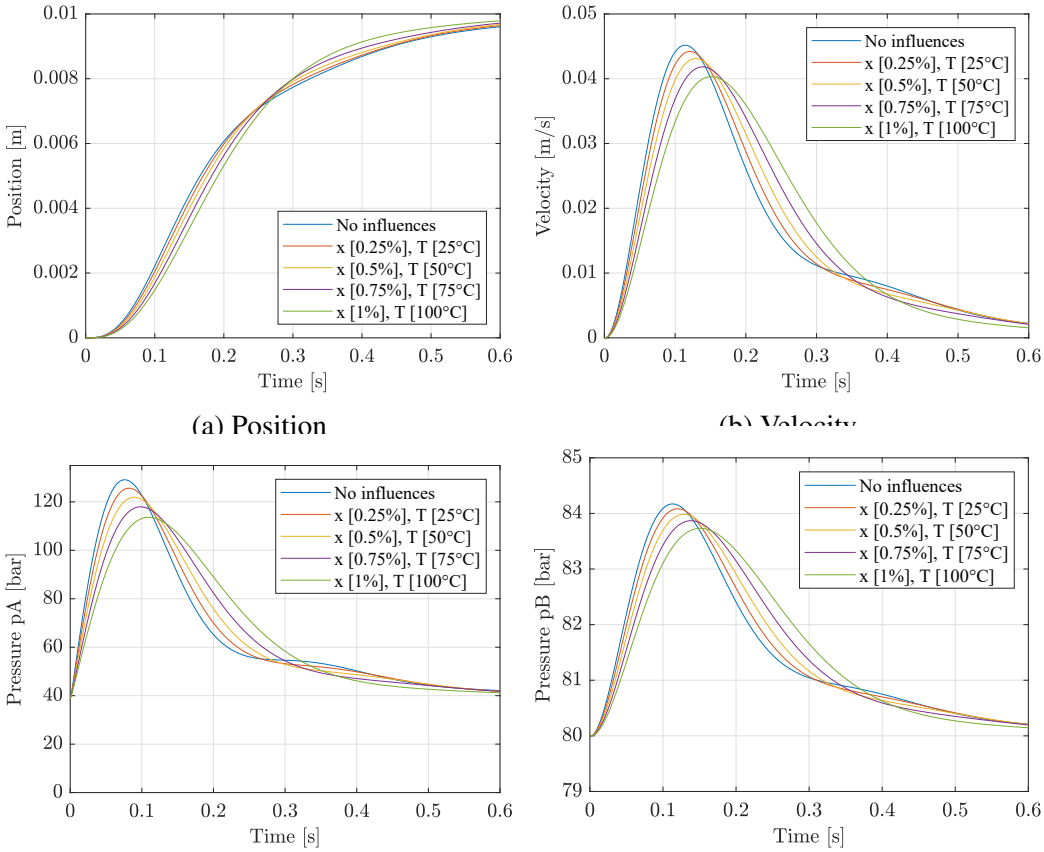

(a) Position

(b) Velocity

(c) Pressure piston side P_A

(d) Pressure rod side P_B

Figure 4.4: The system dynamics are tested at different air content x_{air} and temperature T. With the increased air content and temperature, the system delays, and the pressure decreases.

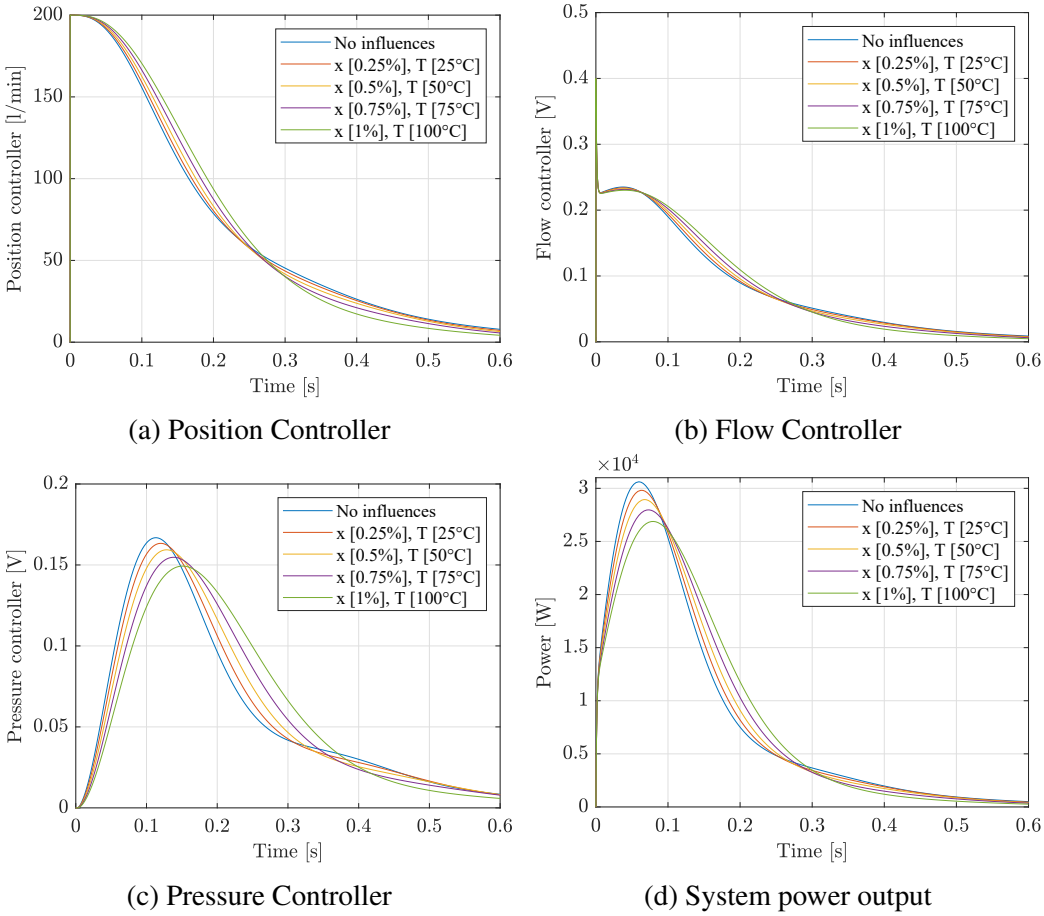

(a) Position Controller

(b) Flow Controller

(c) Pressure Controller

(d) System power output

Figure 4.5: System performance at different air content x_{air} and temperature T. With the increased air content and temperature, the system controllers delay, and the system needs more flow to achieve the same position.

essential to mention that when the value of the bulk modulus is lower, the system power peak value decreases. One of the reasons for this is the decreased pressure values on the piston side. This prompts us to believe that the independent metering system does not consider the change in the bulk modulus value. The reason for this lies at the assumption the valves embedded controllers always make for the value for the bulk modulus. Because the value is almost always assumed to be constant the system cannot recognize its effects on the dynamics. For this reason an adaptive controller was proposed to try to improve the system performance and efficiency. Also, Fig. 4.5 shows that the pressure and the flow-controlled sides do not have an equal contribution to the stiffness of the system.

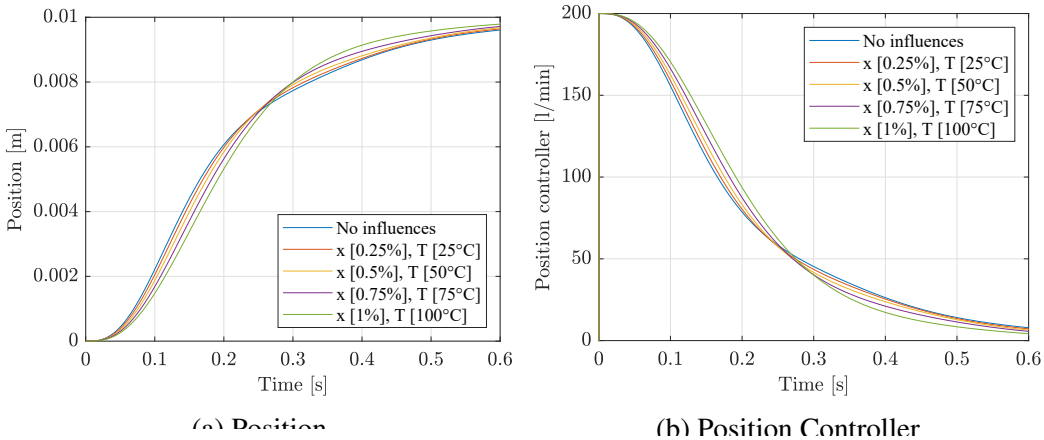

(a) Position

(b) Position Controller

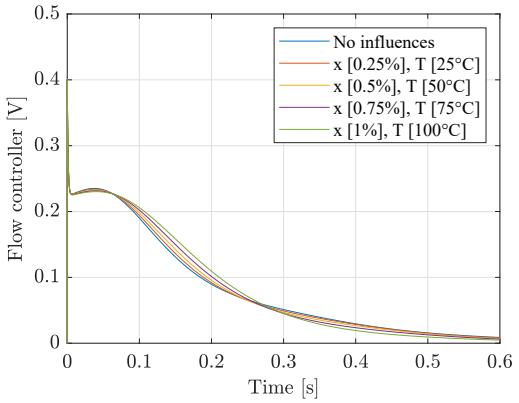

(c) Flow Controller

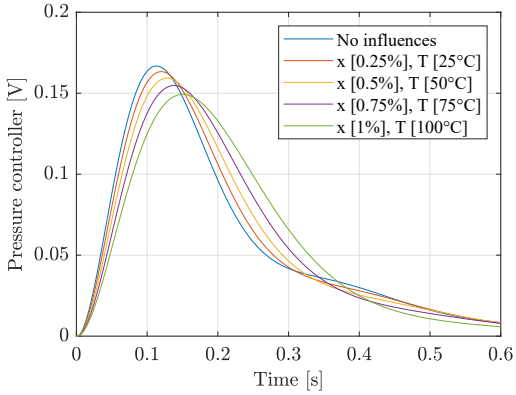

(d) Pressure Controller

Figure 4.6: Outputs of the position and the controllers. The piston side bulk modulus value is affected by: air content (x_{air}), temperature (T) and pressure (P); rod side bulk modulus value is affected by: pressure (P).

4.2.1 Comparison of the Pressure and Flow Controlled Sides

In the previous section, the effects of the bulk modulus on the system dynamics were illustrated. Moreover, it was stated that the flow and the pressure controller have no equal contribution to the mechanical stiffness of the system. In order to test this, two simulations were carried out. In the first simulation, the bulk modulus value on the flow-controlled side was only affected by the oil's temperature, air content, and pressure. The bulk modulus value on the rod side was only affected by the pressure increase. It is evident from Fig. 4.6 that the bulk modulus value significantly affects the system's performance and position. All of the controllers are delaying, and the system needs more power to compensate for the position delay. This shows that the flow controller is severely affected by the value of the bulk modulus. On the other hand, the system shows much better performance

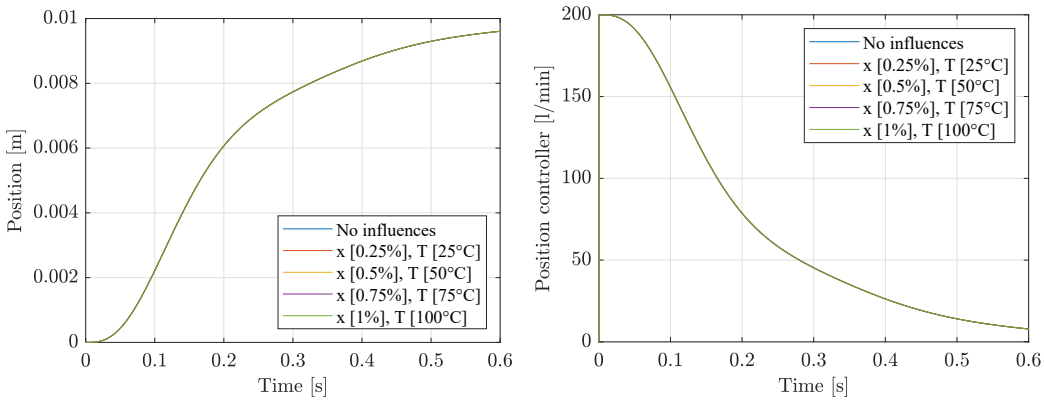

(a) Position

(b) Position Controller

(c) Flow Controller

(d) Pressure Controller

Figure 4.7: Outputs of the position and the controllers. The rod side bulk modulus value is affected by: air content (x_{air}), temperature (T) and pressure (P); piston side bulk modulus value is affected by: pressure (P).

when the pressure-controlled side is affected by the bulk modulus value (Fig. 4.7). The position is almost unaffected, which goes for the system controllers. This leads us to conclude that the pressure controller has a significant advantage in this type of system under the given conditions [124]. It also opens the possibility to regulate the pressure on the rod side according to the value of the bulk modulus.

4.3 Adaptive Control

An adaptive control system is a system that can cope with the changes and the uncertainty of the plant [134]. The first time adaptive control was mentioned was in the early 1950s [135]. The motivation behind this research was the design of an autopilot for a high-performance aircraft. Aircraft dynamics are highly nonlinear and conceptually time-varying. At a given operating point, the system was approximated for a linear state-space model 2.2. When the aircraft goes through different conditions, the system's operating point will change. This will lead to changes in the A, B, C, D matrices values accordingly. The output of the system $\boldsymbol{y(t)}$ carries information about the states Eq. 2.9. If the values of the state matrices change, one can argue that the controller should be able to learn and adjust its performance [136]. This led to the control structure known as adaptive control [137], [138]. This control structure is very commonly used for nonlinear systems and in plants where the model is not well known. Through the years, there have been various methods of how this control scheme has been used [139]. Model Predictive Control (MPC) is used when the system model is known, but the system parameters are unknown. In [140] this control has shown impressive results. Machine learning techniques such as Neural Networks [141], reinforcement learning [142], and even fuzzy logic [143] have shown promising results in an approximation of nonlinear plants.

4.3.1 Adaptive Back Pressure Control

When the bulk modulus value decreases significantly, the value of the pressure on the pressure-controlled side is usually increased to compensate for the loss of pressure. This loss of pressure leads to lower mechanical stiffness of the whole machine, which can cause vibrations, lower accuracy, and efficiency. To avoid this, in praxis, the pressure is usually set to a higher value. However, this leads to a much higher energy consumption of the machine. To alleviate this, a novel adaptive back pressure controller was developed. Because nonlinear equations for the calculation of effective bulk modulus are already implemented in the simulation model, one can easily see how much the value of the bulk modulus is affected by the temperature, the air content, and the pressure of the oil. According to this,

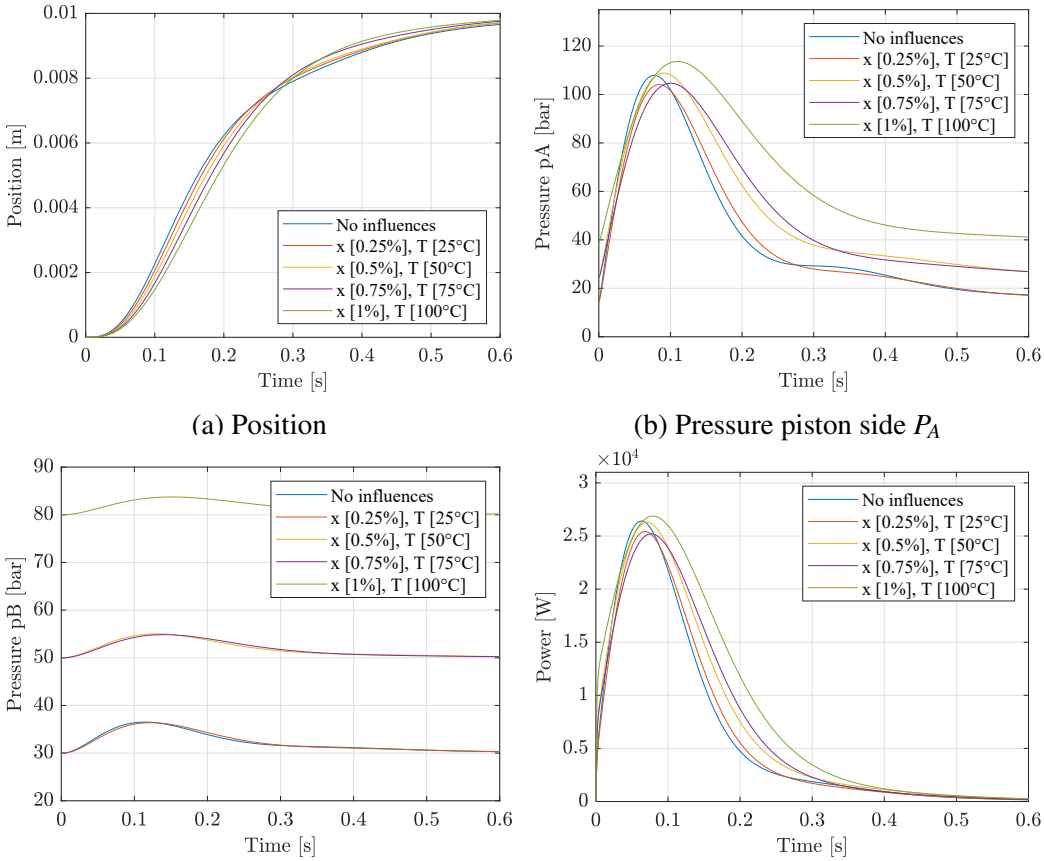

(a) Position

(b) Pressure piston side P_A

(c) Pressure rod side P_B

(d) Power Consumption

Figure 4.8: Outputs of the position, the pressures, and the power consumption with implemented adaptive controller. The back pressure is set experimentally at three different values.

an adaptive controller was developed that regulates the back pressure according to the bulk modulus value. Additionally, because the pressure controller reacts much better at lower bulk modulus values than the flow controller 4.2.1, only the bulk modulus value on the flow controlled side was monitored. In agreement with this, the preset values for the back pressure were set experimentally. In Fig.4.9 it can be seen that the information about the bulk modulus change is acquired from the actuator. The information is then sent to the adaptive controller which regulates the back pressure value. It can be seen from Fig. 4.8 that, as a result of the adaptive controller, the pressure curves for P_A are more balanced, and the peak pressure curves are very near. As a result, when we compare the power curves from Fig.4.5 and Fig. 4.8 the difference in used power is obvious. The adaptive controller uses much less energy when the value of the bulk modulus is higher.

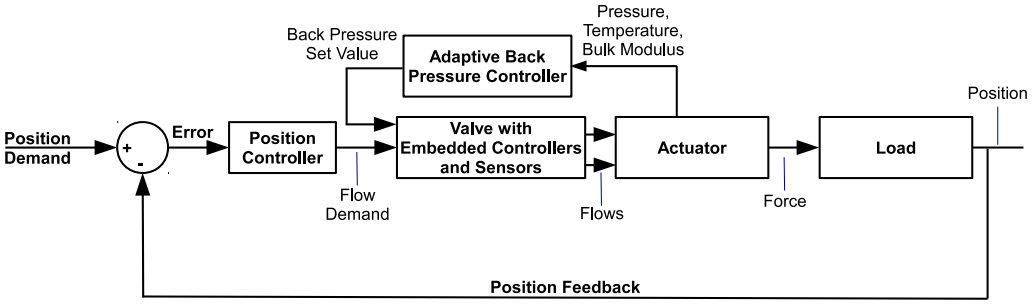

Figure 4.9: Block diagram of the overall system with adaptive back pressure controller. This controller manipulates the back pressure of the system depending on the value of the temperature, pressure and air content in oil.

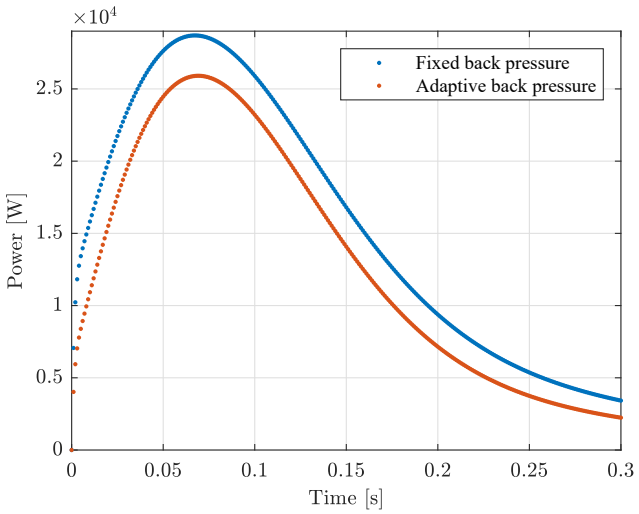

Figure 4.10: Average power consumption for the system with and without adaptive controller.

This improvement is more obvious in Fig. 4.10, where the average consumption for the two scenarios under the given conditions is visible.

Chapter 5

Calculus of Variations Methods for Optimal Control

This chapter derives the fundamentals and solution of two calculus of variation methods for numerically stiff hydraulic systems. The goal was to find the optimal path and implement a path tracking algorithm for the same system that already has embedded controllers in the servo valve. The system is first discretized using the methods described in Chapter 2 and then solved accordingly. Then, the Euler-Lagrange equations are used to minimize the functional. The optimal control method shows better performance compared to LQR and PID controllers. Moreover, both methods show improved energy-efficient performance.

5.1 Introduction

The birth of optimal control is closely connected to the beginnings of the calculus of variations, which stretches back a few centuries. It became very popular in the 1960s with the spectacular success of optimal control trajectory prediction in the aerospace industry [144]. The invitation letter from Bernoulli in year 1969 for the solution of the brachystochrone problem marks the start of the calculus of variation. In his letter, Bernoulli challenged all of the scientists to solve the problem of finding the fastest path between two points in a vertical plane [145]. Multiple authors submitted their results, including Leibnitz, l'Hopital, Newton etc., and they were collected and published by Euler in 1744 in [146]. Before Lagrange, most solution techniques were geometric and not analytical. In 1755, Lagrange offered an analytical approach based on perturbations of the optimal curve using his multipliers which led to the Euler - Lagrange equation [144]. More about early and today's history of the calculus of variations can be found in [147], [148], [149].
Today, the calculus of variation is used in many optimization problems, which dif-

fer from the ordinary calculus of variations problems. Lev Pontryagin and Francis Clarke are some of the most popular authors known for developing new methods using calculus of variation for optimal control theory that are used even nowadays [150], [151]. The most important quantity used in calculus of variations is a functional. A functional can be defined as a correspondence that assigns a definite (real) number to each function (curve) belonging to some class [152]. Calculus of variations is often used to find the extrema of given functions and find curves or surfaces that optimize some process defined by a given cost function. This covers very well the problems that arise very often in mining machinery, for instance: path planning and bringing one hydraulic system from one point to another in the shortest amount of time. These two problems are explained in more detail and solved for the system given in chapter 3.1.1 in section 5.5 and 5.6. Basically, in the calculus of variation, a function is needed, which minimizes a certain integral, facilitating the Euler - Lagrange equations. Or, in Harker's words: 'by introducing variations in functions, it can be shown that a function that minimizes a given functional must satisfy a differential equation' [57].
In this chapter, the calculus of variation will be used to solve several optimal control problems. The numerical stiffness of the system shown in chapter 3 is an enormous challenge when using such methods. Additionally, the system's complexity (non-linearity) and the additional controllers already implemented in the valve make the task even more demanding. However, with the improvements made to the system in Chapter 3 and the numerical methods presented in Chapter 2, an accurate solution can be obtained.

5.2 Partial Differential Equations (PDE)

The research containing first-order PDE dates back to the 18th century. Alex-Claude Clairaut was the first one to encounter PDE's in his work on the shape of the earth [153]. Partial differential equations (PDEs) are equations that contain multiple independent variables (x,y,...), a dependent variable ($u(x,y,...)$), and one or more partial derivatives of the dependent variable. The variable u which we differentiate is called the dependent variable, whereas the variables one differentiates with respect to are called the independent variables [154]. A PDE is an identity that relates the independent variables, the dependent variable u and the partial derivatives of u [155]. This can be written as

$$F(x,y,u(x,y),u_x(x,y),u_y(x,y)) = F(x,y,u,u_x,u_y) = 0. \tag{5.1}$$

where $u_x = \frac{\partial u}{\partial x}$, $u_y = \frac{\partial u}{\partial y}$. If this is extended for a second order, one gets

$$F(x,y,u(x,y),u_x(x,y),u_y(x,y),u_{xx},u_{xy},u_{yy}) = 0, \tag{5.2}$$

where $u_{xx} = \frac{\partial u}{\partial x^2}$, $u_{xy} = \frac{\partial u}{\partial x \partial y}$ and $u_{yy} = \frac{\partial u}{\partial y^2}$. The simplest first order PDE, also known as the transport equation, can be expressed as

$$\begin{aligned} \frac{\partial}{\partial t}u(x,t) + k\frac{\partial}{\partial x}u(x,t) &= 0 \\ u(x,t_0) &= f(x). \end{aligned} \tag{5.3}$$

PDEs are very often used to describe physical processes that happen in nature, such as heat flow, fluid dynamics, electricity, and so on. One of the most commonly used equations in engineering is the heat (diffusion) equation

$$u_{xx}(x,t) + u_x(t) = l(x,t). \tag{5.4}$$

Since it defines how a particular distribution changes (evolves) over time, it is also known as an evolution equation. For the solution of this equation, one can use the Robin boundary conditions as described in [57]. Solving PDEs with matrices numerically is not an easy task. To do so, one must first discretize the dependent variable $u(x,t)$ for both independent variables and their partial derivatives. The dependent variable can be discretized in matrix form as,

$$\mathsf{U} = \begin{bmatrix} u(x_1,t_0) & u(x_1,t_1) & \dots & u(x_1,t_f) \\ u(x_2,t_0) & u(x_2,t_1) & \dots & u(x_2,t_f) \\ \vdots & \vdots & \ddots & \vdots \\ u(x_n,t_0) & u(x_n,t_1) & \dots & u(x_n,t_f) \end{bmatrix} \tag{5.5}$$

If this is extended for the two derivative matrices of x and the time dimension t, the partial derivatives can be discretized as

$$\begin{aligned} \mathsf{U}_x &= \mathsf{D}_x\mathsf{U}, \\ \mathsf{U}_t &= \mathsf{U}\mathsf{D}_t^T. \end{aligned} \tag{5.6}$$

In this manner, the discretized solution of the PDE can be expressed in matrix form. The numerical solution of this PDE is the constrained solution of the linear matrix equation given the boundary conditions.

5.3 The Method of Lagrangian Multipliers

The area of Lagrangian multiplier methods for constrained optimization starts with introducing augmented Lagrangian function and methods of multipliers in 1968 by Hestens and Powell [156]. To grasp the idea of constrained optimization via Lagrangian multipliers, let us consider a straightforward example. Let us

suppose we have two distinct points: A and B and the task is to find the shortest distance between these points. The answer is obviously a straight line connecting the two points. What will happen to the solution if one adds some constraint to the problem? For example, let us find the shortest distance between A and B, but touching some line g. This now becomes a constrained optimization problem that can be easily solved using the Lagrangian multipliers. Since we choose that the minimal path line and the constrained line g are to be tangent, they both have the same slope at that point. Following this, one gets

$$\frac{\partial f}{\partial x} || \frac{\partial g}{\partial x} \quad so \quad \frac{\partial f}{\partial x} = \lambda \frac{\partial g}{\partial x}, \tag{5.7}$$

which leads to the method of Lagrangian multipliers for constrained optimization. If we consider the example for $g(x) = 0$ one can minimize the function $f(x)$ in a few steps. First, one must define the Lagrangian function,

$$\mathscr{L}(x, \lambda) = f(x) - \lambda g(x). \tag{5.8}$$

Secondly, one must differentiate with regards to x and λ

$$\begin{aligned} \frac{\partial \mathscr{L}}{\partial x} &= \frac{\partial f}{\partial x} - \lambda \frac{\partial g}{\partial x}, \\ \frac{\partial \mathscr{L}}{\partial \lambda} &= -g(x). \end{aligned} \tag{5.9}$$

The Lagrange multipliers turns a constrained problem in one variable x into and unconstrained problem into two variables x and λ Eq. 5.9. More details on how Lagrangian multipliers are used in calculus of variation problems can be found in [157].

5.3.1 Least Squares with Equality Constrains via Lagrangian Multipliers

The least-square problem was already discussed in section 2.6, where the problem for constrained optimization was solved via the SVD. To solve the linear square problem subject to a set of linear constraints via the Lagrangian multipliers, one must first define the linear function, and the constraints in the following manner

$$\min ||\mathsf{H}\boldsymbol{\gamma} - \boldsymbol{b}||_2^2 \quad \text{subject to} \quad \mathsf{G}^T\boldsymbol{\gamma} = \boldsymbol{d}. \tag{5.10}$$

Following this, the Lagrangian functional can be written as

$$\mathscr{L}(\boldsymbol{\gamma}, \boldsymbol{\lambda}) = \frac{1}{2}||\mathsf{H}\boldsymbol{\gamma} - \boldsymbol{b}||_2^2 - \boldsymbol{\lambda}^T(\mathsf{G}^T\boldsymbol{\gamma} - \boldsymbol{d}). \tag{5.11}$$

If one follows the same steps as in section 5.3, differentiating w.r.t. both $\boldsymbol{\gamma}$ and $\boldsymbol{\lambda}$ one can find the stationary points by solving the following set of equations

$$\begin{aligned} \mathsf{H}^T\mathsf{H}\boldsymbol{\gamma} - \mathsf{H}^T\boldsymbol{b} - \mathsf{G}\boldsymbol{\lambda} &= \mathbf{0} \\ -\mathsf{G}^T\boldsymbol{\gamma} + \boldsymbol{d} &= \mathbf{0}, \end{aligned} \tag{5.12}$$

or in matrix form

$$\begin{bmatrix} \mathsf{H}^T\mathsf{H} & -\mathsf{G} \\ -\mathsf{G}^T & 0 \end{bmatrix} \begin{bmatrix} \boldsymbol{\gamma} \\ \boldsymbol{\lambda} \end{bmatrix} = \begin{bmatrix} \mathsf{H}^T\boldsymbol{b} \\ -\boldsymbol{d} \end{bmatrix}. \tag{5.13}$$

This becomes an unconstrained problem, which can be solved by any means of matrix inversion (singular value decomposition (SVD), QR decomposition [57]). From Eq. 5.13 it can be seen that the LSE problem under the right circumstances can have a unique solution even if the matrix H is not invertible. This is true if the coefficient matrix of this equation is invertible.

5.4 Euler Lagrange Equations

Variational calculus addresses a wide array of minimization problems. In this section, we will focus on the path minimization problems that focus on our research. To explain this minimization problem, one must start with what might be called

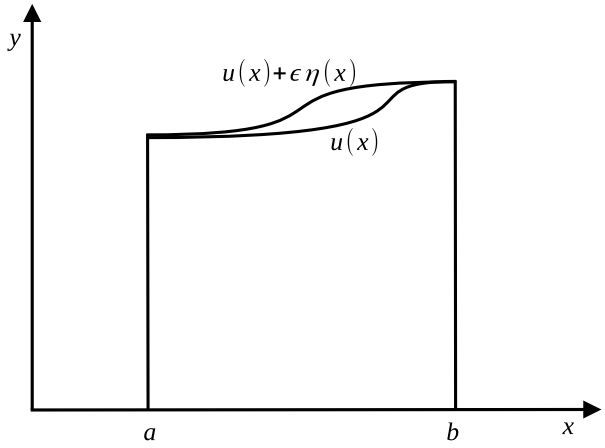

Figure 5.1: Shortest path between two points

the 'simplest' variational problem [152]. What we want is to find the function $y(x)$ such that the following functional is stationary.

$$J = \int_a^b F(x, y, y')dx, \tag{5.14}$$

where $u(x)+\varepsilon\eta(x)$ is the first variation of the minimizing solution $u(x)$. The functional subject to boundary conditions should be minimized. The boundary conditions can be defined as

$$\begin{aligned} a_{11}y(a)+a_{12}y'(a)&=c_1,\\ a_{21}y(b)+a_{22}y'(b)&=c_2. \end{aligned} \tag{5.15}$$

respectively at $x=a$ and $x=b$. Equation 5.14 can also be rewritten as

$$J(\varepsilon)=\int_a^b F(x,y,D_1y)dx. \tag{5.16}$$

where D_1 is a linear differential operator which was already mentioned in section 2.4. The differential operator can be of n^{th} degree and also fractional order derivative. In our case D_1 is the first derivative as given in Eq. 5.14. Now, let's introduce a function (variation) $\eta(x)$ such that $\eta(a)=\eta(b)=0$. Additionally, let's define a function $\bar{y}$ such that

$$\bar{y}=u(x)+\varepsilon\eta(x). \tag{5.17}$$

In Eq. 5.17 $\bar{y}$ represents a family of curves which satisfies the same boundary conditions as y. The idea now is to find $\bar{y}$ which makes J stationary. If we substitute Eq. 5.17 into Eq. 5.14 we get

$$J=\int_a^b F(x,u(x)+\varepsilon\eta(x),u'(x)+\varepsilon\eta'(x))dx. \tag{5.18}$$

Since the functional given in Eq. 5.14 depends on ε one can very easily make J stationary by differentiation with respect to ε and equating this equation to zero. This gives

$$\int_a^b \frac{\partial}{\partial\varepsilon}F(x,u(x)+\varepsilon\eta(x),u'(x)+\varepsilon\eta'(x))dx=0. \tag{5.19}$$

By differentiating one gets

$$\int_a^b(\eta(x)F_y+\eta'(x)F_{y'})dx=\int_a^b(\eta(x)F_y)dx+\int_a^b(\eta'(x)F_{y'})dx=0. \tag{5.20}$$

By integrating by parts only one term of the equation, one gets

$$\int_a^b(\eta'(x)F_{y'})dx=(F_{y'}\eta(x))|_a^b-\int_a^b(\frac{\partial}{\partial x}F_{y'}\eta(x))dx. \tag{5.21}$$

Knowing that the η at the extremes is zero one gets

$$\int_a^b(\eta'(x)F_{y'})dx=-\int_a^b(\frac{\partial}{\partial x}F_{y'}\eta(x))dx. \tag{5.22}$$

Following the same step for the first integral in Eq. 5.20 and combining both of them one gets

$$J'(0) = \int_a^b (F_y - \frac{\partial}{\partial x} F_{y'})\eta(x)dx = 0. \tag{5.23}$$

From Eq. 5.17 it is obvious that the functional is stationary when $\varepsilon = 0$. Because η is an arbitrary function, the only way this integral is guaranteed to be zero is if

$$F_y - \frac{\partial}{\partial x} F_{y'} = 0, \tag{5.24}$$

which represents the Euler Lagrange Equation. For the functional defined with Eq. 5.16 the Euler Lagrange equation can be derived in a similar manner [57].

5.5 Optimal Control for Numerically Stiff Independent Metering System

The hydraulic system presented in section 3.2.3 consists of independent metering valves, which are controlled independently. These valves offer very flexible control strategies for handling inertia loads [126], [79]. However, the systems' servo valves react significantly quicker than the load's inherent frequency, which creates a numerically stiff system [158], [159], [2]. This, and the system's complexity, poses a challenging task to solve it numerically. Additionally, in [160], Rath shows that the exponential matrix method yields an unstable solution to such systems.

Before we start with the optimal control problem, we need to modify the system to improve its numerical stiffness. This is done using the mass matrix presented in Eq. 2.10. Following this, the system presented in Eq. 3.55 can be modified in this manner,

$$\Pi = \begin{bmatrix} \frac{1}{\beta} & 0 & 0 & 0 \\ 0 & \frac{1}{\beta} & 0 & 0 \\ 0 & 0 & 1 & 0 \\ 0 & 0 & 0 & m \end{bmatrix}, \quad \mathsf{A} = \begin{bmatrix} -C_{p_1}\frac{\beta}{V_A} & 0 & -k_A C_{q_1}\frac{\beta}{V_A} & -A_A\frac{\beta}{V_A} \\ 0 & -\left(k_B C_{q_2} + C_{p_2}\right)\frac{\beta}{V_B} & 0 & -A_B\frac{\beta}{V_B} \\ 0 & 0 & 0 & 1 \\ \frac{A_A}{m} & -\frac{A_B}{m} & 0 & -\frac{b}{m} \end{bmatrix},$$

$$\boldsymbol{x} = \begin{bmatrix} P_A \\ P_B \\ y_1 \\ v \end{bmatrix}, \quad \mathsf{B} = \begin{bmatrix} k_A C_{q_1}\frac{\beta}{V_A} & 0 \\ 0 & -k_B C_{q_2}\frac{\beta}{V_B} \\ 0 & 0 \\ 0 & 0 \end{bmatrix}, \quad \boldsymbol{u} = \begin{bmatrix} y_{set} \\ P_{Bset} \end{bmatrix}. \tag{5.25}$$

It is important to note here that a portion of the numerical values for the bulk modulus β and the mass m appears in the mass matrix Π. This step decreases

the numerical stiffness of Eq. 2.10 on the right-hand side of the equation. Historically, numerous attempts have been made to solve the optimal control problem for numerically stiff hydraulic systems. Rath uses the Hamiltonian in [94] to find the optimal hydraulic systems flow. Even with a friction parameter of zero, the system shows stable performance without oscillations. In [161], Dupree solves the Hamiltonian Jakobi Bellman equation using the implicit learning capabilities of the robust integral of the sign of the error (RISE) control. Additional methods like the Lagrangian force method [162] linear quadratic regulator (LQR) [163], [164] have also been used to solve the optimal control problem for hydraulic systems. However, most of these systems lack the complex control algorithm of the system presented in chapter 3.In this section, the mass matrix and interstitial derivatives are used to construct a new strategy for solving the optimal control problem (Euler-Lagrange equations) for numerically stiff systems.

5.5.1 Numerical Solution of the Optimal Control Problem

The idea of optimal control is to move the system from one state to a new one in an optimal manner. In our case, the system's mass shown in Fig. 3.3 must be moved in an optimal way from its initial state $x(t_0)$ to the new state $x(t_f)$. This may be accomplished by minimizing the control variable's norm

$$\int_{t_0}^{t_f} \boldsymbol{u}^T(t)\boldsymbol{u}(t)dt, \tag{5.26}$$

where t_0 and t_f represent the start and final value of the time vector. Before minimizing the control variable norm, one must consider that the system must satisfy a set of differential equations subject to boundary values. This creates a constrained optimization problem that can be addressed using methods from the Calculus of Variations, namely the Lagrange multiplier approach already derived in section 5.3. The functional that has to be minimized will therefore have the following form:

$$\begin{aligned} J(\boldsymbol{x}(t),\dot{\boldsymbol{x}}(t),\boldsymbol{u}(t),\boldsymbol{\lambda}(t)) &= \frac{1}{2}\int_{t_0}^{t_f} \boldsymbol{u}^{\mathrm{T}}(t)\,\boldsymbol{u}(t)\,\mathrm{dt} \\ -\int_{t_0}^{t_f} \boldsymbol{\lambda}^{\mathrm{T}}(t)\,(\Pi\dot{\boldsymbol{x}}(t) - \mathsf{A}\boldsymbol{x}(t) - \mathsf{B}\boldsymbol{u}(t))\,\mathrm{dt} \end{aligned} \tag{5.27}$$

Equation 5.27 can now be solved using the variational approach (Euler Lagrange equations) given in Eq. 5.24. This yields the following solution

$$\begin{aligned} &A^{\mathrm{T}}\boldsymbol{\lambda}(t) + \Pi^{\mathrm{T}}\dot{\boldsymbol{\lambda}}(t) = \mathbf{0}. \\ &\mathsf{B}^T\boldsymbol{\lambda}(t) + \boldsymbol{u}(t) = \mathbf{0} \\ &\Pi\dot{\boldsymbol{x}}(t) - \mathsf{A}\boldsymbol{x}(t) + \mathsf{B}\boldsymbol{u}(t) = \mathbf{0} \end{aligned} \tag{5.28}$$

By substituting the second equation for the control into the third equation, one gets a system of two differential equations which can be expressed as

$$\begin{aligned} \Pi\dot{\boldsymbol{x}}(t) &= \mathsf{A}\boldsymbol{x}(t) - \mathsf{B}\mathsf{B}^T\boldsymbol{\lambda}(t) \\ \Pi^{\mathrm{T}}\dot{\boldsymbol{\lambda}}(t) &= -A^{\mathrm{T}}\boldsymbol{\lambda}(t). \end{aligned} \tag{5.29}$$

These equations can then be written in matrix form as

$$\Pi_1\dot{\boldsymbol{\gamma}}(t) - \mathsf{A}_1\boldsymbol{\gamma}(t) = \mathbf{0} \tag{5.30}$$

where

$$\Pi_1 = \begin{bmatrix} \Pi & 0 \\ 0 & \Pi^{\mathrm{T}} \end{bmatrix}, \boldsymbol{\gamma}(t) = \begin{bmatrix} \boldsymbol{x}(t) \\ \boldsymbol{\lambda}(t) \end{bmatrix} \tag{5.31}$$

and

$$\mathsf{A}_1 = \begin{bmatrix} \mathsf{A} & -\mathsf{B}B^{\mathrm{T}} \\ 0 & -A^{\mathrm{T}} \end{bmatrix}. \tag{5.32}$$

This system can now be discretized following the methods shown in section 2.5. The same goes for the initial and boundary values which can be defined as

$$\begin{aligned} \boldsymbol{I_C} &= \begin{bmatrix} P_A(t_0) & P_B(t_0) & y_1(t_0) & y_2(t_0) \end{bmatrix}^{\mathrm{T}} \\ \boldsymbol{B_C} &= \begin{bmatrix} P_A(t_f) & P_B(t_f) & y_1(t_f) & y_2(t_f) \end{bmatrix}^{\mathrm{T}} \end{aligned} \tag{5.33}$$

where $\boldsymbol{I_C}$ and $\boldsymbol{B_C}$ represent real physical values of the system. To be able to discretize Eq. 5.34 must be first transposed in the following form

$$\dot{\boldsymbol{\gamma}}^{\mathrm{T}}(t)\,\Pi_1{}^{\mathrm{T}} - \boldsymbol{\gamma}^{\mathrm{T}}(t)A_1{}^{\mathrm{T}} = \mathbf{0} \tag{5.34}$$

Now, following the method presented in section 2.5 and 2.5.1 one can discretize this system at the interstitial points i.e. between the samples $t_k < s_k < t_{k+1}$ for $k = 1, \ldots, n-1$. Following this, the state of the system over time, discretized at time instances can be written in discretized matrix form as

$$\begin{bmatrix} \boldsymbol{\gamma_1}^{\mathrm{T}} \\ \boldsymbol{\gamma_2}^{\mathrm{T}} \\ \vdots \\ \boldsymbol{\gamma_n}^{\mathrm{T}} \end{bmatrix} = \begin{bmatrix} \gamma_1(t_0) & \gamma_1(t_1) & \ldots & \gamma_1(t_f) \\ \gamma_2(t_0) & \gamma_2(t_1) & \ldots & \gamma_2(t_f) \\ \vdots & \vdots & \ddots & \vdots \\ \gamma_n(t_0) & \gamma_n(t_1) & \ldots & \gamma_n(t_f) \end{bmatrix} D_0{}^{\mathrm{T}} = \Gamma^{\mathrm{T}} D_0{}^{\mathrm{T}}, \tag{5.35}$$

where D_0 is an interstitial linear operator already derived in section 2.4.2. The rule applies to the derivatives of the state vector

$$\begin{bmatrix} \dot{\boldsymbol{\gamma}}_{\mathbf{1}}^{\mathrm{T}} \\ \dot{\boldsymbol{\gamma}}_{\mathbf{2}}^{\mathrm{T}} \\ \vdots \\ \dot{\boldsymbol{\gamma}}_{\boldsymbol{n}}^{\mathrm{T}} \end{bmatrix} = \begin{bmatrix} \gamma_1(t_0) & \gamma_1(t_1) & \ldots & \gamma_1(t_f) \\ \gamma_2(t_0) & \gamma_2(t_1) & \ldots & \gamma_2(t_f) \\ \vdots & \vdots & \ddots & \vdots \\ \gamma_n(t_0) & \gamma_n(t_1) & \ldots & \gamma_n(t_f) \end{bmatrix} D_1{}^{\mathrm{T}} = \Gamma^{\mathrm{T}} D_1{}^{\mathrm{T}}, \tag{5.36}$$

where D_1 is the interstitial derivative linear operator already derived in section 2.4.2. Combining the last three equations, one gets the system in discretized form,

$$\mathsf{D}_1 \Gamma \Pi_1{}^{\mathrm{T}} - \mathsf{D}_0 \Gamma A_1{}^{\mathrm{T}} = 0 \tag{5.37}$$

where Γ is a matrix derived from the discretization of $\boldsymbol{\gamma}$. Vectorizing Eq 5.37 one gets a system of linear equations which can be expressed as

$$(\Pi_1 \otimes \mathsf{D}_1 - \mathsf{A}_1 \otimes \mathsf{D}_0)\,\mathrm{vec}\,(\Gamma) = 0. \tag{5.38}$$

This system can now be solved for the constraints given in Eq. 5.33. The final form of the system is very similar to the one described in section 2.7.

$$\begin{aligned} \mathsf{L}\boldsymbol{y} &= 0 \\ \mathsf{C}^T \boldsymbol{y} &= \boldsymbol{d} \end{aligned} \tag{5.39}$$

where

$$\mathsf{L} = (\Pi_1 \otimes \mathsf{D}_1 - \mathsf{A}_1 \otimes \mathsf{D}_0), \quad \boldsymbol{y} = \mathrm{vec}\,(\Gamma) \tag{5.40}$$

$$\mathsf{C} = \begin{bmatrix} \mathsf{E} & 0 & 0 & 0 & 0 & \dots & 0 \\ 0 & \mathsf{E} & 0 & 0 & 0 & \dots & 0 \\ 0 & 0 & \mathsf{E} & 0 & 0 & \dots & 0 \\ 0 & 0 & 0 & \mathsf{E} & 0 & \dots & 0 \end{bmatrix}^{\mathrm{T}}, \tag{5.41}$$

$$\boldsymbol{d} = \left[\boldsymbol{I_C}^{\mathrm{T}}, \boldsymbol{B_C}^{\mathrm{T}}\right]^{\mathrm{T}}. \tag{5.42}$$

In addition to that, the matrix E is $2 \times n$ matrix where n is the number of steps used for discretiztation. The matrix E has the form

$$\mathsf{E} = \begin{bmatrix} 1 & 0 & \dots & 0 \\ 0 & 0 & \dots & 1 \end{bmatrix}. \tag{5.43}$$

The solution of the system presented in Eq. 5.39 can be found using the singular value decomposition as described in section 2.7.

$$\mathsf{L} = \mathsf{U}\mathsf{S}\mathsf{V}^T = \begin{bmatrix} \mathsf{U}_\mathsf{r} & \tilde{\mathsf{U}} \end{bmatrix} \begin{bmatrix} \mathsf{S}_\mathsf{r} & 0 \\ 0 & \Delta \end{bmatrix} \begin{bmatrix} \mathsf{V}_\mathsf{r}{}^T \\ \tilde{\mathsf{V}}^T \end{bmatrix}, \tag{5.44}$$

where Δ is a block matrix with zero or very small singular values and r is the rank of the matrix L, imposed by the order of the set of ODE and the number of boundary conditions. It is worth noting that the columns of $\tilde{\mathsf{V}}$ serve as a basis for L's nullspace (which are the homogeneous solutions), hence the solution to the equation $\mathsf{L}\boldsymbol{y} = \mathbf{0}$ will be in the form of

$$\boldsymbol{y} = \tilde{\mathsf{V}}\boldsymbol{\alpha}, \tag{5.45}$$

where $\boldsymbol{\alpha}$ is the vector of parameters. To solve for the parameter values $\boldsymbol{\alpha}$ one must use the constraints given in Eq. 5.39. Following this, one gets

$$\begin{aligned} &\mathsf{C}^T\boldsymbol{y} = \mathsf{C}^T\tilde{\mathsf{V}}\boldsymbol{\alpha} = \boldsymbol{d}, \quad \text{and thus} \\ &\boldsymbol{\alpha} = \left(\mathsf{C}\tilde{\mathsf{V}}\right)^{-1}\boldsymbol{d}, \end{aligned} \tag{5.46}$$

which leads to the solution of the equations in the form

$$\boldsymbol{y} = \tilde{\mathsf{V}}\left(\mathsf{C}\tilde{\mathsf{V}}\right)^{-1}\boldsymbol{d}. \tag{5.47}$$

5.5.2 Experimental Results

In the previous section, the derivation of the optimal control equations for the system shown in Fig. 3.3 was made. To test the system performance, one needs first to define the system parameters. Because the experiment is done for the same system (just linearized), one can use the same parameters as given in section 4.2 with some minor modifications. The value of the back pressure P_B is going to be adjusted accordingly. In addition, the linearized terms C_{q_1},C_{q_2},C_{p_1} and C_{p_2} values were computed for a supply pressure of $300 \cdot 10^5$ Pa with the assumption that the initial values for the pressures on both sides will be $10 \cdot 10^5$ Pa. The values for the proportional controllers k_A and k_B were set experimentally. The same applies for the LQR controller where the weighting matrices Q and R have the following values

$$Q = \begin{bmatrix} 0 & 0 & 0 & 0 \\ 0 & 0 & 0 & 0 \\ 0 & 0 & 0.001 & 0 \\ 0 & 0 & 0 & 0.001 \end{bmatrix}, R = \begin{bmatrix} 0.1 & 0 & 0 \\ 0 & 0.1 & 0 \\ 0 & 0 & 0.1 \end{bmatrix}. \tag{5.48}$$

After that, the optimal control solution was compared to PID and LQR controllers. The major goal was to compare these two controllers' outcomes to the optimal control solution. In this experiment, performance and energy efficiency were defined as key considerations.

For the same system, two different experiments were carried out. For both scenarios the initial values vector is defined as $\boldsymbol{I_C} = \begin{bmatrix} 0 & 0 & 0 & 0 \end{bmatrix}^{\mathrm{T}}$. For the first scenario, the system was simulated for a time of $t \in$ [0,0.3]s. The boundary values vector for this scenario is defined as $\boldsymbol{B_C} = \begin{bmatrix} 0 & 0 & 0.01 & 0 \end{bmatrix}^{\mathrm{T}}$. The input for the position of the PID and LQR controllers is a predefined step function with an amplitude of $y_1 = 0.01$m. The back pressure P_B final value is equal to zero. It is evident from Fig. 5.2 that the optimal control method satisfies the defined constraints at the predefined points. On the other hand, the LQR and the PID controllers overshoot and do not meet the final values at the exact points. Moreover,

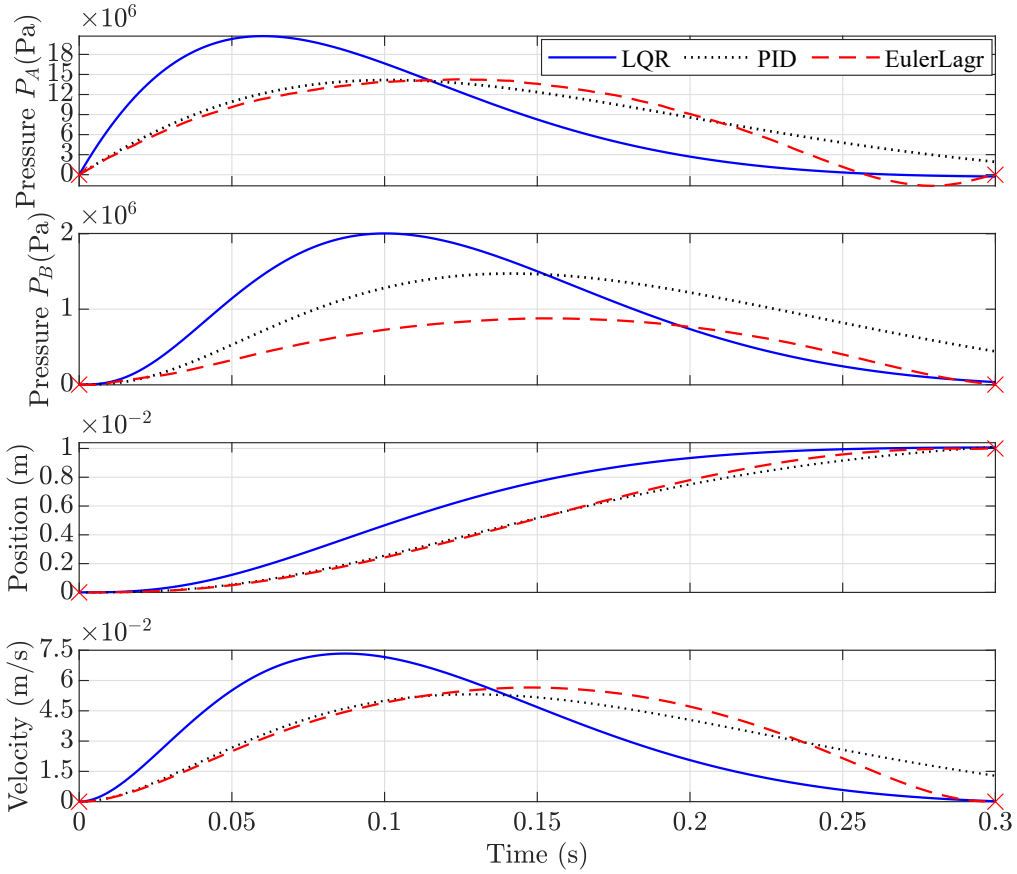

Figure 5.2: The first simulation results ($t \in [0,0.3]$s), with all initial conditions and final values are set to zero, except for the end position, which is set to $y_1 = 0.01\,m$. It can be observed that the LQR and PID controllers overshoot and do not terminate at the required values for position and pressure P_B. On the other hand, the optimal control method satisfies the defined constraints at precise points. It also outperforms PID and LQR in terms of energy efficiency, as evidenced by the velocity and the pressure P_A curves [128].

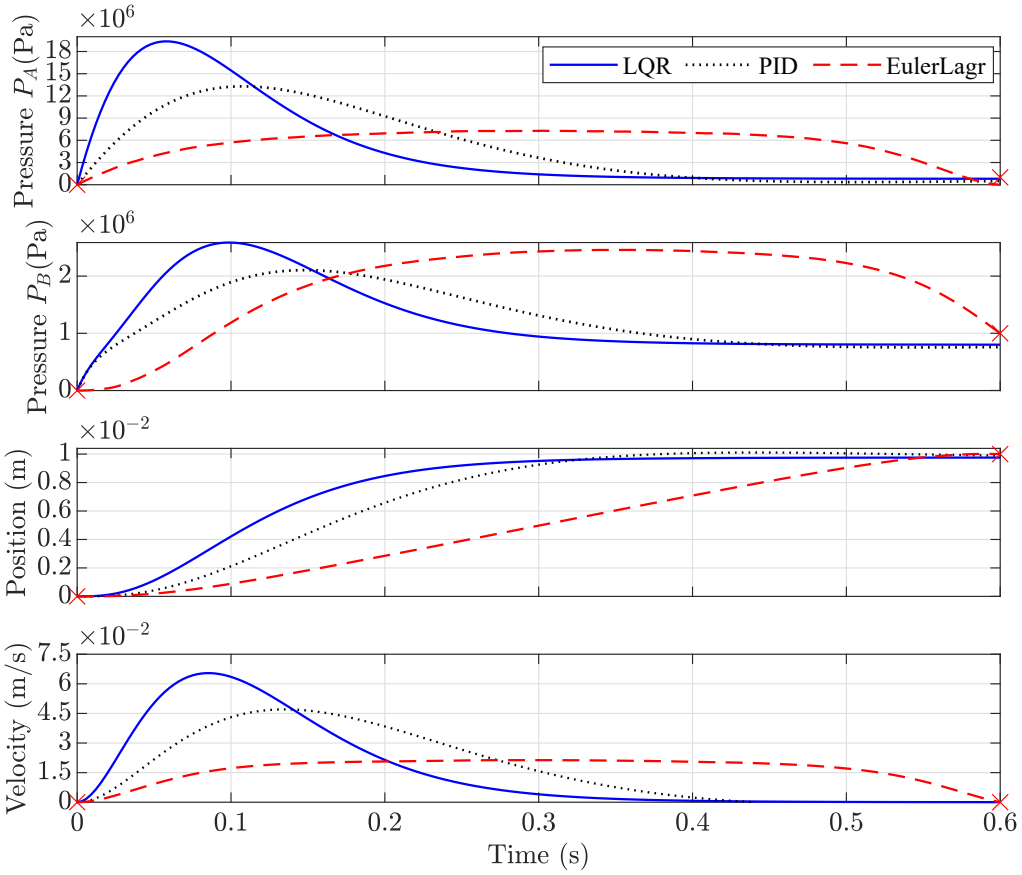

Figure 5.3: The second simulation results ($t \in [0,0.6]$s), with all initial conditions are set to zero, except for the end position, which is set to $y_1 = 0.01\,m$ and back pressure $P_B = 10 \cdot 10^5$. It can be observed that the LQR and PID controllers have a steady-state error and do not terminate at the required values for the position and the pressure P_B. On the other hand, the optimal control method satisfies the defined constraints at precise points. It also outperforms PID and LQR in terms of energy efficiency, as evidenced by the velocity and the pressure P_A curves [128].

the optimal control method has much better energy efficiency when compared with these two methods. For the second scenario, the simulation time was extended to $t \in [0,0.6]$s. The boundary values vector for this scenario is defined as $\boldsymbol{B_C} = \begin{bmatrix} 0 & 10 \cdot 10^5 & 0.01 & 0 \end{bmatrix}^{\mathrm{T}}$. It is obvious that the position value is unchanged and the back pressure value is $P_B = 10 \cdot 10^5$. The back pressure P_B final value is equal to zero. Figure 5.3 shows that in this case, as in the previous one, the optimal control method achieves the desired values for the position and the pressure at the exact values. On the other hand, the PID and the LQR control, once again, show

performance which overshoots. In this case, as in the previous one, the optimal control method significantly improves the energy efficiency of the system.

5.6 Multidimensional Trajectory Tracking for Numerically Stiff Independent Metering System

Tunnel boring machines usually have a predefined profile that needs to be cut. In most circumstances, the system must follow a predetermined course [165][166]. This is the main reason why path tracking algorithms are appropriate for these systems. Additionally, in mining equipment navigation, optimal path tracking is commonly employed instead of other traditional approaches. It improves efficiency and cuts down working time, which improves safety [167],[168]. Model predictive control (MPC) [169], [170] is one of the most often utilized approaches because it can account for the system's constraints [171]. Path tracking is very often used for controlling hydraulic manipulators [172]. To correct and detect the non-linearity of static dead zone input signals, Rudolfsen uses the inverse [173]. The optimal control input for multi-dimensional path tracking of a hydraulic crane controlled by electric motors is determined using a global least-squares technique in [174]. The sliding perturbation observer (SPO) is used to build a new control rule in [175]. The SPO is employed here to minimize all environmental disturbances, dynamic uncertainties, and modeling mistakes. Additional methods like the contour tracking methods [176], D-H (Denavit - Hartenberg) parameters [177], and a PD controller [178] are also very often used to solve the path tracking problem.

All of the approaches described above, however, are focused on tracking one or more parameters with the same unit and magnitude, and in most situations, the position of the provided system is tracked. The hydraulic circuits used in tunnel boring equipment are very complex. In our case, the system presented in Fig. 3.3 has already implemented control inside the valve embedded controllers. The pressure settings on the pressure controllers are very high to compensate for the significant external forces produced by the cutting process. This increases the mechanical stiffness of the hydraulic system, which increases the system's overall mechanical stiffness. Consequently, the high values for the external forces and pressure on one side and the very low values for the valve parameters on the other side make this system numerically stiff. For this reason, as mentioned in the previous section, the mass matrix method and interstitial derivatives are used to obtain a stable solution. The approach suggested in this section, which is based on optimal control theory, uses variational calculus to solve the path tracking issue as a boundary value problem. To demonstrate the method's potential, it is next applied

to a simulated model of the actual system. The results show that the variables tracked can be tracked accurately, although they do not have the same units.

5.6.1 Numerical Solution of the Multidimensional Path Tracking Problem

The path tracking method may be stated as identifying the input vector $\boldsymbol{u}$ in order to obtain the system's intended output. In terms of variational calculus, this issue may be phrased as finding the ideal input vector $\boldsymbol{u}$ for which the cost function is minimized Eq. 5.25

$$\frac{\mu_1^2}{2}\int_{t_0}^{t_f}\left(x_2(t)-\xi_2(t)\right)^2\mathrm{dt}+\frac{\mu_2^2}{2}\int_{t_0}^{t_f}\left(x_3(t)-\xi_1(t)\right)^2\mathrm{dt} \tag{5.49}$$

Taking into account how the vector $\boldsymbol{u}$ is defined Eq. 5.25, x_2 tracks ξ_2 and x_3 tracks ξ_1. Because the states $x_2(t)$ and $x_3(t)$ are of different units and order of magnitude, the least square difference must be normalized. The parameters μ_1 and μ_2 in Eq. 5.49 are used to do this. Additionally, the integrals quantify the least-squares differences between the states $x_2(t)$, $x_3(t)$, and the respective desired outputs $\xi_2(t)$, $\xi_1(t)$[179]. Following this, the equation 5.49 can now be rewritten as

$$\frac{\mu_1^2}{2}\int_{t_0}^{t_f}\left(\boldsymbol{e}_2^{\mathrm{T}}\boldsymbol{x}(t)-\xi_2(t)\right)^2\mathrm{dt}+\frac{\mu_2^2}{2}\int_{t_0}^{t_f}\left(\boldsymbol{e}_3^{\mathrm{T}}\boldsymbol{x}(t)-\xi_1(t)\right)^2\mathrm{dt}, \tag{5.50}$$

where $\boldsymbol{e}_2=\begin{bmatrix}0 & 1 & 0 & 0\end{bmatrix}^{\mathrm{T}}$ and $\boldsymbol{e}_3=\begin{bmatrix}0 & 0 & 1 & 0\end{bmatrix}^{\mathrm{T}}$ are coordinate unit vectors. To obtain a unique solution, regularization parameters are implemented [180], which can be expressed as

$$\frac{\mu_3^2}{2}\int_{t_0}^{t_f}\dot{\boldsymbol{u}}^{\mathrm{T}}(t)\,\dot{\boldsymbol{u}}(t)\,\mathrm{dt}+\frac{\mu_4^2}{2}\int_{t_0}^{t_f}\ddot{\boldsymbol{u}}^{\mathrm{T}}(t)\,\ddot{\boldsymbol{u}}(t)\,\mathrm{dt}, \tag{5.51}$$

where μ_3 and μ_4 are the regularization parameters. The regularization parameters are used to physically limit in such manner that the results obtained can be physically achieved by the real system. Combining all these equations, the functional which needs to be minimized can be written as

$$\begin{aligned}
&J(\boldsymbol{x}(t),\boldsymbol{u}(t),\boldsymbol{\lambda}(t))=\\
&\frac{\mu_1^2}{2}\int_{t_0}^{t_f}\left(\boldsymbol{e}_2^{\mathrm{T}}\boldsymbol{x}(t)-\xi_2(t)\right)^2\mathrm{dt}+\frac{\mu_2^2}{2}\int_{t_0}^{t_f}\left(\boldsymbol{e}_3^{\mathrm{T}}\boldsymbol{x}(t)-\xi_1(t)\right)^2\mathrm{dt}\\
&+\frac{\mu_3^2}{2}\int_{t_0}^{t_f}\dot{\boldsymbol{u}}^{\mathrm{T}}(t)\,\dot{\boldsymbol{u}}(t)\,\mathrm{dt}+\frac{\mu_4^2}{2}\int_{t_0}^{t_f}\ddot{\boldsymbol{u}}^{\mathrm{T}}(t)\,\ddot{\boldsymbol{u}}(t)\,\mathrm{dt}\\
&-\int_{t_0}^{t_f}\boldsymbol{\lambda}^{\mathrm{T}}(t)\left(\Pi\dot{\boldsymbol{x}}(t)-\mathsf{A}\boldsymbol{x}(t)-\mathsf{B}\boldsymbol{u}(t)\right)\mathrm{dt}
\end{aligned} \tag{5.52}$$

Because only the ratio between $\mu_1 : \mu_2 : \mu_3 : \mu_4$ is relevant, one of the parameters can be set to 1 (μ_1 =1). To minimize this functional, one can use the Euler Lagrange Equations, which are [152]

$$\begin{aligned}
&\frac{\partial F}{\partial \boldsymbol{x}} - \frac{d}{dt}\frac{\partial F}{\partial \dot{\boldsymbol{x}}} = \mathbf{0} \\
&\frac{\partial F}{\partial \boldsymbol{u}} - \frac{d}{dt}\frac{\partial F}{\partial \dot{\boldsymbol{u}}} + \frac{d^2}{dt^2}\frac{\partial F}{\partial \ddot{\boldsymbol{u}}} = \mathbf{0} \\
&\frac{\partial F}{\partial \boldsymbol{\lambda}} - \frac{d}{dt}\frac{\partial F}{\partial \dot{\boldsymbol{\lambda}}} = \mathbf{0}.
\end{aligned} \tag{5.53}$$

Solving equation 5.53 for the given functional one gets

$$\begin{aligned}
&\boldsymbol{e}_2\boldsymbol{e}_2^{\mathrm{T}}\boldsymbol{x} - \boldsymbol{e}_2\xi_2 + \mu_2^2\boldsymbol{e}_3\boldsymbol{e}_3^{\mathrm{T}}\boldsymbol{x} - \mu_2^2\boldsymbol{e}_3\xi_1 + A^{\mathrm{T}}\boldsymbol{\lambda} + \Pi^{\mathrm{T}}\dot{\boldsymbol{\lambda}} = \mathbf{0}. \\
&B^{\mathrm{T}}\boldsymbol{\lambda} - \mu_3^2\ddot{\boldsymbol{u}} + \mu_4^2\boldsymbol{u}^{(4)} = \mathbf{0} \\
&\Pi\dot{\boldsymbol{x}}(t) + \mathsf{A}\boldsymbol{x}(t) + \mathsf{B}\boldsymbol{u}(t) = \mathbf{0}.
\end{aligned} \tag{5.54}$$

From these equations a system of differential equations can be derived:

$$\begin{aligned}
&\Pi^{\mathrm{T}}\dot{\boldsymbol{\lambda}} = -\mathsf{E}_{23}\boldsymbol{x} + \boldsymbol{e}_2\xi_2 + \mu_2^2\boldsymbol{e}_3\xi_1 - \mathsf{A}^T\boldsymbol{\lambda} \\
&\boldsymbol{u}^{(4)} = -\frac{1}{\mu_4^2}B^{\mathrm{T}}\boldsymbol{\lambda} + \frac{\mu_3^2}{\mu_4^2}\ddot{\boldsymbol{u}} \\
&\Pi\dot{\boldsymbol{x}}(t) = \mathsf{A}\boldsymbol{x}(t) + \mathsf{B}\boldsymbol{u}(t)
\end{aligned} \tag{5.55}$$

where

$$\mathsf{E}_{23} = \boldsymbol{e}_2\boldsymbol{e}_2^{\mathrm{T}} + \mu_2^2\boldsymbol{e}_3\boldsymbol{e}_3^{\mathrm{T}}. \tag{5.56}$$

Combining these equations in a similar manner as in section 5.5.1, the matrix form for Eq. 5.55 is

$$\Pi_1\dot{\boldsymbol{\gamma}}(t) - \mathsf{V}\boldsymbol{\gamma}(t) - \mathsf{W}\boldsymbol{\xi}(t) = \mathbf{0} \tag{5.57}$$

where

$$\begin{aligned}
\Pi_1 &= \begin{bmatrix} \Pi & 0 & 0 & 0 & 0 & 0 \\ 0 & \Pi^{\mathrm{T}} & 0 & 0 & 0 & 0 \\ 0 & 0 & \mathsf{I} & 0 & 0 & 0 \\ 0 & 0 & 0 & \mathsf{I} & 0 & 0 \\ 0 & 0 & 0 & 0 & \mathsf{I} & 0 \\ 0 & 0 & 0 & 0 & 0 & \mathsf{I} \end{bmatrix}, \boldsymbol{\gamma}(\boldsymbol{t}) = \begin{bmatrix} \boldsymbol{x}(t) \\ \boldsymbol{\lambda}(t) \\ \boldsymbol{u}(t) \\ \dot{\boldsymbol{u}}(t) \\ \ddot{\boldsymbol{u}}(t) \\ \boldsymbol{u^{(3)}}(t) \end{bmatrix}, \boldsymbol{\xi} = \begin{bmatrix} \xi_1 \\ \xi_2 \end{bmatrix}, \\
\mathsf{V} &= \begin{bmatrix} \mathsf{A} & 0 & \mathsf{B} & 0 & 0 & 0 \\ -\mathsf{E}_{23} & -A^{\mathrm{T}} & 0 & 0 & 0 & 0 \\ 0 & 0 & 0 & \mathsf{I} & 0 & 0 \\ 0 & 0 & 0 & 0 & \mathsf{I} & 0 \\ 0 & 0 & 0 & 0 & 0 & \mathsf{I} \\ 0 & -\frac{1}{\mu_4^2}B^{\mathrm{T}} & 0 & 0 & \frac{\mu_3^2}{\mu_4^2}\mathsf{I} & 0 \end{bmatrix}, \mathsf{W} = \begin{bmatrix} \mathbf{0} & \mathbf{0} \\ \boldsymbol{e}_2 & \mu_2^2\boldsymbol{e}_3 \\ \mathbf{0} & \mathbf{0} \\ \mathbf{0} & \mathbf{0} \\ \mathbf{0} & \mathbf{0} \\ \mathbf{0} & \mathbf{0} \end{bmatrix}.
\end{aligned} \tag{5.58}$$

This system can be solved numerically by discretizing using the methods shown in [58]. Any state of this system can be discretized in vector form as

$$\boldsymbol{\gamma}_k = \begin{bmatrix} \gamma_k(t_0) & \gamma_k(t_1) & \dots & \gamma_k(t_f) \end{bmatrix}^{\mathrm{T}}. \tag{5.59}$$

Because the discretization is done in the interstitial points (the point t_i between the samples s_i) this can be written as

$$\begin{bmatrix} \gamma_k(t_1) \\ \gamma_k(t_2) \\ \vdots \\ \gamma_k(t_f) \end{bmatrix} = \begin{bmatrix} \gamma_k(s_0) \\ \gamma_k(s_1) \\ \vdots \\ \gamma_k(s_f) \end{bmatrix} \mathsf{J}_0 \tag{5.60}$$

$$\mathsf{J}_0 = \frac{1}{16}\begin{bmatrix} 5 & 15 & -5 & 1 & 0 & \dots & 0 & 0 & 0 & 0 \\ -1 & 9 & 9 & -1 & 0 & \dots & 0 & 0 & 0 & 0 \\ 0 & -1 & 9 & 9 & -1 & \dots & 0 & 0 & 0 & 0 \\ \vdots & \vdots & \vdots & \vdots & \vdots & \ddots & \vdots & \vdots & \vdots & \vdots \\ 0 & 0 & 0 & 0 & 0 & \dots & -1 & 9 & 9 & -1 \\ 0 & 0 & 0 & 0 & 0 & \dots & 1 & -5 & 15 & 5 \end{bmatrix}. \tag{5.61}$$

Expanding the idea for any vector of states γ can be discretized in a matrix form as

$$\boldsymbol{\Gamma}^{\boldsymbol{T}} = \begin{bmatrix} \boldsymbol{\gamma}_1^{\mathrm{T}} \\ \boldsymbol{\gamma}_2^{\mathrm{T}} \\ \vdots \\ \boldsymbol{\gamma}_n^{\mathrm{T}} \end{bmatrix} = \begin{bmatrix} \gamma_1(t_0) & \gamma_1(t_1) & \dots & \gamma_1(t_f) \\ \gamma_2(t_0) & \gamma_2(t_1) & \dots & \gamma_2(t_f) \\ \vdots & \vdots & \ddots & \vdots \\ \gamma_n(t_0) & \gamma_n(t_1) & \dots & \gamma_n(t_f) \end{bmatrix} {J_0}^{\mathrm{T}} \tag{5.62}$$

The derivative of a state can be discretized as

$$\dot{\boldsymbol{\gamma}}_k \approx \mathsf{D}_1 \boldsymbol{\gamma}_k. \tag{5.63}$$

Following the same analogy as for the discretized states the first derivative

$$\Gamma^{\mathsf{T}} = \begin{bmatrix} \dot{\boldsymbol{\gamma}}_1^{\mathrm{T}} \\ \dot{\boldsymbol{\gamma}}_2^{\mathrm{T}} \\ \vdots \\ \dot{\boldsymbol{\gamma}}_n^{\mathrm{T}} \end{bmatrix} = \begin{bmatrix} \gamma_1(t_0) & \gamma_1(t_1) & \dots & \gamma_1(t_f) \\ \gamma_2(t_0) & \gamma_2(t_1) & \dots & \gamma_2(t_f) \\ \vdots & \vdots & \ddots & \vdots \\ \gamma_n(t_0) & \gamma_n(t_1) & \dots & \gamma_n(t_f) \end{bmatrix} {D_1}^{\mathrm{T}} \tag{5.64}$$

Transposing and discretizing Eq. 5.57 one gets

$$\mathsf{D}_1 \Gamma {\Pi_1}^{\mathrm{T}} - \mathsf{J}_0 \Gamma V^{\mathrm{T}} - \mathsf{D}_1 \Xi W^{\mathrm{T}} = 0. \tag{5.65}$$

where Γ and Ξ are the matrices resulting from the discretization of $\boldsymbol{\gamma}$ and $\boldsymbol{\xi}$ respectively. By vectorizing Eq. 5.65, one gets

$$(\Pi_1 \otimes \mathsf{D}_1 - \mathsf{V} \otimes \mathsf{J}_0)\,\mathrm{vec}\,(\Gamma) = (\mathsf{W} \otimes \mathsf{J}_0)\,\mathrm{vec}\,(\Xi) \tag{5.66}$$

which is a linear system of equations. This system is solved using singular value decomposition (SVD). The appropriate number of boundary conditions must be defined to obtain a unique solution. For the system given in Eq. 5.57 one has 16 differential equations for which the boundary conditions are defined as

$$\begin{array}{lll} \gamma_1(t_0) = 0 & & \\ \gamma_1(t_f) = 0 & \gamma_{4-8}(t_0) = 0 & \gamma_{10}(t_0) = \xi_1(t_0) \\ \gamma_2(t_0) = \xi_2(t_0) & \gamma_{4-8}(t_f) = 0 & \gamma_{10}(t_f) = \xi_1(t_f) \\ \gamma_2(t_f) = \xi_2(t_f) & \gamma_9(t_0) = \xi_2(t_0) & \gamma_{11-16}(t_0) = 0 \\ \gamma_3(t_0) = \xi_1(t_0) & \gamma_9(t_f) = \xi_2(t_f) & \gamma_{11-16}(t_f) = 0 \\ \gamma_3(t_f) = \xi_1(t_f) & & \end{array} \tag{5.67}$$

In Eq. 5.67 γ_2, γ_3, γ_9 and γ_{10} represent the real physical values for the boundary conditions of the physical system.

5.6.2 Experimental Results

The input parameters for the system given in Fig. 3.3 are the same as for the optimal control problem. The only difference will be the values for the normalization and regularization parameters. In this case, the values for the normalization parameter μ_2 were assumed to be $\mu_2 = 10^4$ because of the varied dimensions and magnitudes of the two tracked states. Additionally, the values for the μ_3 and μ_4 were established experimentally to be $5 \cdot 10^{-5}$. For a reference route for the pressure, an oblique rectangular form was chosen. This enhanced the system's total mechanical stiffness during motion. The algorithm was implemented in MATLAB, where the control variables u_1 and u_2 were determined. These variables were then implemented to the real model of the system into MATLAB Simulink as a feed-forward to the system inputs (see Fig. 5.4). This system was then tested for two distinct time intervals: $t \in [0,4]\,s$ and for $t \in [0,8]\,s$. The pressure on the rod side was controlled to a maximum value of 20 bar. This improves the hydraulic stiffness of the system, which improves the whole system's mechanical stiffness. Despite the fact that the pressure changes rapidly, there are no fluctuations in the pressure. This is not the case when utilizing traditional control methods. For the first experiment Fig. 5.5 it can be seen that the system follows its desired paths without any issues. Additionally, the system reaches its maximum speed towards

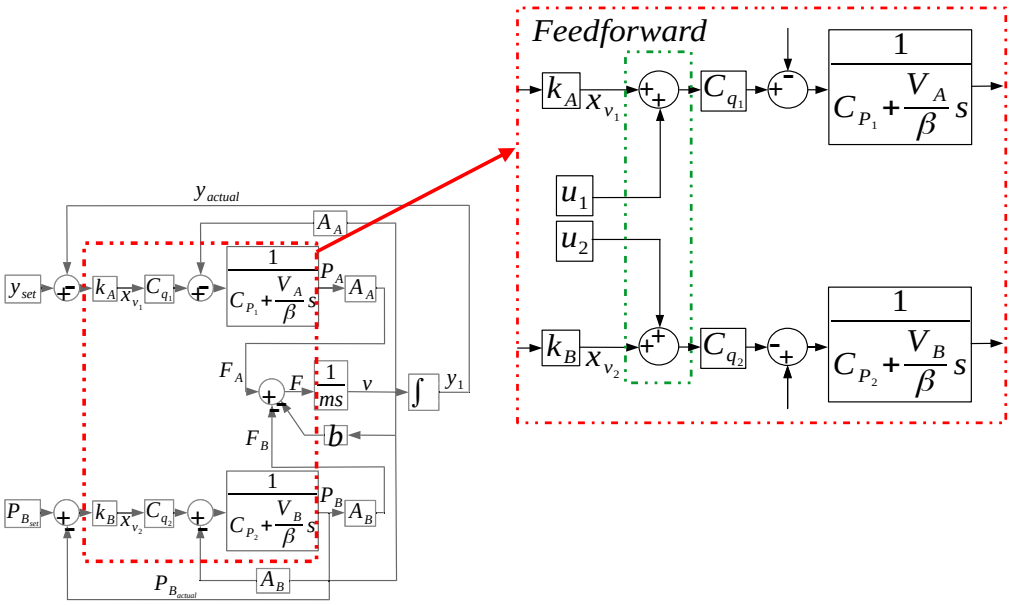

Figure 5.4: As a feed-forward, the estimated control variables u_1 and u_2 are implemented into the simulation model of the system.

the midpoint, which shows the energy efficiency of this method. Since the difference between the desired, followed, and simulated paths and pressures is very small, an error plot was produced. The second experiment was conducted with the same path and values but on a longer time scale. In this case, the time interval is $t \in [0, 8]\, s$. Similar to the first experiment, the path tracking algorithm produces excellent results. The accuracy, in this case is, much higher than in the first experiment. This is shown in the error curves Fig. 5.8 where the maximum offset is 0.005%. Based on the findings, it can be stated that the path tracking approach may be successfully utilized to track states in various units and magnitudes. The estimated control variables, which were then employed as feed-forward inputs for the simulated system, resulted in extremely close pathways to the desired and followed trajectories. In addition, the behavior of the other two states demonstrates that the approach is energy efficient in both cases studied.

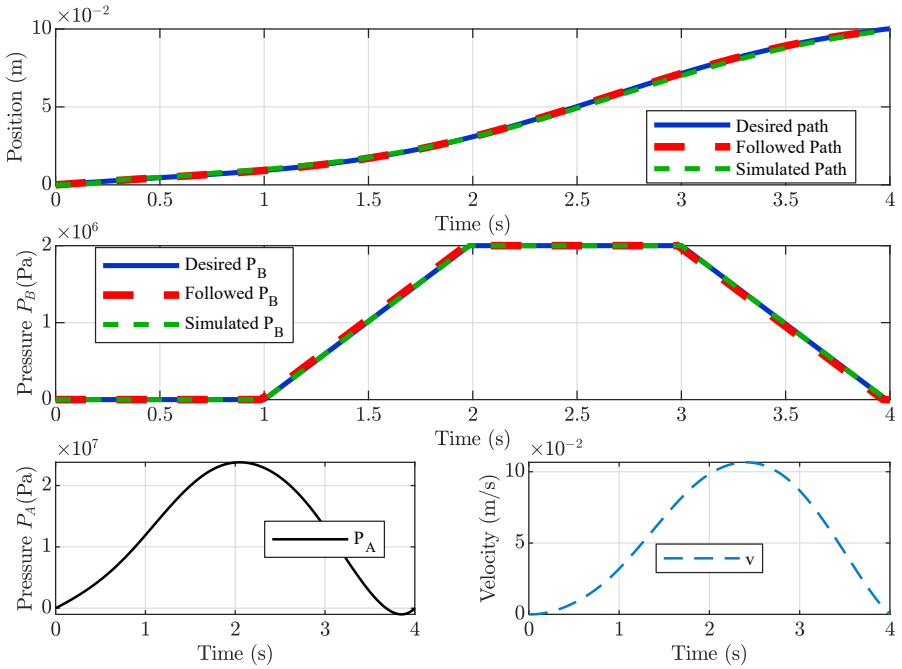

Figure 5.5: (Top and middle graph) - Path tracking results for time $t \in [0,4]\,s$. The states x_3 and x_2 (position and pressure respectively) are being tracked. There is only a small offset between the followed, simulated, and desired values. (Bottom graphs) - The behavior of the remaining two states of the system [179].

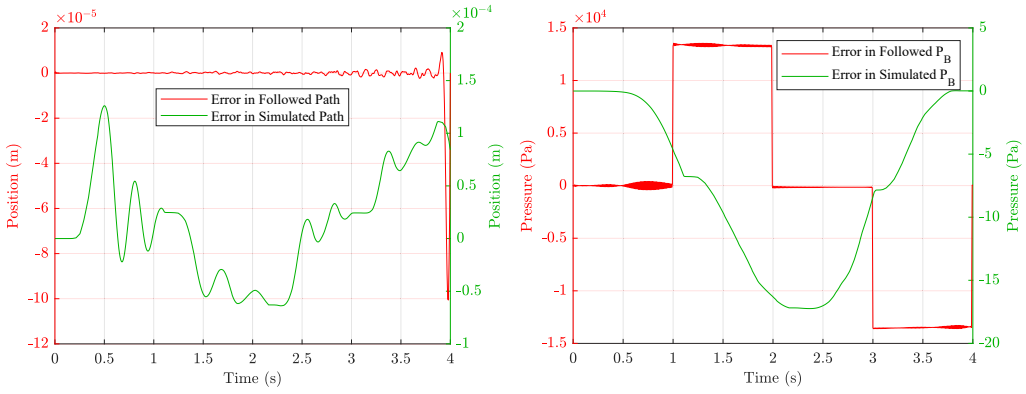

(a) Error curves for the followed and simulated positions in Fig. 5.5

(b) Error curves for the followed and simulated pressures in Fig. 5.5

Figure 5.6: Error curves for the followed and simulated positions and pressures in Fig. 5.5 accordingly. The maximum offset of this method here is 1 % [179].

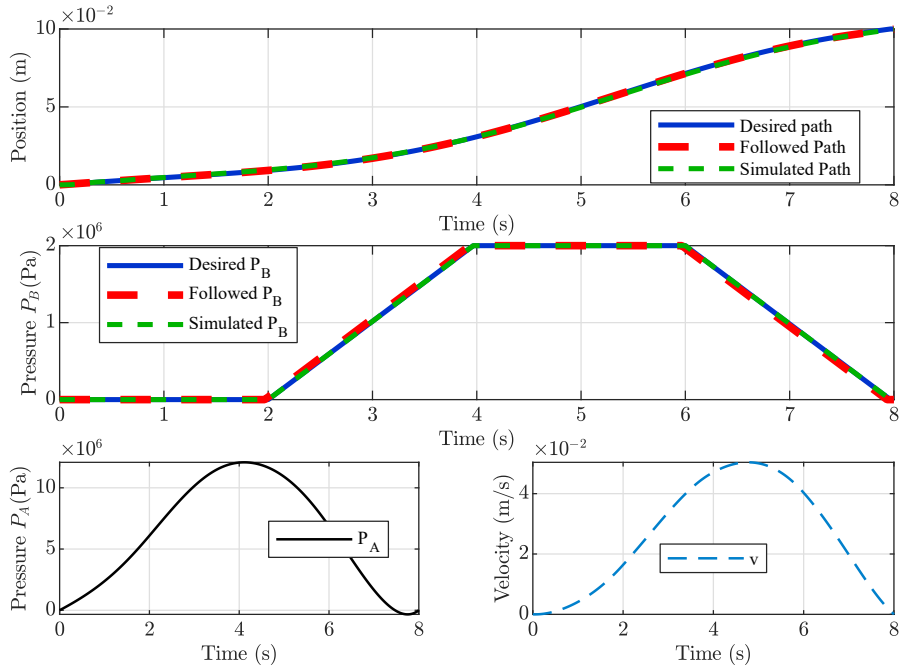

Figure 5.7: (Top and middle graph) - Path tracking results for time $t \in [0,8]\,s$. The states x_3 and x_2 (position and pressure respectively) are being tracked. There is only a small offset between the followed, simulated, and desired values. (Bottom graphs) - The behavior of the remaining two states of the system [179].

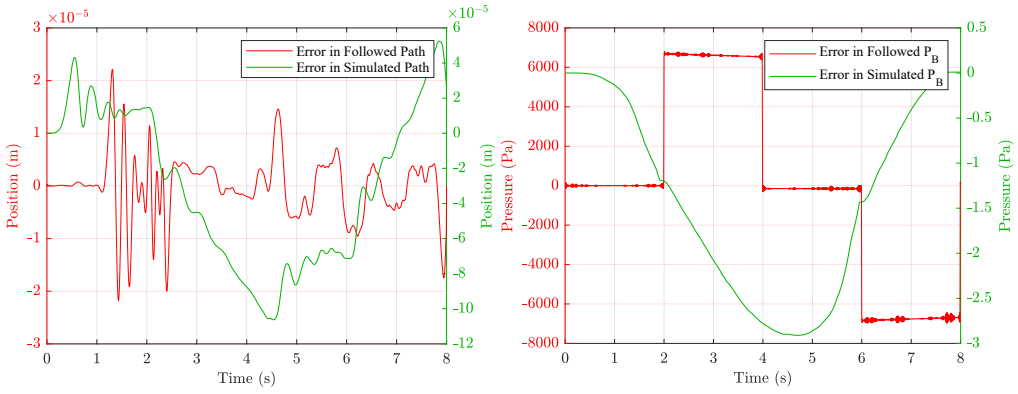

(a) Error curves for the followed and simulated positions in Fig. 5.7

(b) Error curves for the followed and simulated pressures in Fig. 5.7

Figure 5.8: Error curves for the followed and simulated positions and pressures in Fig. 5.7 accordingly. The maximum offset of this method here is 0.005 % [179].

Chapter 6

Potential Future Works

Some elements of this work are still in progress yet or have not been thoroughly studied, thus they will be provided here. The following approaches are provided individually due to their respective incompleteness and largely superficial descriptions. However, they are all a part of the study.

6.1 Optimal Control Parameters

The controller is the heart of the control system [181]. The controller delivers the actuating signal to the actuator to reduce error based on the error between the plant output and the reference value [29]. The PID controller is one of the most used controllers in the industry. It improves the steady-state response of the system and can dampen oscillations [182]. Depending on the parameters, the system performance can be tuned or modified. There are already multiple tuning algorithms that can be modified to tune the performance according to its demands. More information about different tuning algorithms can be found in [183], [184], [185], [186]. Some of these methods are based on calculus of variation techniques [187], [188], [189], [190]. Although most of the tuning methods work on the trial and error principle, the optimal control methods estimate the optimal control parameters for the desired input. In this chapter, a novel method for finding the optimal control parameters for a PID controller for a given system is derived.

6.2 Potential Numerical Solution of the Problem

Before solving for the optimal parameters for a PID controller, we first need to define the system we want to optimize and the desired input. In order to do that, we can use the state-space representation already implemented in Eq. 3.54. Following

this, the state-space representation of the system is defined as

$$\dot{\boldsymbol{x}}(t) = \mathsf{A}\boldsymbol{x}(t) + \mathsf{B}\boldsymbol{x}_{set}(t) \tag{6.1}$$

where $\boldsymbol{x}_{set}$ is the desired input for the system. The initial values for the system can be expressed as

$$\boldsymbol{x}(0) = \mathbf{0}. \tag{6.2}$$

Discretizing this system in a similar manner as in section 5.5.1 and 5.6.1 one gets

$$(\mathsf{I} \otimes \mathsf{D} - \mathsf{A} \otimes \mathsf{I}_n)\boldsymbol{x} = (\mathsf{B} \otimes \mathsf{I}_n)\boldsymbol{x}_{set} \tag{6.3}$$

Following the same methodology as in 5.5.1 and 5.6.1 the constraints of the system can be written in the following manner

$$\underbrace{\begin{bmatrix} 1 & 0 & \dots & 0 & 0 & 0 & \dots & 0 & 0 & 0 \\ 0 & 0 & \dots & 0 & 1 & 0 & \dots & 0 & 0 & 0 \\ 0 & 0 & \dots & 0 & 0 & 0 & \dots & 0 & 0 & 1 \end{bmatrix}}_{\mathsf{C}} \boldsymbol{x} = \mathbf{0}. \tag{6.4}$$

The general numerical solution for Eq. 6.3 using the singular value decomposition (SVD) can be written as

$$\boldsymbol{x} = \mathsf{L}^{-}(\mathsf{B} \otimes \mathsf{I}_n)\boldsymbol{x}_{set} + \tilde{\mathsf{V}}\boldsymbol{\beta}. \tag{6.5}$$

The vector $\boldsymbol{\beta}$ can be calculated using the constraints given in 6.4 in the following way

$$\mathsf{C}\boldsymbol{x} = \mathbf{0} \quad \rightarrow \quad \mathsf{C}\left(\mathsf{L}^{-}(\mathsf{B} \otimes \mathsf{I}_n)\boldsymbol{x}_{set} + \tilde{\mathsf{V}}\boldsymbol{\beta}\right) = \mathbf{0} \tag{6.6}$$

so one gets

$$\boldsymbol{\beta} = -\left(\mathsf{C}\tilde{\mathsf{V}}\right)^{+} \mathsf{C}\mathsf{L}^{-}(\mathsf{B} \otimes \mathsf{I}_n)\boldsymbol{x}_{set}. \tag{6.7}$$

Finally, the solution can be written as

$$\boldsymbol{x} = \left[\mathsf{I} - \tilde{\mathsf{V}}\left(\mathsf{C}\tilde{\mathsf{V}}\right)^{+}\mathsf{C}\right]\mathsf{L}^{-}(\mathsf{B} \otimes \mathsf{I}_n)\boldsymbol{x}_{set}. \tag{6.8}$$

6.3 Potential Numerical Solution of PI Controlled System

For example, let us consider a mass-spring system already defined by Newton's second law equation in Eq. 3.2. This system is position-controlled where the input or the position is defined as $\boldsymbol{x}_{set}$. Taking into account that the external forces for

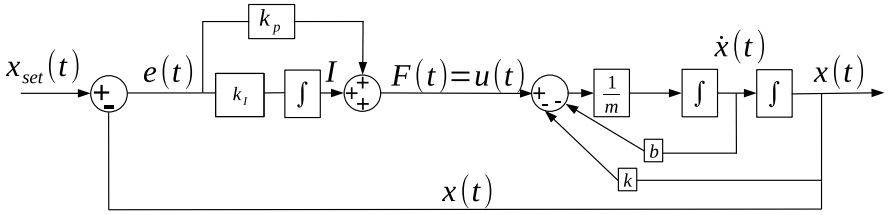

Figure 6.1: PI controlled mass spring system.

the system given in Fig. 6.1 are equal to zero, the control variable u using the Laplace transformation can be expressed as

$$\dot{u} = (\dot{x_{set}} - \dot{x_1})(k_p + k_I) \tag{6.9}$$

where the vector x_1 is actual position of the system, x_{set} is the desired position and k_p and k_I are the proportional and integral part of the PID controller. Taking the system presented in Fig. 6.1 the system differential equations can be expressed as

$$m\ddot{x} + b\dot{x} + kx = (\dot{x_{set}} - \dot{x})(k_p + k_I) \tag{6.10}$$

Following this, the system state space matrices can be expressed as

$$\mathsf{A} = \begin{bmatrix} 0 & 1 & 0 \\ 0 & 0 & 1 \\ -\frac{k_I}{m} & -\frac{(k+k_P)}{m} & -\frac{b}{m} \end{bmatrix} \mathsf{B} = \begin{bmatrix} 0 \\ \frac{k_P}{m} \\ \frac{k_I}{m} \end{bmatrix} \tag{6.11}$$

Now, the cost function Θ we want to minimize can be written as

$$\Theta(\psi) = \|\boldsymbol{x}_{set} - \mathsf{E}_1 \boldsymbol{x}\| \tag{6.12}$$

where

$$\mathsf{E}_1 = \begin{bmatrix} \mathsf{I} & 0 & 0 \end{bmatrix}. \tag{6.13}$$

In Eq. 6.12 ψ is the vector containing the control parameters. In other words, we want to minimize the difference between the first state (which is the position in our case) and the set value. If we substitute 6.8 in 6.12 we get

$$\Theta(\psi) = \left\| \left[\mathsf{I} - \mathsf{E}_1 \left(\mathsf{I} - \tilde{\mathsf{V}} \left(\mathsf{C}\tilde{\mathsf{V}} \right)^{+} \mathsf{C} \right) \mathsf{L}^{-} (\mathsf{B} \otimes \mathsf{I}_n) \right] \boldsymbol{x_{set}} \right\|. \tag{6.14}$$

This cost function reaches a minimum when $k_P, k_I \to \infty$. In the real system we know that if the values of the k_P and k_I are very big the system will be unstable. In order to implement this method to a real system, some kind of limit to the system performance variables is needed (velocity, acceleration). This can be achieved by

the implementation of regularization parameters to the control input, which will prevent its value to become unrealistically large. Now, to be able to see which regularization norm will give us the most suitable solution, three different alterations of regularization parameters were derived, and three different cost functions were defined accordingly

$$\begin{aligned}
\Theta_1(\psi) &= \|\boldsymbol{x_{set}} - \mathsf{E}_1\boldsymbol{x}\|_2^2 + \mu_1 \|k_P\dot{\boldsymbol{x}}_{\boldsymbol{set}} - k_P\mathsf{E}_2\boldsymbol{x}\|_2^2 + \mu_2 \|k_I\boldsymbol{x_{set}} - k_I\mathsf{E}_1\boldsymbol{x}\|_2^2 \\
\Theta_2(\psi) &= \|\boldsymbol{x_{set}} - \mathsf{E}_1\boldsymbol{x}\|_2^2 + \mu_1 \|k_P\dot{\boldsymbol{x}}_{\boldsymbol{set}} - k_P\mathsf{E}_2\boldsymbol{x}\|_2^2 + \mu_2 \|k_I\dot{\boldsymbol{x}}_{\boldsymbol{set}} - k_I\mathsf{E}_1\dot{\boldsymbol{x}}\|_2^2 \\
\Theta_3(\psi) &= \|\boldsymbol{x_{set}} - \mathsf{E}_1\boldsymbol{x}\|_2^2 + \mu_1 \|k_P\dot{\boldsymbol{x}}_{\boldsymbol{set}} - k_P\mathsf{E}_2\boldsymbol{x}\|_2^2 + \mu_1 \|k_I\boldsymbol{x_{set}} - k_I\mathsf{E}_1\boldsymbol{x}\|_2^2 \\
&\quad + \mu_2 \|k_P\ddot{\boldsymbol{x}}_{\boldsymbol{set}} - k_P\mathsf{E}_2\dot{\boldsymbol{x}}\|_2^2 + \mu_2 \|k_I\dot{\boldsymbol{x}}_{\boldsymbol{set}} - k_I\mathsf{E}_1\dot{\boldsymbol{x}}\|_2^2, \qquad (6.15)
\end{aligned}$$

where

$$\mathsf{E}_2 = \begin{bmatrix} 0 & \mathsf{I} & 0 \end{bmatrix}. \qquad (6.16)$$

6.3.1 Results

The three cost functions given in Eq. 6.15 were run in a simulation environment and plotted. For the three simulations, the values for the regularization parameters μ_1 and μ_2 were chosen experimentally. According to these values, the control parameters k_P and k_I values were calculated and plotted accordingly.

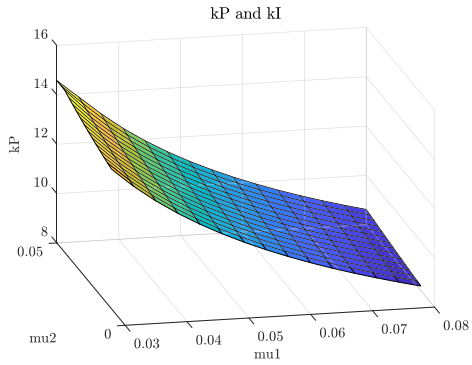

Figure 6.2: Results from the cost function Θ_1. The value of k_P increases with the increase of μ_2 but decreases with the increase of μ_1.

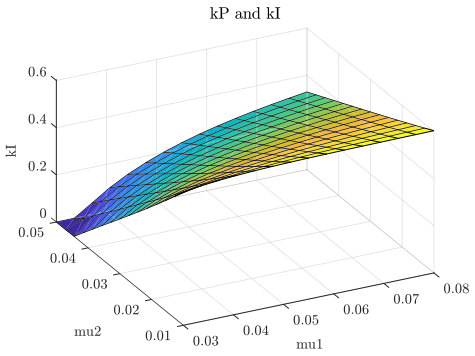

Figure 6.3: Results from the cost function Θ_1. The value of k_I increases with the increase of μ_1 but decreases with the increase of μ_2.

These computed values for k_p and k_I were then tested in a simulation environment (Simulink). It was concluded that the optimal values for $k_p = 10.5$ and $k_I = 0.54$. It is essential to mention that all three cost functions include the solution for different values of μ_1 and μ_2. This should mean that when one plots the control parameters

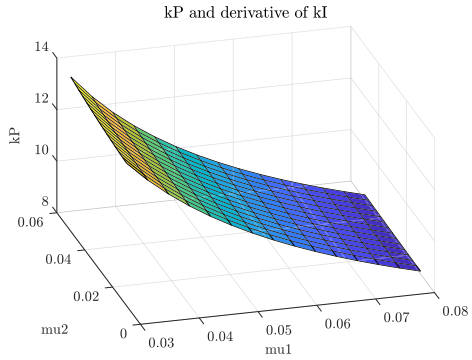

Figure 6.4: Results from the cost function Θ_2. It is obvious that the behavior is very similar to the one in Fig. 6.2. The values for the parameters are slightly different.

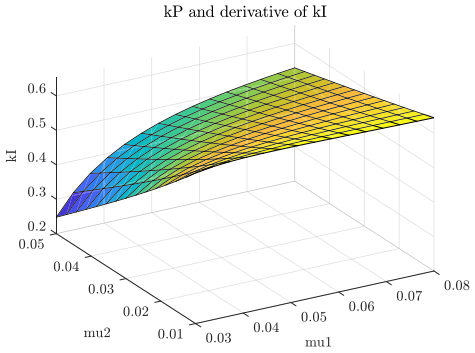

Figure 6.5: Results from the cost function Θ_2. We have the similar behavior in this figure as in the one shown in Fig.6.3.

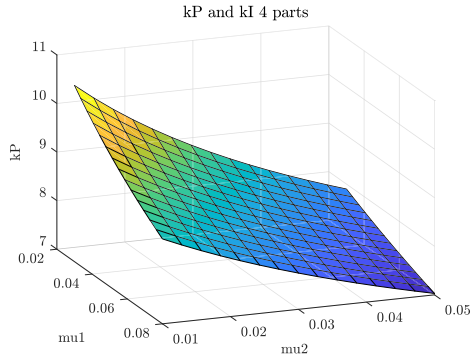

Figure 6.6: Results from the cost function Θ_3. Here the behavior is similar to the ones shown in Fig.6.2 and Fig.6.4 but the values for the regularization parameters are different. This is expected as the regularization parameters in the cost function for this case are very different from the ones before.

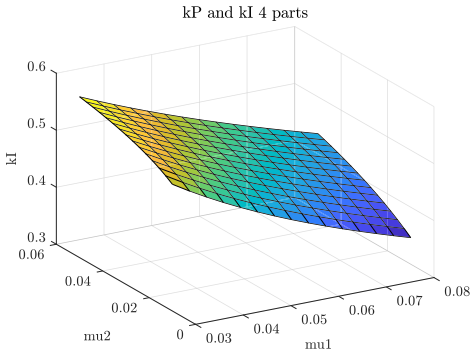

Figure 6.7: Results from the cost function Θ_3. The value of μ_2 does not affect the value of k_I significantly. When compared with Fig.6.3 and Fig.6.5 it is obvious that μ_1 has a bigger effect on the value of k_I.

k_p and k_I with the cost function, one should have a certain minimum at this point (see Fig. 6.8). The optimal parameters were then tested for the system given in Eq. 6.11 for mass $m = 10\ kg$, spring constant $k = 1\ \frac{N}{m}$, and friction parameter b= $20\ \frac{Ns}{m}$. It can be seen from Fig. 6.9 that the system achieves the desired position

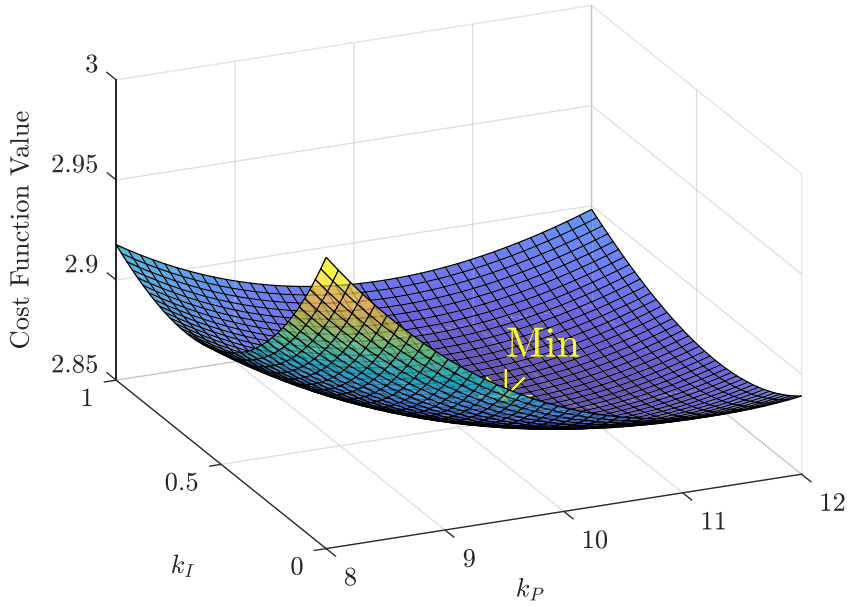

Figure 6.8: Cost function evaluated for the certain range of the control parameters k_p and k_I, which includes the optimal parameters also. It is obvious that the cost function has a minimum at the optimal parameter values previously calculated (k_p = 10.5 and k_I = 0.54).

with no steady-state error and no overshoot. This idea can be then extended to any system and to a PID-controlled system in a similar manner. It is important to note that in this case three regularization parameters will be necessary to get satisfactory results when the system has three control parameters.

6.4 Conclusion and Future Works

The method shown in this chapter calculates the optimal parameters for a PI-controlled system given in a state-space form. Multiple cost functions were derived according to the different definition of the regularization parameters. The results were plotted accordingly, and the optimal parameters for the system were computed. For these optimal parameters, the cost function was plotted where it was illustrated that the function has a minimum at this point. Additionally, the system was tested in Matlab Simulink, where it was concluded that the values calculated are the ones that yield stable solution with no overshoot or steady-state error.
However, this solution can be improved concerning the regularization parameters. In the example given previously, certain values for the regularization parameters

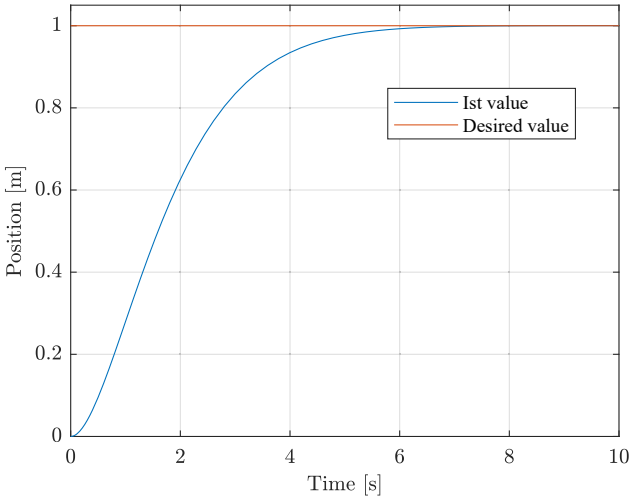

Figure 6.9: Simulation for the system for the calculated optimal parameters k_p = 10.5 and k_I = 0.54. The mass of the system m = 10 kg, the spring constant k = 1 $\frac{N}{m}$ and friction parameters b= 20 $\frac{Ns}{m}$. The system achieves the desired position with no overshoot and no steady state error.

were assumed experimentally, and the optimal control parameters were calculated according to them. To estimate the regularization parameters more structurally, one can use regularization techniques such as L-curve, Tikhonov regularization, etc. More information on these techniques can be found in [191], [192], [193], [194], [195], [196]. This will then allow the algorithm to fully compute the optimal parameters without any need for estimation for the regularization parameters.

Chapter 7

Discussion and Conclusion

The Wylie - Yu model for calculating the bulk modulus was improved to incorporate influence of the temperature, air content, and pressure of the hydraulic oil and successfully incorporated into an independent metering system for tunnel boring machines. The influence that each of these parameters has on the dynamics of such systems was analyzed. In addition, a new adaptive controller was implemented to mitigate some of these effects and improve the system's overall efficiency. In systems under high pressure, such as those used in tunnel boring machines, the temperature has a much higher influence on the bulk modulus value than the air content and pressure.

Given the increasing demand for tunnel boring machines, developing new state-of-the-art control algorithms for these machines is essential. The control of such systems must, on the one hand, increase productivity, but on the other hand, also increase energy efficiency. Despite the numerical difficulties inherent in such systems, two different control algorithms have been developed based on variational calculus methods and implemented in a simulation environment.

Both methods, optimal control and path tracking implemented for an independent metering system in tunnel boring machines, provide numerically stable solutions. Moreover, the system shows improved performance and higher energy efficiency compared to conventional solvers. The computation was based on a matrix-based approach for solving ODE's, using the mass matrix method and interstitial derivatives.

List of Figures

Bibliography

[1] E. Süli and D. F. Mayers, *An Introduction to Numerical Analysis*. Cambridge University Press, aug 2003.

[2] C. F. Curtiss and J. O. Hirschfelder, "Integration of Stiff Equations," *Proceedings of the National Academy of Sciences*, vol. 38, pp. 235–243, mar 1952.

[3] G. G. Dahlquist, "A special stability problem for linear multistep methods," *BIT Numerical Mathematics*, vol. 3, no. 1, pp. 27–43, 1963.

[4] R. C. Aiken, *Stiff Computation*. New York, NY: Oxford University Press, 1985.

[5] C. W. Gear, "The automatic integration of ordinary differential equations," *Communications of the ACM*, vol. 14, pp. 176–179, mar 1971.

[6] C. W. Gear, "Algorithm 407: DIFSUB for solution of ordinary differential equations," *Communications of the ACM*, vol. 14, pp. 185–190, mar 1971.

[7] A. Hindmarsh and G. D. Byrne, "Applications of EPISODE: an experimental package for the integration of systems of ordinary differential equations," 1975.

[8] G. D. Byrne and A. C. Hindmarsh, "A Polyalgorithm for the Numerical Solution of Ordinary Differential Equations," *ACM Transactions on Mathematical Software*, vol. 1, pp. 71–96, mar 1975.

[9] W. Liniger and R. A. Willoughby, "Efficient Integration Methods for Stiff Systems of Ordinary Differential Equations," *SIAM Journal on Numerical Analysis*, vol. 7, pp. 47–66, mar 1970.

[10] W. H. Enright, T. E. Hull, and B. Lindberg, "Comparing numerical methods for stiff systems of O.D.E:s," *BIT*, vol. 15, pp. 10–48, mar 1975.

[11] B. Lindberg, "On smoothing and extrapolation for the trapezoidal rule," *BIT*, vol. 11, pp. 29–52, mar 1971.

[12] J. C. Butcher, "On Runge-Kutta processes of high order," *Journal of the Australian Mathematical Society*, vol. 4, pp. 179–194, may 1964.

[13] B. L. Ehle, "High order a-stable methods for the numerical solution of systems of D.E.'s," *BIT Numerical Mathematics*, vol. 8, no. 4, pp. 276–278, 1968.

[14] A.-K. Kassam, *High order timestepping for stiff semilinear partial differential equations.* PhD thesis, Oxford University, 2004.

[15] J. G. J. M. Sanz-Serna, "Special Issue on Time Integration," *Applied Numerical Mathematics*, no. 25:135–136, 1997.

[16] L. F. Shampine and C. W. Gear, "A User's View of Solving Stiff Ordinary Differential Equations," *SIAM Review*, vol. 21, no. 1, pp. 1–17, 1979.

[17] E. Hairer and G. Wanner, *Solving Ordinary Differential Equations II*, vol. 14 of *Springer Series in Computational Mathematics*. Berlin, Heidelberg: Springer Berlin Heidelberg, 1996.

[18] D. Gafjinkel and C. B. Marbach, "Stiff differential equations," no. 360, 1977.

[19] L. N. Trefethen, *Spectral Methods in MATLAB*. Society for Industrial and Applied Mathematics, jan 2000.

[20] B. Minchev and W. Wright, "A review of exponential integrators for first order semi-linear problems," 2005.

[21] L. N. Trefethen, "Finite Difference and Spectral Methods for Ordinary and Partial Differential Equations," 1996.

[22] B. Fornberg, *A Practical Guide to Pseudospectral Methods.*, vol. 77. Cambridge, Cambridge University Press, cambridge, ed., 1997.

[23] C. Lanczos, "Trigonometric Interpolation of Empirical and Analytical Functions," *Journal of Mathematics and Physics*, vol. 17, pp. 123–199, 1938.

[24] J. Cooley and J. Tukey, "An algorithm for the machine calculation of complex Fourier series," *Mathematics of Computation*, vol. 19, pp. 297–301, 1965.

[25] E. O. Brigham, *The Fast Fourier Transform and Its Applications*. USA: Prentice-Hall, Inc., 1988.

[26] E. Hairer, "A Runge-Kutta Method of Order 10," *IMA Journal of Applied Mathematics*, vol. 21, no. 1, pp. 47–59, 1978.

[27] J. M. Varah, "Stability Restrictions on Second Order, Three Level Finite Difference Schemes for Parabolic Equations," *SIAM Journal on Numerical Analysis*, vol. 17, no. 2, pp. 300–309, 1980.

[28] M. Crouzeix, "Une méthode multipas implicite-explicite pour l'approximation des équations d'évolution paraboliques," *Numerische Mathematik*, vol. 35, pp. 257–276, 1980.

[29] B. Doicin, M. Popescu, and C. Patrascioiu, "PID Controller optimal tuning," in *2016 8th International Conference on Electronics, Computers and Artificial Intelligence (ECAI)*, pp. 1–4, IEEE, jun 2016.

[30] U. M. Ascher, S. J. Ruuth, and B. T. R. Wetton, "Implicit-Explicit Methods for Time-Dependent Partial Differential Equations," *SIAM Journal on Numerical Analysis*, vol. 32, pp. 797–823, jun 1995.

[31] J. Frank, W. Hundsdorfer, and J. Verwer, "On the stability of implicit-explicit linear multistep methods," *Applied Numerical Mathematics*, vol. 25, pp. 193–205, nov 1997.

[32] R. L. Burden and J. D. Faires, *Numerical Analysis*, vol. 148. Wadsworth Group, seventh ed ed., 2001.

[33] U. M. Ascher, S. J. Ruuth, and R. J. Spiteri, "Implicit-explicit Runge-Kutta methods for time-dependent partial differential equations," *Applied Numerical Mathematics*, vol. 25, pp. 151–167, nov 1997.

[34] M. Calvo, J. de Frutos, and J. Novo, "Linearly implicit Runge–Kutta methods for advection–reaction–diffusion equations," *Applied Numerical Mathematics*, vol. 37, pp. 535–549, jun 2001.

[35] S. Cox and P. Matthews, "Exponential Time Differencing for Stiff Systems," *Journal of Computational Physics*, vol. 176, pp. 430–455, mar 2002.

[36] P. W. Livermore, "An Implementation of the Exponential Time Differencing Scheme to the Magnetohydrodynamic Equations in a Spherical Shell," *J. Comput. Phys.*, vol. 220, pp. 824–838, jan 2007.

[37] F. Aluffi-Pentini, V. De Fonzo, and V. Parisi, "A novel algorithm for the numerical integration of systems of ordinary differential equations arising in chemical problems," *Journal of Mathematical Chemistry*, vol. 33, no. 1, pp. 1–15, 2003.

[38] H. Berland, B. Owren, and B. Skaflestad, "Solving the nonlinear Schrödinger equation using exponential integrators," *Modeling, Identification and Control: A Norwegian Research Bulletin*, vol. 27, no. 4, pp. 201–218, 2006.

[39] H. Berland, B. Skaflestad, and W. M. Wright, "EXPINT—A MATLAB package for exponential integrators," *ACM Transactions on Mathematical Software*, vol. 33, p. 4, mar 2007.

[40] M. Hochbruck, C. Lubich, and H. Selhofer, "Exponential Integrators for Large Systems of Differential Equations," *SIAM Journal on Scientific Computing*, vol. 19, pp. 1552–1574, sep 1998.

[41] J. P. Boyd, *Chebyshev and Fourier Spectral Methods*, vol. 49 of *Lecture Notes in Engineering*. Berlin, Heidelberg: Springer Berlin Heidelberg, 1989.

[42] N. J. Higham, "The Scaling and Squaring Method for the Matrix Exponential Revisited," *SIAM Journal on Matrix Analysis and Applications*, vol. 26, pp. 1179–1193, jan 2005.

[43] R. Holland, "Finite-difference time-domain (FDTD) analysis of magnetic diffusion," *IEEE Transactions on Electromagnetic Compatibility*, vol. 36, no. 1, pp. 32–39, 1994.

[44] A.-k. Kassam and L. N. Trefethen, "Fourth - order time - stepping for stiff PDEs," vol. 26, no. 4, pp. 1214–1233, 2005.

[45] S. Krogstad, "Generalized integrating factor methods for stiff PDEs," *Journal of Computational Physics*, vol. 203, no. 1, pp. 72–88, 2005.

[46] J. D. Hoffman and S. Frankel, *Numerical Methods for Engineers and Scientists*. CRC Press, oct 2018.

[47] G. F. Simmons, *Differential equations, with applications and historical notes*. McGraw-Hill New York, 1972.

[48] E. Zaev, *'Hardware-In-The-Loop' for real time simulation of complex mechanical system and their control*. Phd thesis, Ss. Cyril and Methodius University, 2013.

[49] R. L. Williams and D. A. Lawrence, *Linear State-Space Control Systems*. Hoboken, NJ, USA: John Wiley and Sons, Inc., feb 2007.

[50] B. Friedland, *Control System Design: An Introduction to State-space Methods*. Control theory, McGraw-Hill, 1986.

[51] K. Ogata, *Modern Control Engineering*. USA: Prentice Hall PTR, 4th ed., 2001.

[52] S. Skogestad and I. Postlethwaite, *Multivariable feedback control: Analysis and Design*. Hoboken, US-NJ: John Wiley, 2005.

[53] G. G. Rigatos, *State-Space Approaches for Modelling and Control in Financial Engineering*, vol. 125 of *Intelligent Systems Reference Library*. Cham: Springer International Publishing, 2017.

[54] G. C. Goodwin Graebe, Stefan F., Salgado, Mario E.,, *Control system design*. Upper Saddle River, N.J.: Prentice Hall, 2001.

[55] J. F. Steffensen, *Interpolation*. Chelsea Publishing Company, 1950.

[56] S. R. Bakhsha, S. Saurabh, and S. Shukla, *Numerical Accuracies of Lagrange's and Newton Polynomial Interpolation*. Lap Lambert Academic Publishing GmbH KG, 2012.

[57] M. Harker, "Differential Equations, Inverse Problems and Fractional Calculus in Mechatronics," dec 2015.

[58] M. Harker, *Fractional Differential Equations: Numerical Methods for Applications*. Springer International Publishing, 2020.

[59] J. M. Ortega and W. C. Rheinboldt, "On Discretization and Differentiation of Operators with Application to Newton's Method," *SIAM Journal on Numerical Analysis*, vol. 3, no. 1, pp. 143–156, 1966.

[60] A. M. Legendre, *Nouvelles méthodes pour la détermination des orbites des comètes*. Nineteenth Century Collections Online (NCCO): Science, Technology, and Medicine: 1780-1925, F. Didot, 1805.

[61] C. H. Davis and C. F. Gauss, *Theory of the motion of the heavenly bodies moving about the sun in conic sections a translation of Gauss's "Theoria motus."*. Boston,: Little, Brown and company,, 1857.

[62] S. M. Stigler, "Gauss and the Invention of Least Squares," *The Annals of Statistics*, vol. 9, may 1981.

[63] S. M. Stigler, *The history of statistics : the measurement of uncertainty before 1900*. Cambridge, Mass.: Belknap Press of Harvard University Press, 1986.

[64] T. Kariya and H. Kurata, *Generalized Least Squares (Wiley Series in Probability and Statistics)*, vol. 7. 2004.

[65] D. G. Luenberger, *Optimization by Vector Space Methods*. USA: John Wiley and Sons, Inc., 1st ed., 1997.

[66] D. Scholz, *Proportionalhydraulik*. Berlin, Heidelberg: Springer Berlin Heidelberg, 1997.

[67] G. Hansen, P.C., Pereyra, V., and Scherer, *Least Squares Data Fitting with Applications*. Johns Hopkins University Press, 2012.

[68] G. Chavent, *Nonlinear Least Squares for Inverse Problems*. Scientific Computation, Dordrecht: Springer Netherlands, 2010.

[69] R. J. Rossi, *Mathematical Statistics: An Introduction to Likelihood Based Inference*. Wiley, 2018.

[70] R. A. Fisher, "On the mathematical foundations of theoretical statistics," *Philosophical Transactions of the Royal Society of London. Series A, Containing Papers of a Mathematical or Physical Character*, vol. 222, pp. 309–368, jan 1922.

[71] J. Russell and R. Cohn, *Ordinary Least Squares*. Book on Demand, 2012.

[72] G. H. Golub and C. F. Van Loan, *Matrix Computations*. The Johns Hopkins University Press, third ed., 1996.

[73] D. Kalman, "A Singularly Valuable Decomposition: The SVD of a Matrix," *The College Mathematics Journal*, vol. 27, pp. 2–23, jan 1996.

[74] P. Krus, *On Load Sensing Fluid Power Systems*. PhD thesis, Univ. of Linkoping, Linkoping, Sweden, 1988.

[75] K. Heybroek, "Saving Energy in Construction Machinery using Displacement Control Hydraulics Concept Realization and Validation," *Linköping Studies in Science*, no. January 2008, 2008.

[76] D. Gomm, R; Vanderlaan, "Velocity control of unbalanced hydraulic actuator subjected to over-center load conditions," 2009.

[77] T. Schmelzer and L. Trefethen, "Evaluating matrix functions for exponential integrators via Carathéodory–Fejér approximation and contour integrals," *ETNA. Electronic Transactions on Numerical Analysis [electronic only]*, vol. 29, 2007.

[78] Eaton Hydraulics Group, "Advanced Independent Metering Mobile Valve," tech. rep., Eaton, 2015.

[79] B. Eriksson, "Control Strategy for Energy Efficient Fluid Power Actuators - Utilizing Individual Metering," *Science And Technology*, no. 1341, p. 70, 2007.

[80] B. Yao and S. Liu, "Energy-saving control of hydraulic systems with novel programmable valves," *Proceedings of the World Congress on Intelligent Control and Automation (WCICA)*, vol. 4, no. June, pp. 3219–3223, 2002.

[81] B. Eriksson and J. O. Palmberg, "Individual metering fluid power systems: Challenges and opportunities," *Proceedings of the Institution of Mechanical Engineers. Part I: Journal of Systems and Control Engineering*, vol. 225, no. 3, pp. 196–211, 2011.

[82] M. Linjama and M. Vilenius, "Energy-Efficient Motion Control of a Digital Hydraulic Joint Actuator," *Proceedings of the JFPS International Symposium on Fluid Power*, vol. 2005, no. 6, pp. 640–645, 2005.

[83] Bin Yao and Song Liu, "Energy-saving control of hydraulic systems with novel programmable valves," in *Proceedings of the 4th World Congress on Intelligent Control and Automation (Cat. No.02EX527)*, vol. 4, pp. 3219–3223, IEEE.

[84] Xiangdong Kong, Dongsheng Shan, Jing Yao, and Yingjie Gao, "Study on experiment and modeling for the multifunctional integrated valve control system," in *2004 International Conference on Intelligent Mechatronics and Automation, 2004. Proceedings.*, pp. 455–459, IEEE.

[85] T. O. Andersen, M. E. Münzer, and M. R. Hansen, "Evaluations of Control Strategies for Separate Meter-In Separate Meter-Out Hydraulic Boom Actuation in Mobile Applications," in *17th International Conference of Hydraulics and Pneumatics, Ostrava, Czech Republic, June*, 2001.

[86] G. Rath and E. Zaev, "Cylinder Pressures in a Position Controlled System With Separate Meter-in and Meter-out," *Proceedings from the 13th Scandinavian International Conference on Fluid Power, June 3-5, 2013, Linköping, Sweden*, vol. 92, pp. 251–259, 2013.

[87] S. Ufheil, S; Rector, "Programmable ride control," *United States Patent*, 1996.

[88] P. Krus and J.-O. Palmberg, "DAMPING OF MOBILE SYSTEMS IN MACHINES WITH HIGH INERTIA LOADS," *Proceedings of the JFPS International Symposium on Fluid Power*, vol. 1989, no. 1, pp. 63–70, 1989.

[89] K. Moon, "Control system for suppression of boom or arm oscillation," *United States Patent*, 2007.

[90] K. Yoshino, "Vibration control method and vibration control system for fluid pressure control circuit," *United States (US) Patent*, 2007.

[91] B. Yu, Z. Wang, D. Zhu, G. Wang, D. Xu, and J. Zhao, "Optimization and testing of suspension system of electric mini off-road vehicles," *Science Progress*, vol. 103, p. 003685041988187, jan 2020.

[92] J. Leavitt, F. Jabbari, and J. Boborw, "Optimal control and performance of variable stiffness devices for structural control," in *Proceedings of the 2005, American Control Conference, 2005.*, pp. 2499–2504, IEEE.

[93] P. Hołobut, "Time-optimal control of hydraulic manipulators with path constraints," *Journal of Theoretical and Applied Mechanics*, vol. 43, no. 3, pp. 523–538–538, 2005.

[94] G. Rath and E. Zaev, "Optimal Control for Hydraulic System With Separate Meter-in and Separate Meter-Out," *The 15th Scandinavian International Conference on Fluid Power, SICFP'17, June 7-9, 2017, Linköping, Sweden*, pp. 125–134, 2017.

[95] G. Stojanoski, *Modelling , Simulation and Control of a Hydraulic System with Individual Meter-in and Meter-out*. Master thesis, University of Leoben, 2017.

[96] G. Tao and F. L. Lewis, eds., *Adaptive Control of Nonsmooth Dynamic Systems*. London: Springer London, 2001.

[97] J. Na, Q. Chen, and X. Ren, *Adaptive Identification and Control of Uncertain Systems with Non-smooth Dynamics*. Academic Press, 2018.

[98] H. E. Merrit, *Hydraulic Control Systems*. John Wiley and Sons, Inc., 1967.

[99] P. Chapple, *Principles of Hydraulic Systems Design*. Momentum Press, vol. 2 ed., 2015.

[100] Y. F. Liu, J. Li, Z. M. Zhang, X. H. Hu, and W. J. Zhang, "Experimental comparison of five friction models on the same test-bed of the micro stick-slip motion system," pp. 15–28, 2015.

[101] A. E.-N. Gene F. Franklin, J. David Powell, *Feedback Control of Dynamic Systems*, vol. 23. Prentice Hall Press, One Lake Street Upper Saddle River, NJ, United States, 1987.

[102] C. M. Bender and S. A. Orszag, *Advanced Mathematical Methods for Scientists and Engineers I*. New York, NY: Springer New York, 1999.

[103] A. Harnoy, B. Friedland, and C. Cihn, "Modeling and measuring friction effects," *IEEE Control Systems*, vol. 28, pp. 82–91, dec 2008.

[104] R. Stribeck, *Kugellager für beliebige Belastungen*. Buchdruckerei AW Schade, Berlin N., 1901.

[105] B. Jacobson, "The Stribeck memorial lecture," *Tribology International*, vol. 36, pp. 781–789, nov 2003.

[106] R. Stribeck, "Die wesentlichen Eigenschaften der Gleit-und Rollenlager," *Zeitschrift des Vereines Deutscher Ingenieure*, vol. 46, pp. 1341–1348,1432–1438,1463–1470, 1902.

[107] D. Karnopp, "Computer Simulation of Stick-Slip Friction in Mechanical Dynamic Systems," *Journal of Dynamic Systems, Measurement, and Control*, vol. 107, pp. 100–103, mar 1985.

[108] R. I. Leine, D. H. van Campen, A. de Kraker, and L. van den Steen, "Stick-Slip Vibrations Induced by Alternate Friction Models," *Nonlinear Dynamics*, vol. 16, no. 1, pp. 41–54, 1998.

[109] R. H. A. Hensen, *Controlled Mechanical Systems With Friction*. PhD thesis, Technische Universiteit Eindhoven, 2002.

[110] B. Armstrong-Hélouvry, P. Dupont, and C. C. De Wit, "A survey of models, analysis tools and compensation methods for the control of machines with friction," *Automatica*, vol. 30, pp. 1083–1138, jul 1994.

[111] P. R. Dahl, "Solid friction model," *The Aerospace Corporation, Technical report*, 1968.

[112] P. R. Dahl, "Measurement of solid friction parameters of ball bearings," *The Aerospace Corporation, Techical report*, 1977.

[113] C. Canudas de Wit, H. Olsson, K. Astrom, and P. Lischinsky, "A new model for control of systems with friction," *IEEE Transactions on Automatic Control*, vol. 40, pp. 419–425, mar 1995.

[114] H. Gholizadeh, *Modeling and Experimental Validation of the Effective Bulk Modulus of a Mixture of Hydraulic Oil and Air*. Phd thesis, University of Saskatchewan, 2014.

[115] H. Feng, Q. Du, Y. Huang, and Y. Chi, "Modelling study on stiffness characteristics of hydraulic cylinder under multi-factors," *Strojniski Vestnik/Journal of Mechanical Engineering*, vol. 63, no. 7-8, pp. 447–456, 2017.

[116] A. U. E. Nykänen.THA, S Esque, "Comparasion of different fluid models.pdf," 2000.

[117] B.-H. Cho, H.-W. Lee, and J.-S. Oh, "Estimation Technique of Air Content in Automatic Transmission Fluid by Measuring Effective Bulk Modulus," tech. rep., 2000.

[118] Y. Jinghong, C. Zhaoneng, and L. Yuanzhang, "The Variation of Oil Effective Bulk Modulus With Pressure in Hydraulic Systems," *Journal of Dynamic Systems, Measurement, and Control*, vol. 116, pp. 146–150, mar 1994.

[119] E. B. Wylie and V. L. Streeter, "Fluid Transients," p. 384, 1980.

[120] M. Kajaste, J., Kauranne, H., Ellman, A., and Pietola, "Experimental Validation of Different Models for Bulk Modulus of Hydraulic Fluid," *The 9th Scandinavian International Conference on Fluid Power, SICFP'05*, 2005.

[121] Y. X. J. Watton, "A new direct measurement method for determining fluid bulk modulus in oil hydraulic systems 1994.pdf," 1994.

[122] E. Kuss, "PVT Daten bei hohen Drücken," *DGMK Berichte, Forschungsbericht 4510*, 1976.

[123] S. Kim and H. Murrenhoff, "Measurement of Effective Bulk Modulus for Hydraulic Oil at Low Pressure," *Journal of Fluids Engineering*, vol. 134, p. 021201, feb 2012.

[124] G. Stojanoski, G. Rath, and M. Gimpel, "The Effects of Bulk Modulus on the Dynamics of Hydraulic Independet Metering Systems," *The Sixteenth Scandinavian International Conference on Fluid Power, May 22-24, 2019, Tampere, Finland*, 2019.

[125] H. Gholizadeh, D. Bitner, R. Burton, and G. Schoenau, "Modeling and experimental validation of the effective bulk modulus of a mixture of hydraulic oil and air," *Journal of Dynamic Systems, Measurement and Control, Transactions of the ASME*, vol. 136, no. 5, pp. 1–14, 2014.

[126] Q. Yuan, E. Corporation, J. Y. Lew, and E. Corporation, "Electronic Flow Control Valve (EFCV) with Pressure Compensation Capability,"

[127] D. Will, H. Stohl, and N. Gebhardt, *Hydraulik*. Berlin, Heidelberg: Springer Berlin Heidelberg, 2008.

[128] G. Stojanoski, D. Ninevski, G. Rath, and M. Harker, "A novel method for solving an optimal control problem for a numerically stiff independent metering system," *2020 Australian and New Zealand Control Conference, ANZCC 2020*, pp. 108–113, 2020.

[129] J. Kajaste, H. Kauranne, A. Ellman, and M. Pietola, "Computational Models for Effective Bulk Modulus of Hydraulic Fluid," *2nd International Conference on Computational Methods in Fluid Power, FPNI'06*, pp. 1–7, 2006.

[130] S. Cetin and A. V. Akkaya, "Simulation and hybrid fuzzy-PID control for positioning of a hydraulic system," *Nonlinear Dynamics*, vol. 61, pp. 465–476, aug 2010.

[131] J. Wang, Guofang Gong, and Huayong Yang, "Control of bulk modulus of oil in hydraulic systems," in *2008 IEEE/ASME International Conference on Advanced Intelligent Mechatronics*, pp. 1390–1395, IEEE, jul 2008.

[132] B. Suif, "Effect of Oil Temperature on the Performance of a Hydraulic Linear System Controlled With Electro," vol. 32, no. 1, pp. 188–195, 2013.

[133] J. M. Hassan and S. Y. Ibrahim, "An Experimental Study Into The Effect Of Temperature And Pressure on The Hydraulic System," pp. 2531–2545, 2009.

[134] O. Yechiel, "A Survey of Adaptive Control," *International Robotics and Automation Journal*, vol. 3, oct 2017.

[135] J. Aseltine, A. Mancini, and C. Sarture, "A survey of adaptive control systems," *IRE Transactions on Automatic Control*, vol. 6, pp. 102–108, dec 1958.

[136] P. A. Ioannou and J. Sun, *Robust Adaptive Control*. USA: Prentice-Hall, Inc., 1995.

[137] S. Sastry and M. Bodson, *Adaptive Control: Stability, Convergence, and Robustness*. USA: Prentice-Hall, Inc., 1989.

[138] B. Egardt, ed., *Stability of Adaptive Controllers*, vol. 20 of *Lecture Notes in Control and Information Sciences*. Berlin/Heidelberg: Springer-Verlag, 1979.

[139] C. Cao, L. Ma, and Y. Xu, "Adaptive Control Theory and Applications," *Journal of Control Science and Engineering*, vol. 2012, pp. 1–2, 2012.

[140] K. S. Narendra and A. M. Annaswamy, *Stable Adaptive Systems*. USA: Prentice-Hall, Inc., 1989.

[141] K. Narendra and K. Parthasarathy, "Identification and control of dynamical systems using neural networks," *IEEE transactions on neural networks*, vol. 1 1, pp. 4–27, 1990.

[142] K. Narendra and K. Parthasarathy, "Reinforcement learning is direct adaptive optimal control," *IEEE Control Systems*, vol. 12, pp. 19–22, apr 1992.

[143] C. Lee, "Fuzzy logic in control systems: fuzzy logic controller. II," *IEEE Transactions on Systems, Man, and Cybernetics*, vol. 20, no. 2, pp. 419–435, 1990.

[144] R. Sargent, "Optimal control," *Journal of Computational and Applied Mathematics*, vol. 124, pp. 361–371, dec 2000.

[145] J. Bernoulli, "Curvatura laminae elasticae. Ejus identitas cum curvatura lintei a ponder inclusi fluidi expansi. Radii circulorum osculantium in terminis simplicissimis exhibiti, una cum novis quibusdam theorematis huc pertinentibus.," *Acta Eruditorum*, no. In Opera, V.1, 1744, 576–600., pp. 262–276, 1694.

[146] L. Euler, "Methodus inveniendi lineas curvas maximi minimive proprietate gaudentes, sive solutio problematis isoperimetrici latissimo sensu accepti," 1744.

[147] H. H. Goldstine, *A history of the calculus of variations from the 17th through the 19th century*. New York: Springer-Verlag, 1980.

[148] R. Vinter, *Optimal Control*. Systems & Control: Foundations & Applications, Birkhäuser Boston, 2000.

[149] A. Bryson, "Optimal control-1950 to 1985," *IEEE Control Systems*, vol. 16, pp. 26–33, jun 1996.

[150] R. Bellman, L. S. Pontryagin, V. G. Boltyanskii, R. V. Gamkrelidze, and E. F. Mischenko, "The Mathematical Theory of Optimal Processes.," *The American Mathematical Monthly*, vol. 70, p. 1114, dec 1963.

[151] F. Clarke, *Functional Analysis, Calculus of Variations and Optimal Control*. Graduate Texts in Mathematics, Springer London, 2013.

[152] I. M. Gelfand and S. V. Fomin, *Calculus of Variations*. Dover Books on Mathematics, Dover Publications, 2012.

[153] A. C. Clairaut, "Solution de plusieurs problèmes où il s'agit de trouver des Courbes dont la propriété consiste dans une certaine relation entre leurs branches, exprimée par une Équation donnée.," *Histoire de l'Académie royale des sciences*, pp. 196 – 215, 1734.

[154] A. Portela, *Parital differential equations for scientists and engineers*, vol. 6. 1989.

[155] A. D. R. Choudary, S. Parveen, and C. Varsan, *Partial Differential Equations An Introduction*. 2010.

[156] M. R. Hestenes, "Multiplier and gradient methods," *Journal of Optimization Theory and Applications*, vol. 4, pp. 303–320, nov 1969.

[157] K. Ito and K. Kunisch, *Lagrange Multiplier Approach to Variational Problems and Applications*. Society for Industrial and Applied Mathematics, jan 2008.

[158] C. Ciftci, H. S. S. Cayci, M. T. Atay, B. Toker, B. Guncan, and A. T. Yildirim, "The numerical solutions for stiff ordinary differential equations by using interpolated variational iteration method with comparison to exact solutions," *AIP Conference Proceedings*, 2018.

[159] S. A. M. Yatim, Z. B. Ibrahim, K. I. Othman, and M. B. Suleiman, "A Numerical Algorithm for Solving Stiff Ordinary Differential Equations," *Mathematical Problems in Engineering*, vol. 2013, pp. 1–11, 2013.

[160] G. Rath, M. Harker, and E. Zaev, "Direct numerical solution of stiff ODE systems in optimal control," in *2017 6th Mediterranean Conference on Embedded Computing (MECO)*, pp. 1–5, 2017.

[161] K. Dupree, P. M. Patre, Z. D. Wilcox, and W. E. Dixon, "Asymptotic optimal control of uncertain nonlinear Euler-Lagrange systems," *Automatica*, vol. 47, no. 1, pp. 99–107, 2011.

[162] T. N. Ta, C. S. Tran, and Y. L. Hwang, "The Kinematic and Dynamic Analysis of Hydraulic Control System Based on the Lagrangian Force Method," *International Journal of Computational Methods*, vol. 15, no. 5, pp. 1–18, 2018.

[163] M. Pourebrahim, A. S. Ghafari, and M. Pourebrahim, "Designing a LQR controller for an electro-hydraulic-actuated-clutch model," *Proceedings of 2016 2nd International Conference on Control Science and Systems Engineering, ICCSSE 2016*, pp. 82–87, 2016.

[164] S. E. Skariya, B. Sebastian, and M. Namboodiripad, "Integrated Optimal Control of Reusable launch Vehicle and Actuation system using Linear Quadratic Regulator," *IFAC Proceedings Volumes*, vol. 47, no. 1, pp. 840–846, 2014.

[165] X. Ji, Y. Liu, X. He, K. Yang, X. Na, C. Lv, and Y. Liu, "Interactive Control Paradigm-Based Robust Lateral Stability Controller Design for Autonomous Automobile Path Tracking With Uncertain Disturbance: A Dynamic Game Approach," *IEEE Transactions on Vehicular Technology*, vol. 67, no. 8, pp. 6906–6920, 2018.

[166] H. Andersen, Z. J. Chong, Y. H. Eng, S. Pendleton, and M. H. Ang, "Geometric path tracking algorithm for autonomous driving in pedestrian environment," in *2016 IEEE International Conference on Advanced Intelligent Mechatronics (AIM)*, pp. 1669–1674, IEEE, 2016.

[167] B. Alshaer, T. Darabseh, and M. Alhanouti, "Path planning, modeling and simulation of an autonomous articulated heavy construction machine performing a loading cycle," *Applied Mathematical Modelling*, vol. 37, no. 7, pp. 5315–5325, 2013.

[168] B. Alshaer, T. Darabseh, and A. Momani, "Modelling and control of an autonomous articulated mining vehicle navigating a predefined path," *International Journal of Heavy Vehicle Systems*, vol. 21, no. 2, p. 152, 2014.

[169] G. Bai, L. Liu, Y. Meng, W. Luo, Q. Gu, and B. Ma, "Path tracking of mining vehicles based on nonlinear model predictive control," *Applied Sciences (Switzerland)*, vol. 9, no. 7, 2019.

[170] J. Ji, A. Khajepour, W. W. Melek, and Y. Huang, "Path Planning and Tracking for Vehicle Collision Avoidance Based on Model Predictive Control With Multiconstraints," *IEEE Transactions on Vehicular Technology*, vol. 66, no. 2, pp. 952–964, 2017.

[171] J. M. Maciejowski, *Predictive Control with Constraints.* England.: Prentice Hall, 2002.

[172] G. Kalaiarassan and K. Krishnamurthy, "Digital hydraulic single-link trajectory tracking control through flow-based control," *Measurement and Control (United Kingdom)*, vol. 52, no. 7-8, pp. 775–787, 2019.

[173] M. H. Rudolfsen, T. N. Aune, O. Auklend, L. T. Aarland, and M. Ruderman, "Identification and Control Design for Path Tracking of Hydraulic Loader Crane," *IEEE/ASME International Conference on Advanced Intelligent Mechatronics, AIM*, pp. 565–570, 2017.

[174] J. Handler, M. Harker, and G. Rath, "Multidimensional Path Tracking With Global Least Squares Solution," *21st IFAC World Congress*, vol. 21, 2020.

[175] J. Wang, M. C. Lee, K. D. Kallu, S. J. Abbasi, and S. Ahn, "Trajectory tracking control of a hydraulic system using TSMCSPO based on sliding perturbation observer," *Applied Sciences (Switzerland)*, vol. 9, no. 7, pp. 1–17, 2019.

[176] J. H. Chin, Y. H. Sun, and Y. M. Cheng, "Force computation and continuous path tracking for hydraulic parallel manipulators," *Control Engineering Practice*, vol. 16, no. 6, pp. 697–709, 2008.

[177] B. Zhang, S. Wang, Y. Liu, and H. Yang, "Research on Trajectory Planning and Autodig of Hydraulic Excavator," *Mathematical Problems in Engineering*, vol. 2017, pp. 1–10, 2017.

[178] S. Kang, J. Park, S. Kim, Bongju Lee, Y. Kim, P. Kim, and H. J. Kim, "Path tracking for a hydraulic excavator utilizing proportional-derivative and linear quadratic control," in *2014 IEEE Conference on Control Applications (CCA)*, pp. 808–813, IEEE, 2014.

[179] G. Stojanoski, D. Ninevski, G. Rath, and M. Harker, "Multidimensional Trajectory Tracking for Numerically Stiff Independent Metering System," *17th Scandinavian International Conference on Fluid Power SICFP21*, no. 17th Scandinavian International Conference on Fluid Power SICFP21, 2021.

[180] R. Belman, *Mathematical Optimization Techniques*. 1963.

[181] J. Singh, B. Singh, and N. Joshi, "Tuning Techniques of PID controller: A review," *International Journal on Emerging Technologies (Special Issue NCETST*, vol. 8, no. 1, pp. 481–485, 2017.

[182] K. J. Åström and T. Hägglund, *PID Controllers: Theory, Design, and Tuning*. ISA - The Instrumentation, Systems and Automation Society, 1995.

[183] A. Y. Jaen-Cuellar, R. D. J. Romero-Troncoso, L. Morales-Velazquez, and R. A. Osornio-Rios, "PID-controller tuning optimization with genetic algorithms in servo systems," *International Journal of Advanced Robotic Systems*, vol. 10, 2013.

[184] A. Cultrera and L. Callegaro, "A simple algorithm to find the L-curve corner in the regularisation of ill-posed inverse problems," *IOP SciNotes*, vol. 1, no. 2, p. 025004, 2020.

[185] T. R. Biyanto, N. Sehamat, N. A. Sordi, and H. Zabiri, "Optimization of PID controller tuning parameters for multivariable system using Duelist algorithm," *IOP Conference Series: Materials Science and Engineering*, vol. 458, no. 1, 2018.

[186] X. Shi, T. Lan, and J. P. Hu, "PID controller tuning using optimization based on gradient-immune algorithm," *Proceedings - 2012 International Symposium on Instrumentation and Measurement, Sensor Network and Automation, IMSNA 2012*, vol. 1, pp. 173–175, 2012.

[187] V. B. S. Thulasi dharan, K, Kavyarasan, "Tuning of PID controller using optimization techniques for a MIMO process," no. 1, pp. 367–372, 2000.

[188] D. Vrančić, J. Petrovčič, Y. Peng, and R. Hanus, "A New Tuning Method for PID Controllers," *IFAC Proceedings Volumes*, vol. 30, pp. 399–404, oct 1997.

[189] T. George and V. Ganesan, "Optimal tuning of PID controller in time delay system: a review on various optimization techniques," *Chemical Product and Process Modeling*, oct 2020.

[190] R. T. O'Brien and J. M. Howe, "Optimal PID controller design using standard optimal control techniques," in *2008 American Control Conference*, pp. 4733–4738, IEEE, jun 2008.

[191] M. Harker and P. O'Leary, "Regularized Reconstruction of a Surface from its Measured Gradient Field: Algorithms for Spectral, Tikhonov, Constrained, and Weighted Regularization," *Journal of Mathematical Imaging and Vision*, vol. 51, no. 1, pp. 46–70, 2015.

[192] G. Landi and E. Loli Piccolomini, "An iterative Lagrange method for the regularization of discrete ill-posed inverse problems," *Computers and Mathematics with Applications*, vol. 60, no. 6, pp. 1723–1738, 2010.

[193] D. Calvetti, S. Morigi, L. Reichel, and F. Sgallari, "Tikhonov regularization and the L-curve for large discrete ill-posed problems," *Journal of Computational and Applied Mathematics*, vol. 123, no. 1-2, pp. 423–446, 2000.

[194] Hansen P.C., "REGULARIZATION TOOLS: A Matlab package for analysis and solution of discrete ill-posed problems," *Numerical Algorithms*, vol. 6, no. I 994, pp. 1–35, 1994.

[195] L. E. Widman, "Computational inverse problems in electrocardiography," *Journal of Biomedical Informatics*, vol. 35, no. 1, p. 51, 2002.

[196] O. Grodzevich and H. Wolkowicz, "Regularization using a parameterized trust region subproblem," *Mathematical Programming*, vol. 116, no. 1-2, pp. 193–220, 2009.